SAHC

Numerical Modelling of the seismic performance of Romanian traditional timber-framed buildings

Francesco Parisse

Portugal | 2019

ADVANCED MASTERS IN STRUCTURAL ANALYSIS
OF MONUMENTS AND HISTORICAL CONSTRUCTIONS

Master's Thesis

Francesco Parisse

Numerical Modelling of the seismic performance of Romanian traditional timber-framed buildings

University of Minho

Portugal | 2019

ADVANCED MASTERS IN STRUCTURAL ANALYSIS
OF MONUMENTS AND HISTORICAL CONSTRUCTIONS

Master's Thesis

Francesco Parisse

Numerical Modelling of the seismic performance of Romanian traditional timber-framed buildings

Portugal | 2019

DECLARATION

Name:	Francesco Parisse
Email:	francesco.parisse@alumni.unitn.it

Title of the Msc Dissertation:	Numerical Modelling of the seismic performance of Romanian traditional timber-framed buildings
Supervisor(s):	Elisa Poletti, Andreaa Dutu
Year:	2018/2019

I hereby declare that all information in this document has been obtained and presented in accordance with academic rules and ethical conduct. I also declare that, as required by these rules and conduct, I have fully cited and referenced all material and results that are not original to this work.

I hereby declare that the MSc Consortium responsible for the Advanced Masters in Structural Analysis of Monuments and Historical Constructions is allowed to store and make available electronically the present MSc Dissertation.

University:	University of Minho
Date:	17/07/2019
Signature:	Francesco Parisse

This page is left blank on purpose.

This page is left blank on purpose.

ACKNOWLEDGEMENTS

I would like to thank you my supervisors Elisa Poletti and professor Andreea Dutu for their availability and politeness. They were active and present since the very beginning.

I thank professor Hugo for its advices and its availability too.

This page is left blank on purpose.

ABSTRACT

Traditional architecture made of timber-framed masonry (TFM) system is widespread around the world and has already been recognized as a unique cultural heritage to be preserved. These structures have shown a good seismic performance compared to other typologies because their configuration and construction details were constantly updated as soon as the builders addressed the causes of damage mechanisms when earthquakes occurred. Romanian TFM structures can be considered a representative example of this typology also because they experienced several seismic events showing their good earthquake-resistance. Although these buildings are still inhabited nowadays and constructed, no recommendation is provided in the Romanian building code and its structural behavior is not properly characterized and modelled yet. Thus, bearing in mind that the building's global response depends on many parameters such as TFM walls, floor and roofing system as well as the connections between them, the calibration of shear walls is crucial to define the non-linear behavior under cyclic loading. A simplified modelling strategy was chosen to simulate TFM wall response consisting of an equivalent frame with linear elastic elements and non-linearities lumped at the joints.

The present thesis aimed at investigating the seismic performance of Romanian TFM walls and a representative TFM building located originally in Sarbova area, Timis County, but relocated to the National Village Museum "Dimitrie Gusti" in Bucharest, by comparing the numerical results with the measurements taken during the experimental campaign performed at Technical University of Civil Engineering of Bucharest and the *in situ* dynamic investigation, respectively. The wall numerical model was calibrated by performing the procedure of inverse fitting to obtain a good approximation between the experimental hysteretic curve and the numerical one in terms of initial stiffness, maximum base shear and total dissipated energy. This model was built in the FEM software OpenSees concentrating at the joints a non-linear hysteretic spring per degree of freedom and updating its parameters starting from some experimental tests performed on comparable types of connections. Once the wall response was matched, the Romanian traditional building was modelled by applying the same equivalent frame method, but, in this case, the dynamic properties did not match perfectly to those recorded by ambient vibration tests since microtremors involve the wall in the elastic range while the wall calibration was carried out for its non-linear one. Thus, the model was updated considering an additional contribution of infill since the type of masonry was different from the one infilling the tested wall. Eventually, non-linear static analysis was performed to assess the maximum shear and deformation capacity and predict some local failures at the timber joints.

The simplified equivalent frame model shows a good performance in simulating the wall response, but, for the already explained reasons, it was not completely capable of approximating the building dynamic properties. However, this strategy allows to reduce the computational efforts and, at the same time, provide information about the behavior of each connection.

This page is left blank on purpose.

RESUMO

Modelação numerica do desempenho sísmico de edifícios tradicionais mistos madeira-alvenaria romenos

A arquitetura vernacular constituída por paredes madeira com enchimento de alvenaria com estrutura de madeira (TFM) é difundida em todo o mundo e já foi reconhecida como um patrimônio cultural único que precisa de ser preservado. Essas estruturas mostraram um bom desempenho sísmico em comparação com outras tipologias, porque as suas configurações e os seus detalhes constitutivos foram constantemente atualizados assim que os construtores abordaram as causas dos mecanismos de danos quando os terremotos ocorreram. As estruturas TFM Romenas podem ser consideradas um exemplo representativo desta tipologia também porque experimentaram vários eventos sísmicos mostrando a sua boa resistência a sismos. Se bem que estes edifícios ainda sejam habitados hoje em dia e continuem a ser construídos, nenhuma recomendação é fornecida no código de construção romeno e o seu comportamento estrutural ainda não está devidamente caracterizado e modelado. Assim, tendo em conta que a resposta global do edifício depende de muitos parâmetros, tais como paredes TFM, piso e sistema de cobertura, bem como as ligações entre eles, a calibração das paredes de corte é crucial para definir o comportamento não linear sob carga cíclica. Uma estratégia simplificada de modelação foi escolhida para simular a resposta da parede TFM constituída por uma estrutura equivalente com elementos elásticos lineares e não-linearidades concentradas nas ligações.

A presente tese tem como objetivo investigar o desempenho sísmico das paredes romenas TFM e de um edifício TFM representativo localizado originalmente na área de Sarbova, no distrito de Timis, mas transferido para o National Village Museum “Dimitrie Gusti” em Bucareste, comparando os resultados numéricos com os resultados obtidos durante a campanha experimental realizada na Universidade Técnica de Engenharia Civil de Bucareste e na investigação dinâmica in situ, respetivamente. O modelo numérico da parede foi calibrado utilizando um procedimento de ajuste inverso para obter uma boa aproximação entre a curva histerética experimental e a curva numérica em termos de rigidez inicial, capacidade máxima e energia total dissipada. Este modelo foi desenvolvido no software a elementos finitos OpenSees, concentrando nas ligações uma mola histerética não linear por grau de liberdade e atualizando os parâmetros a partir de alguns ensaios experimentais existentes realizados em ligações comparáveis. Uma vez que a resposta da parede foi calibrada, o edifício tradicional romeno foi modelado aplicando o mesmo método da estrutura equivalente, mas, neste caso, as propriedades dinâmicas não se ajustaram perfeitamente àquelas obtidas através dos ensaios de vibração ambiental, pois os microtremores envolvem a parede na fase elástica inicial, enquanto a calibração da parede foi realizada para a sua resposta não-linear. Assim, o modelo foi atualizado considerando uma contribuição adicional do preenchimento de alvenaria, uma vez que o tipo de alvenaria foi diferente daquele da

parede ensaiada. Após desta calibração, foi realizada uma análise estática não linear para avaliar a capacidade máxima e deformação e prever alguns danos locais nas ligações de madeira.

O modelo simplificado equivalente da parede mostra um bom desempenho na simulação da resposta da parede, mas, pelas razões acima explicadas, não foi completamente possível aproximar as propriedades dinâmicas do edifício. No entanto, essa estratégia permite reduzir os esforços computacionais e, ao mesmo tempo, fornecer informações sobre o comportamento de cada ligação.

SINTESI

Modellazione numerica del comportamento sismico dell'architettura tradizionale Rumena con sistema misto legno-muratura

La tipologia architettonica tradizionale a sistema misto legno-muratura è ampiamente diffusa in ogni parte del mondo. La sua unicità è stata riconosciuta come patrimonio culturale da salvaguardare. Tali edifici hanno dimostrato un buon comportamento sismico se paragonati ad altre tipologie strutturali. La loro configurazione, nonché I loro dettagli costruttivi, si sono costantemente evoluti per opera dei costruttori, non appena questi ultimi hanno compreso le cause dei principali meccanismi di danno che si verificano a seguito di un terremoto. Il sistema misto Rumeno può essere considerato rappresentativo di questa tipologia strutturale, soprattutto perchè il territorio è stato soggetto ad innumerevoli eventi sismici dimostrando la sua capacità resistente. Nonostante molti di questi edifici siano attualmente abitati o in costruzione, non è presente nessuna informazione riguardo la loro progettazione nel codice edilizio Rumeno, inoltre il loro comportamento non è stato ancora propriamente caratterizzato ne modellato numericamente. La risposta globale di un edificio è funzione di diverse variabili tra cui la tecnologia costruttiva di pannelli murari, diaframmi orizzontali, sistema di copertura, nonché del loro grado di connessione. Per questo motivo, la calibrazione del comportamento non lineare delle pareti resistenti soggette a carichi ciclici è di fondamentale importanza per approssimare tale risposta globale. A questo proposito è stata scelta una strategia di modellazione semplificata basata su un telaio equivalente con elementi lineari elastici e non linearità concentrate nelle connessioni.

Il lavoro di tesi si rivolge in particolare allo studio del comportamento sismico dei pannelli murari Rumeni a sistema misto legno-muratura e di un edificio rappresentativo localizzato originariamente nell'area di Sarbova, contea di Timis (poi successivamente riassemblato nel Museo Nazionale "Dimitrie Gusti" di Bucarest). Tale ricerca è condotta attraverso la comparazione dei risultati numerici con quelli misurati sperimentalmente nelle prove di laboratorio eseguite su un pannello murario rappresentativo presso il Dipartimento di Ingegneria Civile di Bucarest e i test di identificazione dinamica eseguiti *in situ* sull'edificio. Il modello numerico relativo alla parete è stato calibrato attraverso una procedura iterativa per ottenere una buona approssimazione tra la curva isteretica ottenuta sperimentalmente e quella numerica, in termini di rigidezza iniziale, forza di taglio massima alla base ed energia totale dissipata. Tale schema è stato realizzato nel software OpenSees modellando molle non lineari per ogni grado di libertà ed aggiornando i relativi parametri che definiscono la risposta isteretica partendo da test sperimentali condotti su connessioni simili. Una volta calibrato il pannello murario, è stato modellato l'edificio con la stessa strategia a telaio equivalente. In questo caso, tuttavia , le proprietà dinamiche non sono risultate perfettamente comparabili con quelle ottenute dall'identificazione dinamica, i muri dell'edificio rispondono in campo lineare elastico, mentre le proprietà delle connessioni sono state calibrate in campo non lineare plastico. Per questo motivo, il modello è stato modificato considerando il

contributo di rigidezza aggiuntivo dato da una muratura in mattoni pieni, più rigida di quella presente nelle maglie del telaio testato. Infine, è stata svolta un'analisi non lineare statica al fine di stimare la massima forza alla base, la capacità deformativa del muro nonché alcune rotture locali nelle connessioni.

Il modello semplificato a telaio equivalente ha evidenziato un buon grado di approssimazione con la risposta del pannello murario, ma, per le ragioni precedentemente esposte, non è stato in grado di caratterizzare dal punto di vista dinamico l'edificio. Ad ogni modo tale strategia di modellazione permette di ridurre l'onere computazionale e, allo stesso tempo, fornisce informazioni sul comportamento di ogni connessione.

TABLE OF CONTENTS

TABLE OF FIGURES

LIST OF TABLES

1 INTRODUCTION

Timber-framed masonry vernacular architecture can be considered a product of centuries' long accumulation of knowledge and experience that is passed down through generations of local people from around the world. This process may have been accelerated by damages and deaths after devastating earthquakes since many systems were improved to achieve a good seismic behavior. Local workers were involved during the reconstruction processes; thus, the structures were rebuilt without any guideline except in some countries, where governments issued guidelines with specific rules to follow for the reconstruction. The basic concepts of earthquake engineering were developed through damage observations and comparing the response of different structural typologies. Indeed, builders, architects and engineers learnt from history how to prevent the building's global collapse reducing both economic losses and human casualties. This can be demonstrated by the fact that timber-framed masonry (TFM) structures have shown a good performance compared to other typologies when earthquakes occurred.

Vernacular architecture with mixed system has already been recognized as valuable and should be preserved as cultural heritage. This means that any potential intervention should respect authenticity of the structure to ensure compatibility and the retrofitting solutions should be properly designed and adopted only after a process of understanding the structural and architectural typology, which includes qualitative and quantitative information and data gathered by several sources. It is worth to point out that mixed structures remain built in some areas where wood can be easily harvested, and they are considered sustainable buildings.

The seismic behavior of timber-framed structures should be studied to identify and understand the main principles behind the mixed system (timber, bricks, mortar and their connections at the interface) as well as to predict its structural capacity with both complex and simplified numerical analysis. Although the scientific community has increased its research on this issue, the available numerical and experimental analysis on TFM walls is limited and very few tests are carried out considering the building as a whole, taking into account wall-to-wall, wall-to-floor, wall-to-roof connections. Analytical works on hysteretic models and design methodologies are limited as well. They are carried out just for one structural typology, but they should take into account also the several configurations observed *in situ,* which can vary in types of infill and timber joints, arrangement of bracings and frame layout.

In many countries, such as Romania, China, Greece, etc. the building codes do not provide any recommendation on timber-framed masonry structures although this system is still built nowadays. This means that TFM typology should be studied even more with respect to the most common ones and the future results may provide some guidelines or simple regulations about design and/or retrofitting strategies that can be followed either by technicians or non-specialized people.

1.1 Research objectives

The main objective of the thesis is analyzing the cyclic response of traditional timber-framed structures in Romania using a simplified numerical model capable of approximating their linear and, in particular, non-linear behavior when subjected to in-plane horizontal cyclic loading. This research aims to answer the question: Based on experimental results (even if limited) can a simplified numerical model be developed able to be applied to the analysis of a complete building?

1.2 Outline

In order to fulfill the objective of this thesis, the work is organized into the following chapters:
Chapter 2 presents a brief literature review, reporting the main TFM systems found around the world which are divided into engineered and non-engineered systems if they are based on any recommendation or code. In addition, experimental results related to similar TFM systems are described to better understand their mechanical properties and the types of failure mechanisms as well as the potential numerical approaches to simulate their behavior. Romanian timber-framed masonry architecture is characterized in its geometrical features such as typology of structures, construction techniques, types of masonry walls, floors and roofs, foundations as well as the connections between them. The application of TFM system in Romania is due to its seismic hazard that is studied to estimate its main properties and obtain a representative peak ground acceleration for the area under investigation.
Chapter 3 summarizes the Romanian experimental campaign on TFM walls, and its results are discussed to calibrate the numerical model on the actual behavior of the tested panel.
Chapter 4 presents the numerical modelling of some representative examples of traditional carpentry joints used in the Romanian wall specimens, modelled with non-linear hysteretic springs to simulate their maximum capacity in terms of force and deformation. This preliminary calibration was carried out since the connections play an important role in the wall response.
Chapter 5 presents the modelling and calibration of the TFM wall with low diagonals. Its local and global response was approached by understanding how and which connections control the initial and yielding stiffness as well as the ultimate softening branch that can be simulated by stiffness and strength degradations parameters. In this case, hysteretic material properties are modified and iteratively updated to match the experimental results of the in-plane cyclic quasi-static tests. After reaching a good approximation between the behavior of the numerical model and the experimental one, the same modelling strategy applied to the wall was adopted for the building.
Chapter 6 summarizes the *in situ* survey and dynamic identification performed on existing timber-framed buildings in Romania.
In Chapter 7 a representative Romanian building is finally analyzed. It was located originally in Sarbova area, Timis County, but relocated to the National Village Museum “Dimitrie Gusti” in Bucharest, and it is considered as a reference for Romanian TFM traditional architecture. Its seismic behavior was assessed

through eigenvalue analysis and non-linear static analysis, but, in this case, the modelling strategy of equivalent frame model with plasticity lumped at the joints was compared with the same model infilled with shell elements to simulate the increase in stiffness due to a different type of masonry (clay brick instead of mud brick) and also because the dynamic properties were obtained from the *in situ* investigations that measures microtremors only involving the building in the elastic range while the connections were calibrated to approach the non-linear response. Anyway, periods and mode shapes of the two modelling strategies were compared and the differences are commented. Regarding the pushover analysis, the resulting curves were overlapped with those resulting when some local maximum deformations at the joints were reached showing how this simplified model can capture even local failure mechanisms. However, it is worth to point out that the simplified modelling strategies can be implemented to obtain a reliable numerical model calibrated on the experimental measurements.

Finally, Chapter 8 presents conclusions from this thesis and recommendations for future work.

2 TIMBER-FRAMED MASONRY (TFM) STRUCTURES

Timber-framed structures with masonry or other kind of infills can be considered as some of the oldest vernacular architecture. This construction system is widespread all over the world and throughout the history even though each area shows different architectural and structural characteristics according to the available materials, techniques and knowledge (Bianco 2010). Several structural configurations of timber frame can be observed, therefore the dimensions and arrangement of wooden elements, infills, and / or tree species have varied from area to area (Bianco 2010). The system can be found in particular in seismic areas where builders adapted the configurations to make the structures as earthquake resistant as possible, Figure 2.1. This long-term process accelerated when an earthquake occurred because they could observe the structures that showed a good seismic performance and developed a certain experience addressing the causes of damage. In this section, timber-framed masonry (TFM) systems are classified as non-engineered or engineered structures, depending on them being based on design recommendations and codes or not, and their main characteristics are briefly described.

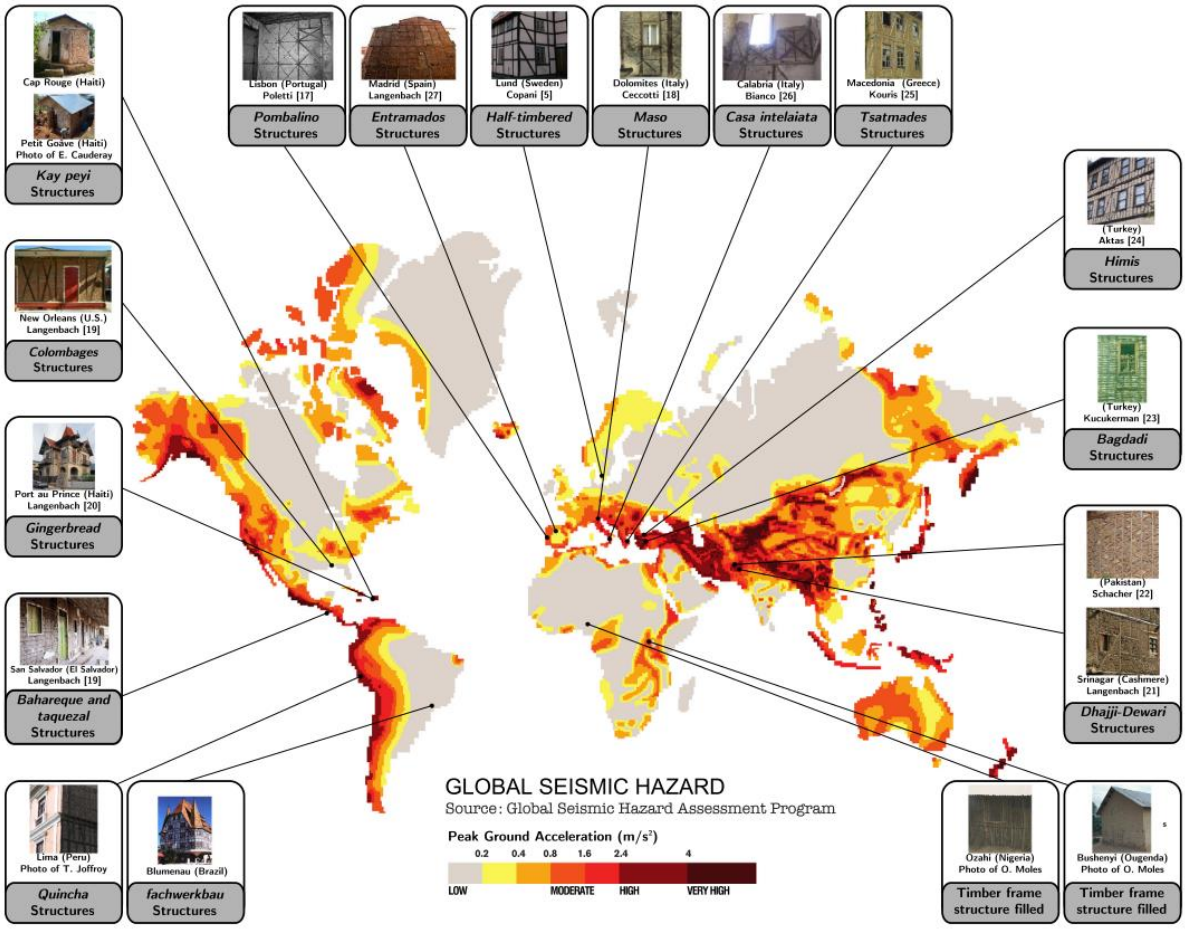

Figure 2.1 Timber-framed masonry structures (Vieux-Champagne et al. 2014).

2.1 Overview of the Timber-Framed Masonry Structures

Timber structures with wattle and daub infill have been built since the Iron Age when wooden posts were driven into a horizontal base with timber planks and branches bonded with mud (clay). The system developed and improved up to the Roman Era when some examples of TFM buildings can be observed such as Casa di Ercolano. The arrangement of the walls, defined as *opus craticium,* consists of timber frame infilled with irregular stones bonded with clay mortar. Initially the frame was applied just to make the upper structures lighter with no apparent seismic purposes (Bianco 2010). However, builders realized that TFM system was not prone to severe damages after an earthquake compared to other types of structures, thus it has spread especially across seismic areas. The vast majority of these structures was built without following any design code even though there are a few systems based on recommendations, whose configurations may have varied according to the background of builders or engineers.

2.1.1 Non engineered systems

The timber skeleton is widespread not only in seismic areas but it can be found even in countries with a low seismic hazard such as Canada, Sweden, Norway, England (*half-timber*), Denmark, Germany (*fachwerk*), Czech Republic, France (*colombages* or *pan de bois*) and Spain (*entramados*), Figure 2.2 and Figure 2.3. Sometimes timber masonry panels were applied only for architectural or aesthetical reasons but, in many cases, they have a structural role at least under static loads (Dima and Dutu 2016). On the other hand, TFM panels play an important role for dynamic actions, as a result TFM systems have developed especially in seismic countries. TFM structures can be observed in several configurations ranging from half-timbered type, masonry reinforced with wooden skeleton, to mixed systems between the ground floor and upper storeys. Figure 2.4 shows examples of TFM vernacular architecture in Albania, Romania (*paianta*), Greece, Turkey, where three systems are found such as *Hatil*, horizontal timber elements embedded into load-bearing masonry walls, *Himis*, TFM system with masonry infill and *Bagdadi*, timber-framed walls with infill made of rough timber elements, Figure 2.5 (Gülkan and Langenbach 2004). Mixed construction systems can be also observed in Northern Pakistan known as *Cator and Cribbage* technique and *Bhatar* method, Figure 2.6a and b. They can be defined as masonry reinforced with horizontal timber elements even though *Bhatar* building method uses less timber members due to the limited availability of the material (Schacher 2008). This system relates also to *Taq* technique in Kashmir, Figure 2.6c, where another construction method, known as *Dhajji-dewari*, is applied as well. It consists of highly subdivided light timber frames with masonry infills that seems a patchwork quilt wall, Figure 2.7 (NDMA - National Disaster Management Authority n.d.). Moreover, TFM structures have spread across Central and South America since these areas are prone to seismic events. They are known as *Bahareque* in Colombia, *Vareque* in Ecuador (Figure 2.8a and b), *Pajareque* in Honduras (Figure 2.9a), *Pared Francesa* in Argentina, *Quincha* in Perù (Figure 2.9b), *Adobillo* in Chile and *Taquezal* in Nicaragua, Figure 2.9c (Cruz et al. 2015). In particular, *Quincha* shows good seismic performance and consists of a timber frame infilled with canes plastered with earth and gypsum (Ortega

et al. 2017). These buildings have the ground floor in adobe and the upper storeys built with the TF panels. Miyanmar (Figure 2.10a) and China (Figure 2.10b) also have examples of TFM buildings and proved that they can withstand damages due to earthquakes, but rarely collapse.

(a) (b) (c)

Figure 2.2 Non-engineered TFM systems: Sweden (a); half-timber, England (b); fachwerk, Germany (c) (Bianco 2010); (Copani 2007); (Lukic 2016).

(a) (b) (c)

Figure 2.3 Non-engineered TFM systems: pletivo dùm, Czech Republic (a); colombages, France (b); entramados, Spain (c) (Bianco 2010).

(a) (b) (c)

Figure 2.4 Non-engineered TFM systems: Albania (a); *paianta*, Romania (b); Greece (c) (Vintzileou et al. 2004).

(a) (b) (c)

Figure 2.5 Non-engineered TFM systems: *hatil* construction technique in the ground floor and *himis* above (a); detail of *himis* (b) and *bagdadi* (c) in Turkey (Gülkan and Langenbach 2004).

(a) (b) (c)

Figure 2.6 Non-engineered TFM systems: c*ator and cribbage* (a) and *bhatar* (b) technique in Pakistan; *taq,* Kashmir (c) (Langenbach 2009).

(a) (b) (c)

Figure 2.7 Non-engineered TFM systems: details of patchwork quilt of d*hajji-dewari* with large panels (a), small panels (b), random layout (c) in Kashmir (Langenbach 2009).

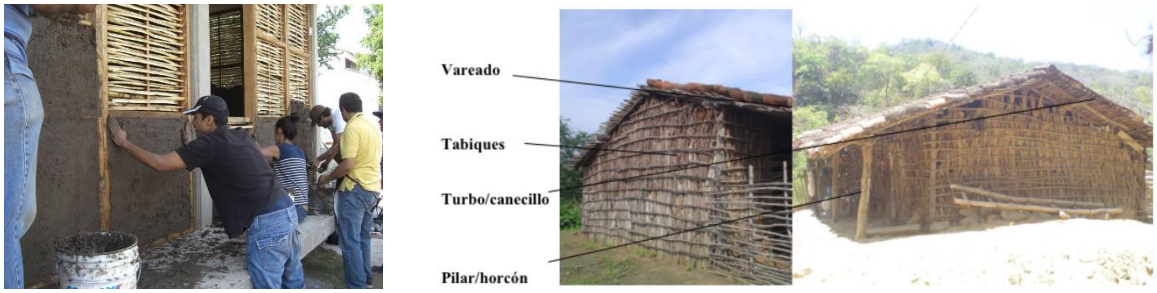

(a) (b)

Figure 2.8 Non-engineered TFM systems: b*ahareque,* Colombia (a), v*areque,* Ecuador (b) (Sánchez et al. 2006).

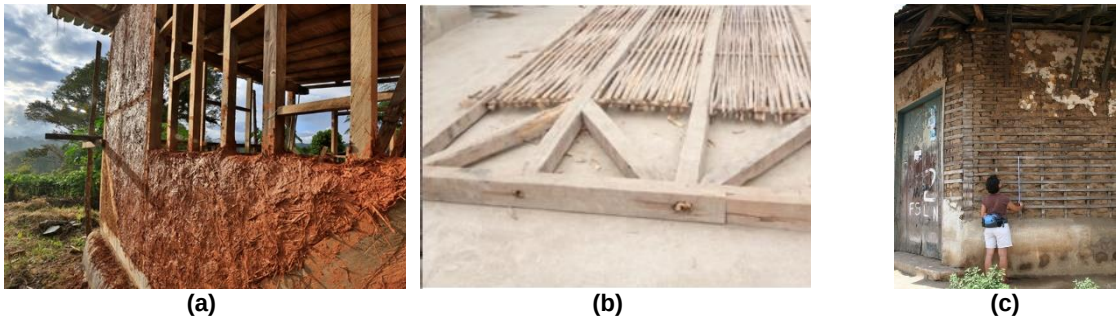

(a) (b) (c)

Figure 2.9 Non-engineered TFM systems: p*ajareque* in Honduras (a), q*uincha* in Perù (b), photo E. Vicente, *taquezal* in Nicaragua (c) (Quinn 2017); (Holliday et al. 2011).

(a) **(b)**

Figure 2.10 House in Miyanmar (a) and China (b) after the earthquake in 2016, August 24th (courtesy of dr. Matsutaro Seki) and the Lushan earthquake in 2013, respectively (Qu et al. 2015).

2.1.2 Engineered systems

The engineered systems, developed in few countries such as Portugal, Italy and Greece (Lefkas island) were based on design recommendations provided by the corresponding governments that lead the reconstruction process after two large earthquakes with catastrophic consequences. Since the construction materials, techniques and knowledge were diverse, the arrangement of timber elements, infill but also the structural role of masonry vary between the two systems.

The Portuguese "*gaiola pombalina*" can be defined as a half-timber structure with masonry infill. The system was not actually innovative since it was already used in existing buildings, although in a simplified way (Mascarenhas 2009). However, after the Great Lisbon earthquake in 1755, it was improved by the engineers of the government and applied systematically to the building as a whole to achieve a box-like behavior. Buildings should have been built with *Pombalino* system during the reconstruction process of Lisbon, thus the provided guidelines can be considered the first technical regulation on seismic design (Poletti and Vasconcelos 2015). Typical buildings can have up to five storeys with the ground floor made of stone masonry walls and columns supporting arches and / or masonry vaults, while the superstructure shows walls with "*gaiola*" system. The timber structure consists of vertical and horizontal elements with diagonal bracings to make the panel stiffer. Wooden elements are made of softwood (pinewood), but hardwood (oak) can be found in windows frames and in humid environment. The infill consists of small stones bonded with lime mortar or brick masonry, which not only makes the panel stiffer, but also increases the energy dissipation during cyclic loading. However, the detachment of the masonry infill is not prevented during an earthquake due to low adhesion between the timber frame and infill. Sometimes, timber-framed panels present an external layer of wooden strips covered by plaster to make the structure lighter and more flexible but this type of infill was observed only for internal walls (Mascarenhas 2009). TFM panels are connected to timber joists at floor level and to trusses and rafters at roof level to increase the overall seismic performance by ensuring proper constraints.

The Italian engineered TFM system spread across the south of peninsula and Sicily during the reconstruction process after the catastrophic earthquake in 1783, although this system was already present in the area and its good seismic resistance led the engineers to adopt such structures for the reconstruction process, similarly to what happened in Lisbon. Borbone government enacted one of the first European seismic codes (*Istruzioni per gli Ingegneri commissionati nella Calabria Ulteriore*) which provided guidelines based on the advanced criteria of seismic engineering of that period (Ruggieri 2016). One configuration of a structure that followed the seismic guidelines is called "*casa Baraccata*", and is composed of masonry walls reinforced with internal and external timber frames. These frames are connected by transversal elements, especially at the corners, which allowed to achieve the confinement of masonry in each direction. Floors and roofs with truss configurations are made of timber as well, with each joist and truss tie-beam linked to the inner skeleton to improve the box-like behavior and avoid overturning mechanisms. This behavior can be approached if the following requirements are fulfilled such as monolithic walls, well-connected structural members and regularity in plan and elevation. Despite other TFM structures, "*casa Baraccata*" was still dependant on the masonry structure as it played the main role under static loads due to having higher elasticity modulus and cross-sectional dimensions than timber. On the other hand, when an earthquake occurred, the timber frames provided most of the seismic capacity due to higher tensile strengths and flexibility (Ruggieri 2016).

2.2 Experimental Studies on the Cyclic Behavior of Timber-framed Masonry Walls

Timber-framed masonry walls show a good behavior under cyclic and dynamic loads which has been investigated by some research programs in recent years. Although the scientific community has increased its research on this issue, experimental tests are still limited since TFM walls may have different geometries and cross-sections, their infill can vary from brick masonry to wattle and daub as well as timber members can be made of different species. Thus, the seismic assessment of these structures was mainly qualitative with several reports that proved a good seismic capacity based on damage observation after severe earthquakes (Gülkan and Langenbach 2004). TFM structural behavior depends on three materials with different mechanical properties thus its seismic capacity is difficult to be predicted by numerical analysis. Moreover, their construction process plays an important role for their seismic capacity since the vast majority of TFM structures were built without following any standard code or recommendation. In the present section, some experimental test on TFM walls are presented as well as a brief discussion about the outcomes.

The first experimental tests on *Pombalino* walls were performed by (Santos 1997) in LNEC. These walls were taken out from an existing structure and tested under static cyclic loads with no vertical load, Figure 2.11a. Their hysteretic behavior shows high ductility and good energy dissipation capacity, Figure 2.12b. However, the base of the wall was embedded into a RC beam, which is not consistent with reality.

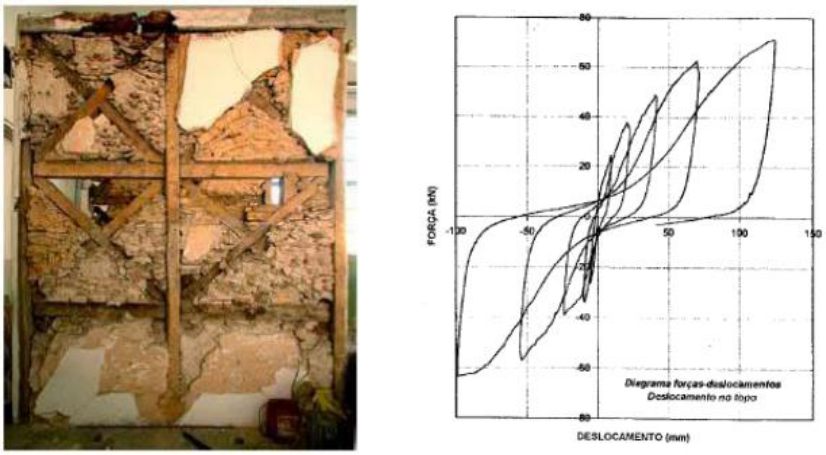

(a) **(b)**

Figure 2.11 *Pombalino* wall (a) and its hysteretic behavior (b) (Santos 1997).

(Meireles et al. 2012) tested timber-framed "*frontal*" walls subjected to in-plane cyclic loading and obtained comparable results to the previous study. Frame geometry, member cross-section, connections and masonry infill simulated those observed in existing structures, Figure 2.12. The timber elements, connected by nails, were made of softwood (*Pinus pinaster*) even though timber species that can be found in *Pombalino* structures can vary from hardwood to softwood. In this case, a vertical load of 30 kN/m was applied to the upper beam which can be representative of a wall located on the first floor in a four storey building. CUREE testing program was chosen to study the in-plane response of "*frontal*" wall which resulted highly ductile. Figure 2.13a ad b show the non-linear hysteretic curves with pinching behavior related to strength degradation and large loops representing the dissipated energy (Meireles et al. 2012).

Figure 2.12 Pombalino "frontal" wall (Meireles et al. 2012).

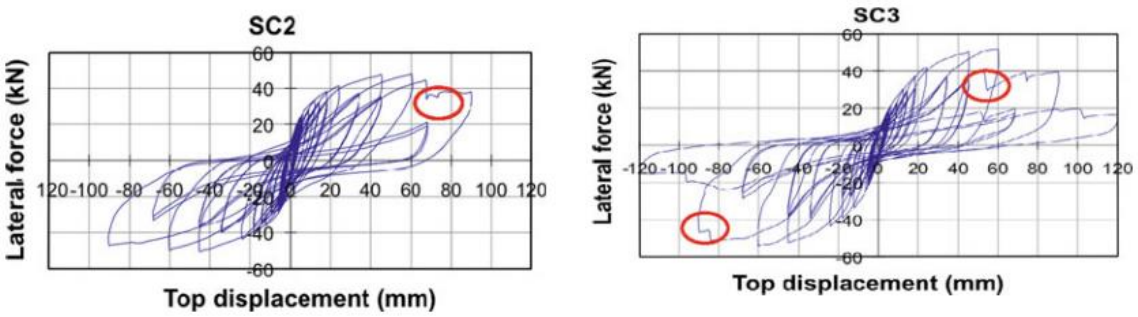

Figure 2.13 Hysteretic behavior of *Pombalino* "frontal" wall (Meireles et al. 2012).

Other in-plane static cyclic tests on *Pombalino* structures were performed by (Gonçalves et al. 2012) and (Poletti and Vasconcelos 2014). Both programs were aimed at obtaining the hysteretic behavior of "*frontal*" walls with and without infill to understand its contribution for the seismic capacity. In the experimental work by (Gonçalves et al. 2012), two types of specimen were tested: timber-framed (TF) wall and timber-framed masonry (TFM) wall, Figure 2.14a and b. Stone pine was used for timber members that are arranged in the same configuration of the following experimental program by (Poletti and Vasconcelos 2014) and have same cross-sections even though the global dimensions are slightly different. The connections are cross-halved type fastened with nails whose dimensions and performance can vary from those found in existing structures. Moreover, the mechanical properties of masonry infill were higher than the traditional ones since cement was added to lime mortar to ensure a faster curing. Before applying the cyclic loading, a vertical load of 30 kN/m was applied to the masonry wall to simulate the typical weight of the upper structures supported by it. Regarding the test setup and its configuration, the loading protocol was CUREE for ordinary ground motion to compare the results with the already described tests. The hysteretic behavior showed again non-linear response with high ductility, Figure 2.15. As expected, the initial stiffness of TFM walls is higher than TF walls since the presence of infill make the connections stiffer. Moreover, it prevents any buckling mechanism of the bracings and, at the same time, increases the dissipated energy resulting in higher damping effect. This is due to the friction at the interfaces between timber frame and masonry infill and at masonry joints.

(a) **(b)**

Figure 2.14 Tested walls: timber-framed wall (a), timber-framed masonry wall (b) (Gonçalves et al. 2012).

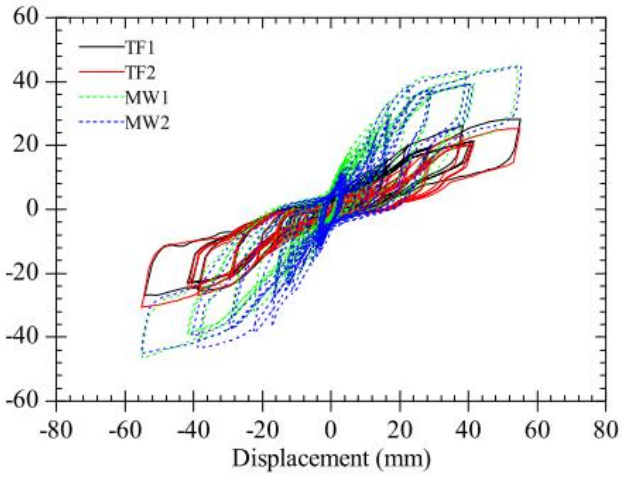

Figure 2.15 Hysteretic behavior of timber-framed walls without (TF) and with masonry (MW) infill (Gonçalves et al. 2012).

The experimental campaign by Poletti *et al*. (2014) was performed to timber-framed walls without infill, with brick masonry infill and lath and plaster to study how the response changes depending on the type of infill, Figure 2.16a, b and c. Timber species was the same of the previous test, *Pinus pinaster*, as well as nailed cross-halved connections. Regarding the frame geometry, walls have the same configuration of those tested by Gonçalves et al. (2012), but present diagonal bracings and horizontal members with different cross-sections. In this case, the dimensions and cell size were determined according to those found in literature to get results more compatible with existing structures (Mascarenhas 2009). Moreover, the influence of vertical load on the in-plane response was studied since the original weight of traditional structures may have been modified after restoration processes. This is the reason why two different vertical loads, 25 kN and 50 kN per post, were considered representative of the dead and live loads supported by the wall. The testing procedure based on protocol ISO DIS 21581 (2010) was chosen to obtain a better approximation of the highly non-linear response. Figure 2.17a and b show the force-displacement curves related to the wall specimens with brick masonry infill per each vertical load, UIW25 and UIW50 respectively.

(a) **(b)** **(c)**

Figure 2.16 Timber-framed walls without infill (a), with brick masonry infill (b), lath and plaster (c) (Poletti and Vasconcelos 2014).

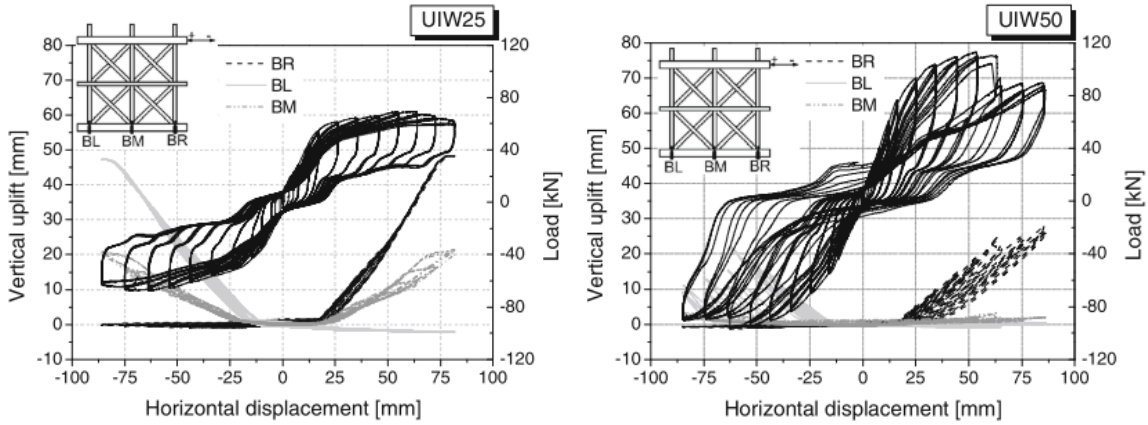

Figure 2.17 Hysteretic behavior of TFM walls with different vertical loads: 25 kN/post (a), 50kN/post (b) (Poletti and Vasconcelos 2014).

It is worth to stress that the presence of infill influences the structural response of "*frontal*" walls since the specimens with infill showed a predominant flexural or mixed shear/flexural behavior instead of a straightforward shear behavior without it. Vertical precompression affects the resisting mechanism as well. The higher the vertical load, the more evident was the flexural/shear behavior, but a flexural/rocking mechanism was also observed with the lower load (25 kN). Moreover, higher vertical loads result in higher values of seismic parameters such as ductility and energy dissipation, but at the same time increases damages for infill walls. Regarding timber-framed wall without infill, damages were mainly located at the central connection and they were not influenced by the vertical load. TF walls showed lower load capacity, stiffness and ductility compared to TFM walls as well as higher damages due to shear deformation at the same lateral drifts. The presence of infill can be considered as a strengthening strategy that reduces damage progression by confining timber joints and limiting deformations (Poletti and Vasconcelos 2014).

Experimental tests on Romanian timber-framed structures were carried out as well. Different infill and arrangement of timber members such as diagonal bracings were studied by Dutu *et al.* (2015) and the results are discussed in detail in Section 3.

Other studies were carried out on Turkish timber-framed walls varying the type of infill (Aktaş et al. 2014), Haitian TFM walls by Vieux-Champagne *et al*. (2014) and *baraccato* system (Ruggieri 2015) and *quincha* system (Torrealva and Vicente 2012).

The experimental campaign about traditional Ottoman houses was aimed at studying the influence of frame geometry, timber species, infill and cladding. The presence of infill or cladding enhances the stiffness and lateral load strength of the timber-framed walls but at the same time increases the mass. It is worth to stress that wood species does not play a significant role in the experimental tests since the failure occurs at the connection. The measured response was again highly ductile and good energy dissipation capacity was observed (Aktaş et al. 2014).

Regarding the *Baraccato* construction system, a full-scale specimen of Mileto masonry reinforced with timber elements was tested under quasi-static cyclic loading. A second specimen without the infill was also built and analyzed to better understand the contribution of masonry infill. In this case, it plays an important role due to the lack of diagonal bracings, thus the in-plane stiffness depends mostly on masonry characteristics. Wood species was Calabrian chestnut and all the connections are half-lap type nailed by pyramidal pinsFigure 2.18a and b show the frame geometry and wall configuration that presents also a centered opening. A uniformly distributed vertical load of 18.7 kN/m was considered as representative of the self-weight of upper structure of Mileto building. Moreover, the standard protocol provided by UNI EN 12512:2003 was adopted as cyclic loading procedure (Ruggieri 2015). Figure 2.19 shows the load-displacement curve (grey) and envelope (blue with yellow dots) of the tested wall.

(a) **(b)**

Figure 2.18 Timber frame (a) and tested wall (b) (Ruggieri 2015).

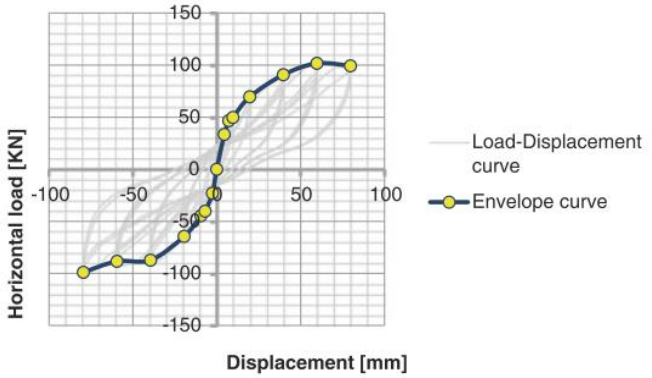

Figure 2.19 Load-displacement and envelope curve (Ruggieri 2015).

The TFM panel shows linear elastic behavior during the first cycles where the flexibility of wooden members allows the masonry infill to get back to the initial position. At the same time, timber elements are confined by masonry that increases in-plane stiffness and reduces deformability of the frame. When larger displacements are imposed, inelastic deformation was observed with cracks along mortar joints up to slip and expulsion of stones. Moreover, energy dissipation increased due to friction at the interface between timber frame and masonry infill and at masonry joints. The behavior of TFM panel was mainly flexural with a limited rocking mechanism and post uplift (30 mm max), while TF specimen showed a shear behavior with high deformations, but neither rocking nor significant uplift (2.9 mm). It is worth to

stress that a high damping ratio was measured for each displacement (6-7%) and the response was highly ductile (maximum value 7.6).

2.3 Numerical Modelling Strategies

The available models for timber-framed masonry structures can vary in their level of complexity and sensitivity. They can predict the structural behavior of mixed panels since they are calibrated based on experimental tests. If the panels are assembled and their connections are taken into account as well as the connections between wall-to-floor, wall-to-roof, it is possible to analyze the building as a whole. The modeling strategy should be chosen according to the building's size and goal of the analysis since more detailed and complex models require higher computational efforts and experience by the user.

2.3.1 Simplified Equivalent Frame Model

A simplified model was proposed by Kouris and Kappos (2012) to assess the non-linear response of full-scale TFM buildings. In this model, non-linearities are lumped to point hinges while timber posts and lintels are linear-elastic beam elements. Diagonal bracings are modelled with link (truss) elements pinned at their ends; thus, they can transmit only axial forces. Moreover, they have non-linear axial springs whose constitutive law was derived from a bi-linearized pushover curve of the assessed panels. This curve results from the pushover analysis of a detailed model in ANSYS, calibrated with the experimental tests, where vertical loads in the timber posts are estimated by a preliminary elastic analysis (Kouris and Kappos 2012). The residual branch of the constitutive law is defined assuming reasonable ratios for residual strength and maximum strain at maximum capacity. In the elastic range, the sliding of the bracings is also taken into account since it influences the initial stiffness of the panel, thus a correction factor is applied to the beam element stiffnesses (Kouris and Kappos 2012).

After performing a non-linear static analysis, the inelastic behavior of a full-scale TFM building can be obtained and its pushover curve results in a bi-linear curve. However, a more detailed study on the connections is required since they affect the local and global behavior of the structures. The simplified approach was validated comparing its results with cyclic load tests on mixed panels and it seems appropriate for seismic vulnerability assessment of timber-framed masonry buildings in the island of Lefkas, Greece (Kouris and Kappos 2012).

2.3.2 Ceccotti and Sandhaas Macro-models

The macro-model proposed by Ceccotti and Sandhaas (2010) can be used to represent a timber-framed masonry panel, but also an entire wall and a building if the connections between single panels, wall-to-floor, wall-to-roof and the flexibility of horizontal diaphragms are taken into account, respectively. This macro-model consists of masses lumped at nodes, rigid members for the timber frame and rotational springs, Figure 2.20. The rotational springs are calibrated with cyclic test results and they represent the panel behavior under lateral loading. The calibration takes into account also friction effects and movements such as uplifting and translation. It is worth to stress that the panel deforms only in shear

because of the initial assumptions. Moreover, equivalent viscous damping should be defined to perform non-linear dynamic analysis since it influences the mechanical behavior of the walls.

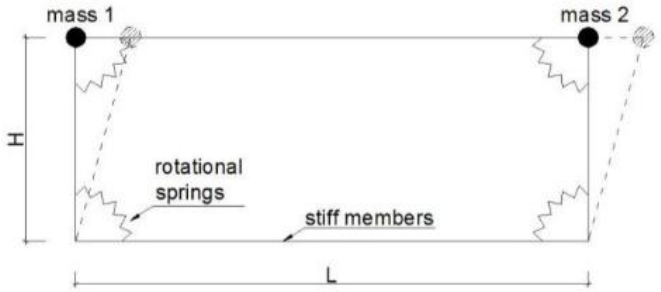

Figure 2.20 Timber frame panel (Ceccotti and Sandhaas 2010).

This approach is intended to model constructions that show a seismic behavior governed by horizontal displacements with negligible uplift. However, several experimental tests demonstrate that vertical uplift is experienced by timber elements since the flexural rocking mechanism is observed due to the presence of masonry infill.

2.3.3 Hysteretic Models of Sheathed Shear Walls

Folz and Filiatrault (2004) proposed a simplified numerical model for the structural analysis of sheathed shear walls. This model can predict the load-displacement response and energy dissipation of sheathed panels under quasi-static cyclic loading (Folz and Filiatrault 2004). The framing members are modelled as rigid elements since their in-plane bending deformation does not influence significantly the wall response (Gupta and Kuo 1985). They are linked through pinned connections at their ends thus the in-plane stiffness is provided only by the sheathed panels that have linear elastic properties. These panels are linked to the frame through non-linear dowel-type connectors with a hysteretic model showing pinched behavior with strength and stiffness degradation under cyclic loading, Figure 2.21. The load-displacement relationship depends on six parameters that should be determined by fitting the model to the experimental tests (Dolan and Madsen 1992).

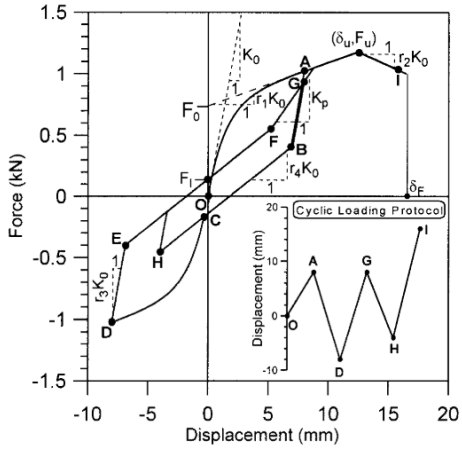

Figure 2.21 Force-displacement response of sheathing-to-framing connector under monotonic and cyclic loading (Folz and Filiatrault 2004).

A similar simplified approach can be applied also to timber-framed buildings. This model aims to predict the seismic behavior of TF structures by characterizing their dynamic properties and to obtain quasi-static pushover curves (Folz and Filiatrault 2004). The three-dimensional structure consists of rigid horizontal diaphragms and non-linear shear walls with negligible out-of-plane stiffness. However, an equivalent two-dimensional planar model is used by assuming the shear walls as zero-height non-linear spring elements linked to the rigid floor and the foundation, Figure 2.22.

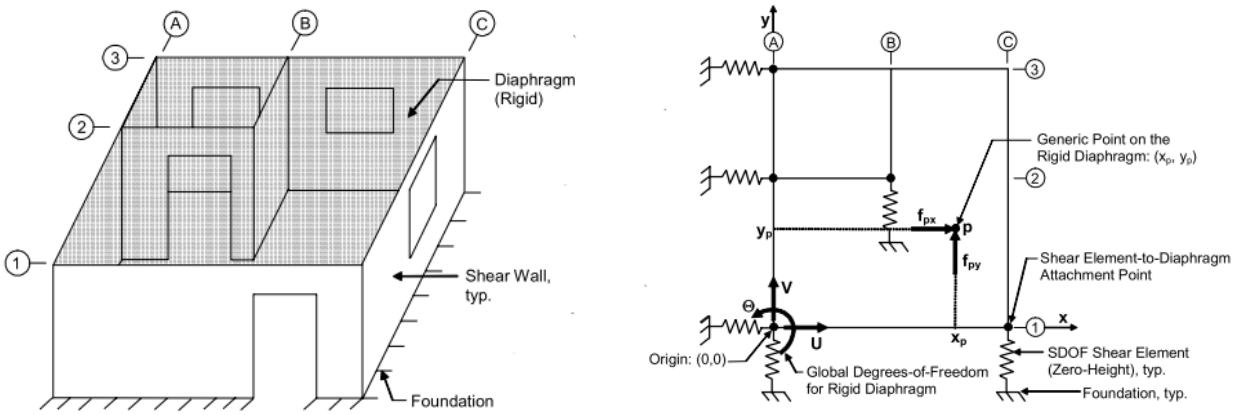

(a) **(b)**

Figure 2.22 One-storey timber frame structure (a) and its schematization (Folz and Filiatrault 2004).

The hysteretic behavior of each SDOF spring can be obtained by calibrating the previous hysteretic model to the global cyclic response of sheathed shear walls. Figure 2.23 shows the force-displacement response of shear wall subjected to monotonic and cyclic loading. Their hysteretic behavior is qualitatively similar to the one of dowel-type sheathing-to-framing connectors of Figure 2.21 since it shows pinched behavior with strength and stiffness degradation under cyclic loading.

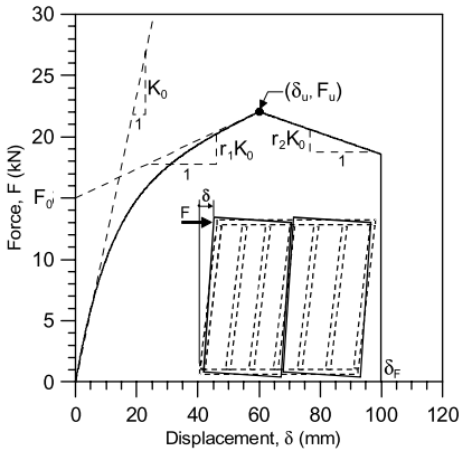

Figure 2.23 Force-displacement response of shear wall under monotonic and cyclic loading (Folz and Filiatrault 2004).

The structural response can be characterized by three DOF per floor (two translations and one rotation) in the simplified building model, Figure 2.22. It is worth to stress that planar model misses both overturning response and flexural deformation, but timber-framed structural behavior is not influenced

significantly by these limitations since buildings are low-rise and shear deformation is predominant (Folz and Filiatrault 2004)The computer program *SAWS* (Seismic Analysis of Woodframe Structures) incorporates the simplified model that requires few input data and has shown a good approximation with a full-scale two-storey wood frame structure in terms of dynamic properties and seismic behavior.

2.3.4 Detailed Non-linear Finite Element Model

The most complex and detailed model is intended for analysis of a single panel due to the high computational effort and amount of input parameters. The planar non-linear finite element model proposed by Kouris and Kappos (2012) considers orthotropic behavior for timber members and their interface is modelled with Mohr-Coulomb yield surface with no cohesion.

Wood is defined as an orthotropic material with a trilinear constitutive law under monotonic axial loading with a stiffness reduction (10% E_{ela}) after reaching 40% of the maximum strength and a horizontal branch at the maximum strength. Thus, after the initial yield, isotropic work-hardening can be observed and since a trilinear behavior is applied, an isotropic expansion of the yielding area can be achieved. It is based on the Hill's yield criterion that considers anisotropy in ductile materials.

In order to define the constitutive laws, wood specimens should be tested to estimate their mechanical properties. However, destructive tests are not allowed in historical buildings and even if they can be performed, the results can be affected by the state of conservation varying from element to element. Therefore, the flexural capacity is defined as the main parameter to assess the other properties with relationships of the EN338 standard. The finite elements are four-node plane-stress ones with two degrees of freedom per node. In addition, connections between timber members play an important role in ensuring strength and stability of the whole panel. They are modelled with contact elements that can transfer only compressive loads and shear stress up to an upper bond when sliding occurs. Their behavior is highly non-linear and the contact area varies with the external loading as well as the boundary conditions at each step. The constitutive law for the contact area is Mohr-Coulomb yield criterion considering a friction coefficient equal to 0.5 and neglecting cohesion (Kouris and Kappos 2012). Since the ultimate resistance to seismic loading is not significantly influenced by the masonry infill, its contribution is neglected, but its weight is considered indirectly (Kouris and Kappos 2012). The validation of the proposed model is demonstrated by the comparison between the analytical and the experimental results which shows a good approximation of the wall behavior under horizontal loading (Kouris and Kappos 2012).

After the pushover analysis, the softening branch of the wall response can be obtained and the whole curve can provide the constitutive law for simplified model. Thus, one of its aims is to calibrate the simplified approaches to analyze the entire buildings or if a detailed displacement-focused analysis is required.

2.4 Seismic Characterization

In this section the seismic characterization of Romania is discussed to define the seismic hazard that is likely to affect the timber-framed masonry structures under investigation. Since vernacular architectures were built without any design code, a seismic vulnerability assessment is required to predict the potential scenarios in case of earthquakes. This safety assessment should be performed taking into account not only the macroseismic intensities, but also the earthquake characteristics related to the studied area.

Romania, as the surrounding countries (Bulgaria, Serbia) can be classified as a country with high seismic risk as well. The active tectonic processes are lumped at the pointed arch of the Carpathians, Vrancea region. This area results from subduction processes and presents an unusual strain rate per volume at subcrustal depths (Pavel et al. 2016). A continental collision characterizes the general tectonic frame: pre-alpine platforms against alpine orogen units involving western margin of the East European Platform (Moldavian Platform), Scythian and Moesian Platforms, Eastern, Southern and Western (Apuseni Mountains) Carpathians, North Dobrogean orogeny, Transylvanian Depression and Eastern margin of the Pannonian Depression. The collision yields to rapid deformations in the mantle beneath Vrancea which propagate toward extra-Carpathians area where strike-slip and normal faults are found along with a SE-NW oriented system of major crustal fractures (Pavel et al. 2016). The moderate seismicity in front of Carpathians Arc is due to the overlapping between the platforms and external units of the Carpathian Orogen, which results in the sinking of their basement and fracturing the crust along alignments parallel to Carpathian Arc (Pavel et al. 2016). Seismic activity is recorded along the Southern Carpathians up to the Danube River as well. Small-to-moderate crustal earthquakes are caused by the strike-slip deformations between the Moesian platform and Carpathians Orogen. In this case, a system of NE-SW oriented faults crosses the Danubian region, which results from the clockwise rotation of the upper Carpathians units with respect to Moesia. On the contrary the back-Arc region, Transylvanian Depression) has a lower seismicity compared to the fore-Arc. Indeed, the seismic activity varies greatly from the back-Arc to the fore-Arc due to the different attenuation phenomenon of the seismic waves between the two regions.

Considering the energy and number of events, there are two main seismic areas in its territory: Vrancea and Banat region. However, the most important one is located in the fore-Arc of Carpathians, which is highlighted with red-to-purple color with an expected PGA of 0.4 g. Figure 2.24 and Figure 2.25 show the seismic zonation according to MSK scale and expected PGA from Romanian Indicativ P 100-1/2013, respectively.

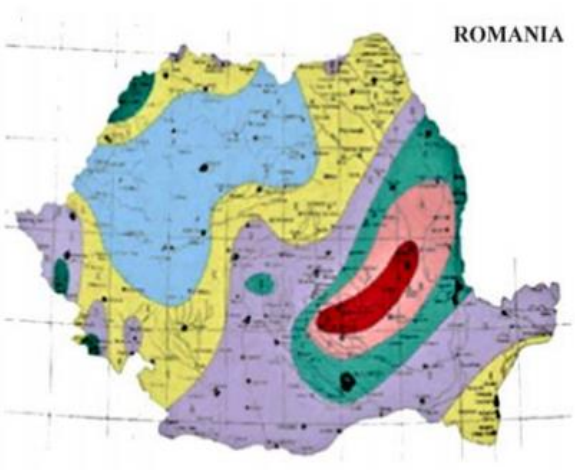

Figure 2.24 Seismic zonation map: MSK scale 1992 (Narita et al. 2016).

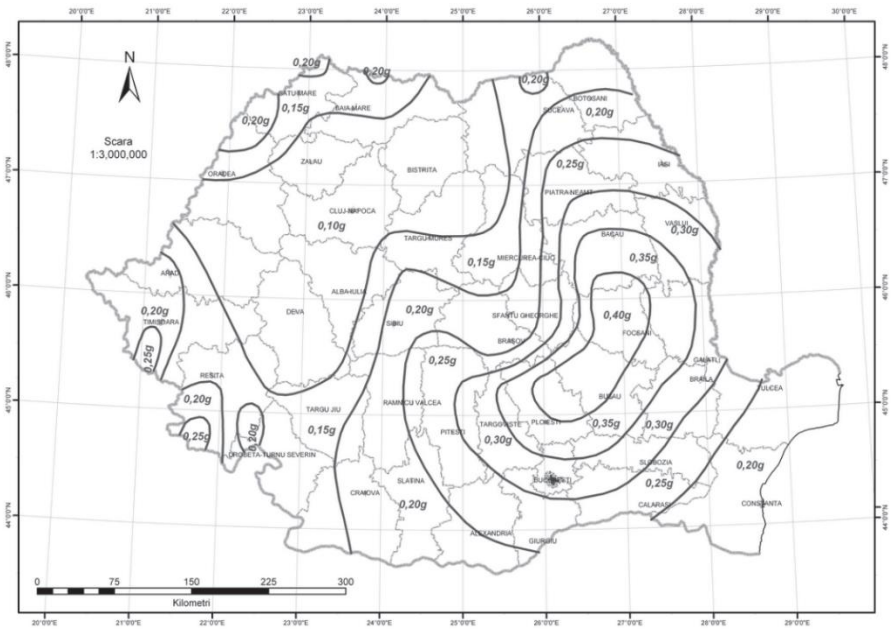

Figure 2.25 Expected PGA 2013 (*Indicativ P 100-1/2013* n.d.).

Figure 2.26 shows the epicenters of the main earthquakes with the related magnitude recorded in ROMPLUS seismic catalogue. It has 6322 events that occurred in Romania or nearby countries from 984 to 2015. They are also organized in three histograms showing the earthquakes classified by magnitude, focal depth and year of occurrence, Figure 2.27a, b and c. The fore-Arc region presents a large concentration of seismic events ranging from low-to-high magnitude and it was affected also by earthquakes occurred in Danubian region, Bulgaria. Banat region shows a lower concentration of seismic activity with moderate magnitude, but again it is influenced by the western seismic area of Serbia.

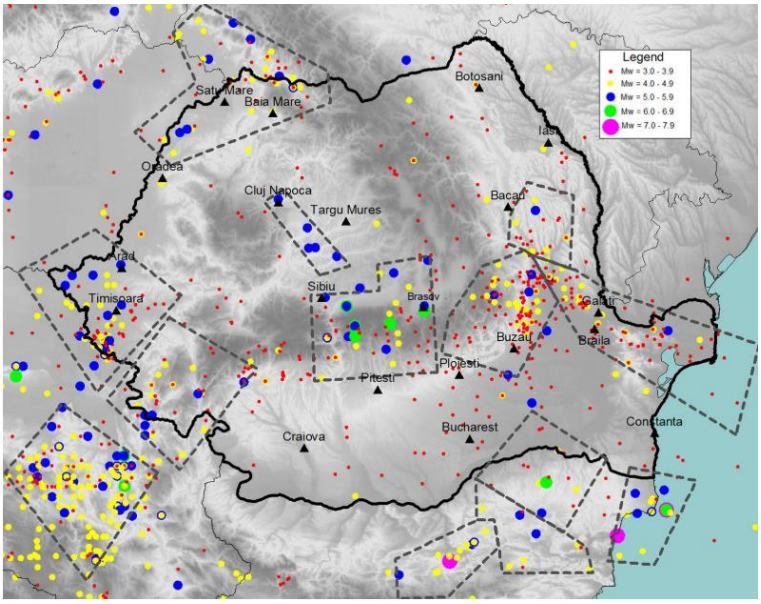

Figure 2.26 Epicentres of crustal earthquakes from ROMPLUS seismic catalogue (Pavel et al. 2016).

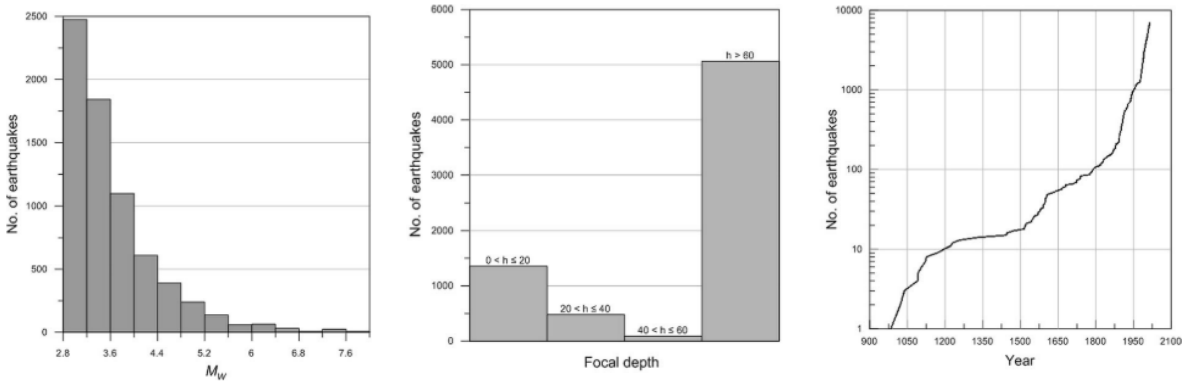

(a) **(b)** **(c)**

Figure 2.27 Histograms of magnitude (a), focal depth (b) and the evolution (c) of the total number of earthquakes with time in the ROMPLUS catalogue (Pavel et al. 2016).

Vrancea area, located at the curvature of the Carpathian Mountains in the eastern part of the country, is the most important seismic region in Romania. It is far from any active plate boundaries, but its seismic activity is also influenced by nearby regions (Ismail-Zadeh et al. 2012). Figure 2.28 shows the intermediate-depth earthquakes ranging from 90 to 150 km according to the ROMPLUS seismic catalogue. Vrancea seismic source has produced nine earthquakes with a M_w higher than 7 during the last two centuries (Pavel et al. 2016). In particular, in the twentieth century, this region was affected by several seismic events occurred in October 6, 1908 (M_w = 7.1, h = 125 km); November 10, 1940 (M_w = 7.7, h = 150 km); March 4, 1977 (M_w = 7.4, h = 94 km); August 30, 1986 (M_w = 7.1, h = 131 km). Sometimes aftershocks are characterized by similar magnitude of the main shock since there are many cases of doublet and triplet seismic events with comparable magnitude (triplet earthquakes in 1893 and 1945, doublet ones in 1894, 1896 and 1990).

The last crustal earthquake occurred in November 2014 with a magnitude M_w of 5.6 and focal depth 40 km. It was characterized by a peak ground acceleration (PGA) of 0.26 g, one of the largest ever recorded in Romania. However, the most severe crustal seismic events were those in Bulgaria in 1901 (Shabla seismic region, $M_w \cong 7.2$) and 1913 (Gorna seismic region, $M_w \cong 7.0$); the Fagaras earthquake in 1916 ($M_w \cong 6.4 \div 6.5$) as well as Banat and Danubius earthquakes in 1991 ($M_w \geq 5.5$).

Regarding earthquake characteristics, Vrancea seismic moment release is similar to that of Southern California (Wenzel et al. 2001). The seismic events have long duration and a large number of cycles that cause severe inelastic deformations (Gioncu and Marius 2009). The maximum expected PGA is 0.4 g, as previously mentioned. It is worth to stress that the TFM structures under investigation are mainly located in this area, for further details see Section 0.

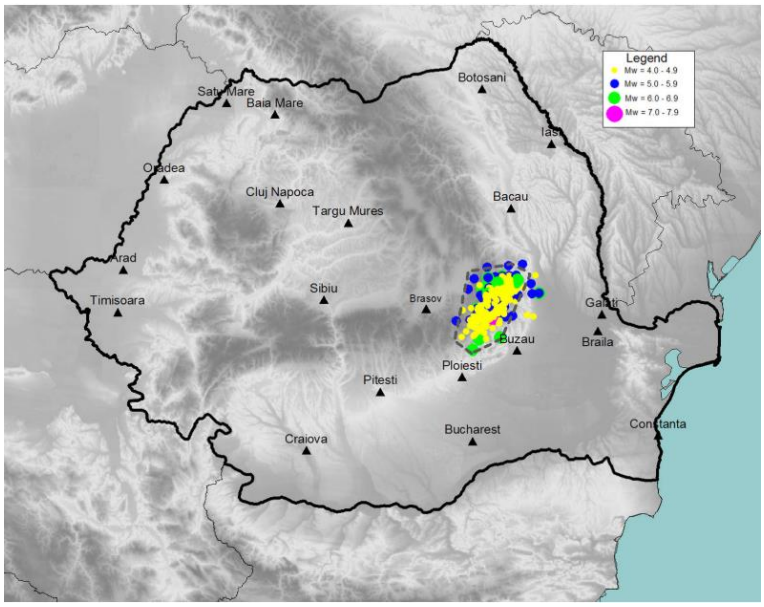

Figure 2.28 Epicentres of intermediate-depth earthquakes considered in the analysis from the Vrancea subcrustal seismic source according to the ROMPLUS seismic catalogue (Pavel et al. 2016).

Banat district, located in the western part of Romania, is affected by shallow earthquakes of crustal type (Mosoarca et al. 2014). They are characterized by small depth of the seismic source (between 5 and 15 km) and by reduced surface of the epicenter area. Moreover, earthquakes can have a PGA ranging between 0.1 g to 0.25 g with similar values in terms of vertical component. Recorded accelerograms show powerful pulse actions during the first cycles and reduced intensity for the following cycles (Narita et al. 2016). They affect structures with short period of vibration below 0.2 sec to 0.3 sec. The main shock is usually preceded by a small number of pre-shocks and followed by a large number of aftershocks. The seismic activity depends on faults with different orientations and depths. The largest earthquakes have seismic sources located at the intersection of seismic faults or close to geological faults of different ages (Mosoarca et al. 2014). Table 2.1 shows the most severe earthquakes occurred in this region with their epicenter, macro seismic intensity and year of occurrence.

Table 2.1 Zones with most important earthquakes, intensities and year of occurrance (Mosoarca et al. 2014).

Epicenter zone	Maximum recorded intensity	Year
Sanicolaul Mare	VII	1879
Barateaz	VII	1900
Periam – Varias	VII	1859
Jimbolia – Bulgarus	VII	1941
Carpinis	V	1889
Sanandrei – Hodoni	V	1950
Recas	V	1896; 1902
Timisoara (Mehala) Sanmihai	VII	1879
Sanmihai – Sacalaz	VI	1973
Sag – Parta	VII	1959
Rudna – Ciacova	V	1907
Liebling – Voiteg	VII-VIII	1991
Banloc – Ofsenita	VII-VIII	1915; 1991
Moldova Noua	VIII	1879

2.5 Building Stock Characterization

The investigation presented in this thesis focuses on the Romanian vernacular architecture. Its features result from a long-term process that is still ongoing and has boosted the local seismic culture especially after severe earthquakes. Since many people realized that traditional buildings did not show significant damages after seismic events, they started to rebuild as their ancestors did. However, there are no guidelines about traditional timber-framed masonry structures in the Romanian code and most of the builders have lost their technical background, thus more detailed studies on existing buildings are required as well as their safety assessment. The structural typology should be characterized and then analyzed to guide the restoration processes and provide guidelines for new TFM structures. Bearing in mind these aims, the building characterization of Romanian TFM buildings is presented in the following paragraphs explaining their geometrical configuration, materials and construction details.

The Romanian traditional architecture can be defined as a half-timber masonry structure, because the timber frame plays the main structural role under static loads and also when an earthquake occurs. The infill provides additional in-plane stiffness, but it is susceptible to out-of-plane collapse mechanisms. Residential buildings are generally one storey high although they may present one additional storey. In this latter case, the ground floor, made of stone brick masonry, has the storage rooms, while the upper level with half-timber structure has the living space. There are several structural configurations of the timber frame, therefore the dimensions and arrangement of wooden elements, infills, and / or tree species could have varied from structure to structure. Starting from the "*paianta*" structural typology,

some characteristics have been modified depending on location, availability of materials and construction techniques (Duțu et al. 2017). The "*paianta*" structure consists of a timber frame with bracings and brick masonry infill. Floors and roofs with truss configurations are made of timber as well, with each joist and truss tie-beam, linked to the timber frame to improve the box-like behavior and avoid overturning mechanisms, Figure 2.29. In the drawing, wooden piles support the structures, but deep foundations are not required due to the light loads that have to be transmitted to the soil and such foundations were not frequently observed during the field survey. In general, they consist of a brick masonry wall-footing with a lower beam made of hardwood where vertical posts are driven into, Figure 2.32. Softwood such as pinewood is applied in the superstructure while hardwood such as oak, locust, walnut is used for the bottom stringers and piles.

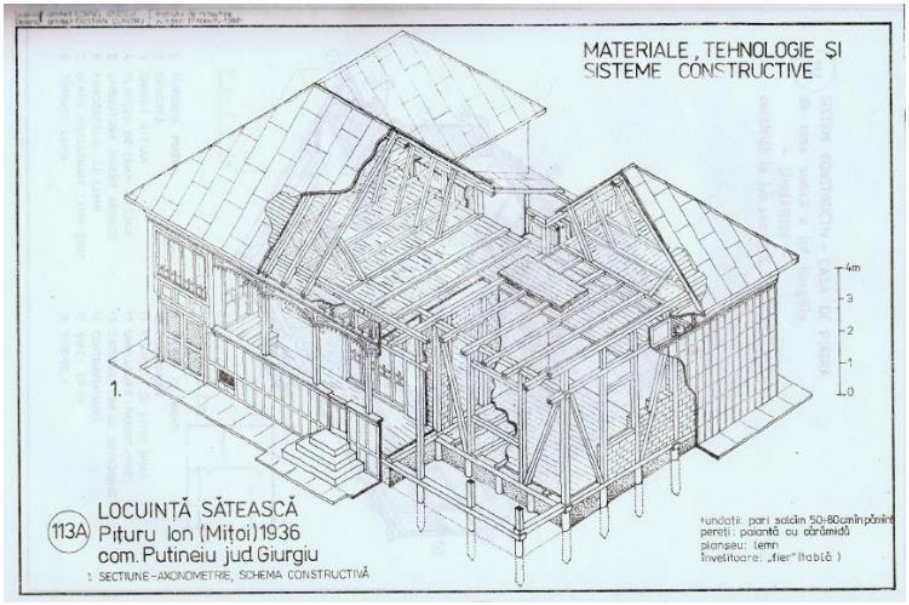

Figure 2.29 The paianta residential architecture (Duțu et al. 2017).

A field investigation was performed across the fore-Arc seismic area, highlighted in blue in Figure 2.30. After the evaluation of 129 buildings, several types of traditional houses were found in the districts of Vrancea, Buzău, Dambovita, Prahova, Argeș and Valcea (Duțu et al. 2017). They have slightly different characteristics from the one recognized in a previous investigation (Institutul Central de Cercetare, Proiectare si Directivare in Constructii, Studii de arhitectura traditionala in vederea conservarii si valorificarii prin tipizare: Locuinta sateasca din Romania, 1989).

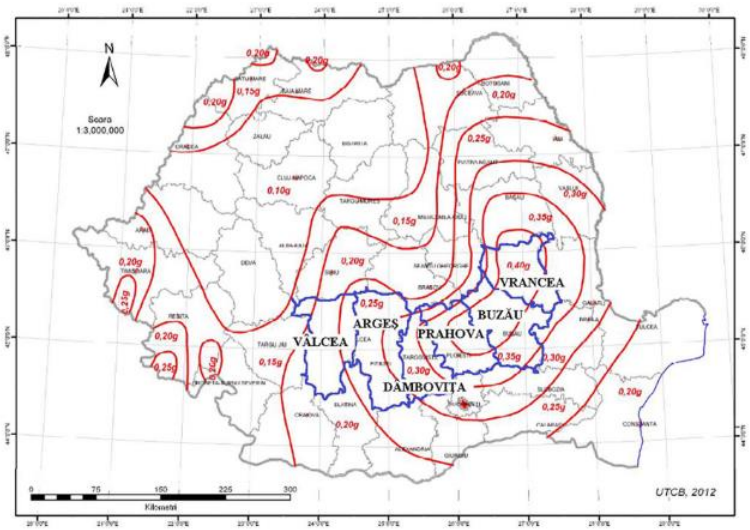

Figure 2.30 Investigated counties against Romanian zonation of PGA according to national seismic code P100-1/2013 (Dutu et al. 2018b).

Five types of TFM houses were identified depending on the their features and infill such as: (Type 1) timber skeleton with brick masonry infill (Figure 2.31a), (Type 2) timber skeleton and strips applied at 45° with clay plaster (Figure 2.31b), (Type 3) timber skeleton and wattle and daub "*gradele*" (Figure 2.31c), (Type 4) timber and earth with straw infill structure (Figure 2.31d) and (Type 5) timber skeleton and AAC (autoclaved aerated concrete) masonry infill (Figure 2.31e).

(a)

(b)

(c)

(d)

(e)

Figure 2.31 Building classified as Type 1 (a), 2 (b), 3 (c), 4 (d), 5 (e) in Romania (Dima and Dutu 2016).

Type 1 is the most common (70%) and approaches the *paianta* typology even if there are some different construction details such as the type of foundations, the position of the bracings, masonry bond and a perimeter beam at the roof level.

Most of the buildings have stone foundations that consist of damp river rocks round or rectangular in shape laid up one over the others on the entire footprint of the structure, Figure 2.32 (Dutu et al. 2018b). As already mentioned, this foundation type was found in most of the building stock despite it was not drawn in Figure 2.29 representing *paianta* typology. The rocks can be processed on 2 or all sides, but they are generally non-processed. The foundations may be dry-stacked masonry, stacked masonry with clay mortar or just river sand that provides seismic energy dissipation (Dutu et al. 2018b). Over the stone platform, an inferior stringer, called “soles”, has the important role to distribute uniformly the load of the superstructure to the foundations. It can be processed on 4 or just 2 sides, but sometimes it consists of logs or half logs, peeled of bark, with cross-halved connections. These elements, made of hardwood, are connected at the corners or overlapped by cross-halving joints, Figure 2.32b. It is worth to stress that if the superstructure is well executed, but not properly connected to the foundations, it may slide as a whole box during an earthquake (Duțu et al. 2017).

(a)

(b)

Figure 2.32 Foundation example for a traditional house at the National Village Museum “Dimitrie Gusti (a) and half-lap joints between elements (b) (Dima and Dutu 2016).

The timber frame consists of posts and beams with a cross-section between 15x15 cm to 20x20 cm and 12x12 cm to 20x20 cm, respectively (Dima and Dutu 2016). The bracings range from 10x10 cm to 15x15 cm and their position does not match exactly the diagonal of the frame but they are connected to the post, not at the frame corner, Figure 2.33a. This may be due to construction: one hypothesis is that they may be just temporary supports of the post (Dutu et al. 2018a). Sometimes it was observed that the bracings are just connected to the lower beam because there is no column, Figure 2.33b. However, it is worth to stress that they are effective only in compression since they detach from the frame in tension due to the type of connections.

(a) **(b)**

Figure 2.33 Timber frame geometry of building in Ocnesti (a) and Vrancea (b), Romania (Dima and Dutu 2016).

The masonry infill is made of mud brick masonry stacked with mud mortar. It is obtained by mixing raw earth with sand and water even though the mix design varies from area to area depending on the type of soil and construction techniques. If the mortar includes a significant amount of clay, it will be more cohesive and harder, but it is likely to crack during the setting process, thus sand is required anyway. It should be noticed that the interaction between infill and timber frame is characterized by the lack of adherence, therefore out-of-plane mechanisms are not prevented (Dutu et al. 2018b). Moreover, the masonry infill bond varies along the height of the panel, Figure 2.34a and b. Units are placed horizontally up to the connection between post and bracing and then they are inclined to increase the friction in the upper part of the wall as well as the stiffness (Dutu et al. 2018b). Figure 2.34b shows a mixed perimeter beam above the upper stringer.

(a) (b)

Figure 2.34 Diagonal bricks below the upper beam in Ocnesti (a) and mixed perimeter beam (b) (Dutu et al. 2018b)~.

The floor above the foundation is made of wooden planks while the upper floors show timber beams with wooden planks, or wattle and daub, or sometimes reed, Figure 2.35a. An additional layer of mud can be found above the planks. Floors can be considered flexible diaphragms since the in-plane stiffness is provided by just one layer of planks nailed to the beams.

The roofing system is made of timber as well. In some cases, it is connected to the walls through a perimeter beam that ensure a proper bond since it is a mixed timber-masonry beam. The most common types are hip or gable roof with king post trusses with no struts, Figure 2.35b. The traditional roof covering consists of shingles or ceramic tiles. Since the wooden shingles are prone to biological attacks, most of them have been replaced by steel sheets (Dutu et al. 2018b).

(a) (b)

Figure 2.35 Detail of timber floor (a) and roofing system (b) (Dutu et al. 2018b).

The timber joints are mainly half-lap, cross-halved or tee-halved type between post and beams, but mortise and tenon type can be also found, Figure 2.36a and b. Sometimes the connections are also improved with nails to increase ductility and occasionally with steel clamps to increase their resistance and stiffness (Dutu et al. 2018b). Since they are not carefully executed, tolerances are quite large therefore many gaps can be seen.

(a) **(b)**

Figure 2.36 Cross-halved (a) and mortise and tenon (b) joints (Dutu et al. 2018b).

Type 2 was found in 15% of the building stock and it differs from the *paianta* typology because of the infill and the presence of wooden strips rotated at 45° and nailed to the frame, Figure 2.37. Although the internal timber structure is hidden by the external layer, the frame should consist of timber posts with mud infill and no diagonal bracings (Duțu et al. 2017).

Figure 2.37 Building classified as Type 2 in Romania (Dutu et al. 2018b).

Type 3 was observed in 15% of the evaluated buildings and its frame approaches the Type 2 in terms of structure, but has also smaller size posts in between. They are required to support the hazelnut branches that are braided and bonded with mud mortar, Figure 2.38. This system is similar to wattle and daub system (Duțu et al. 2017).

Figure 2.38 Building classified as Type 3, timber-framed with wattle and daub infill in Romania (Dutu et al. 2018b).

Type 4 was found just in 3 cases (2%) and it is a low-cost constructive system, Figure 2.39. In this case, many buildings have no foundations and the connections show gaps due to the cheap workforce employed in the construction. There are no nails or steel clamps to increase strength and stiffness of the timber joints (Dușu et al. 2017).

Figure 2.39 Building classified as Type 4, timber-framed with mud mortar infill in Romania (Dutu et al. 2018b)).

Type 5 shows new masonry infill with AAC blocks that provides good thermal insulation, but the timber frame is not properly designed as well as the position of the bracings. This construction system can be dangerous when an earthquake occurs due to the misunderstanding of the traditional architecture (Dușu et al. 2017). However, it was found in just 2 cases and it is not the objective of the thesis.

3 SUMMARY OF EXPERIMENTAL CAMPAIGN ON TFM WALLS

In the present section, the experimental tests on Romanian timber-framed masonry walls are described and their results are discussed. Even though the construction details vary from structure to structure, few wall typologies were identified after the *in situ* investigation described in Section 2.5 and eventually tested. Their main geometrical features, materials and constructive techniques were studied to make the wall specimens comparable with those observed.

3.1 Geometry

Four wall specimens were built by a non-specialized construction company to study their behavior when subjected to lateral forces, Figure 3.1 and Figure 3.2. During the field survey, an average height of 2.7 m was measured from foundation up to the upper beam, but wall dimensions were 3 x 2.4 m due to the maximum height allowed by the testing frame setup. The arrangement, dimensions and connections of the timber elements are the same except for the first (S1) and third (S3) specimen that have lower bracings and no diagonal elements, respectively. Specimens S1 and S2 have masonry infill with traditional mud bricks (rough dimensions of 24x11.5x6.3 cm) and earth (mud) mortar. These specimens differ in the arrangement of the bracings: S1 has bracings connected to the external timber posts, while S2 presents diagonal bracings linked to the upper timber joints. The third wall S3 is infilled with wattle and daub system covered by plaster made of mud and straw. Lastly, S4 specimen has horizontal rectangular wooden strips (cross-section 2.5x5 cm) nailed to the columns and plastered with mud and straw. The bottom timber joints are mortise and tenon type while the upper ones are half lap cross halving type, Figure 3.3. Moreover, all the bottom and upper connections are nailed as well as those linking the diagonal bracings to the columns through plain nails, 6x100 mm (Dutu et al. 2018a). Although the construction process was supervised, some imperfections such as gaps were observed at the joints, which may slightly affect the wall global response.

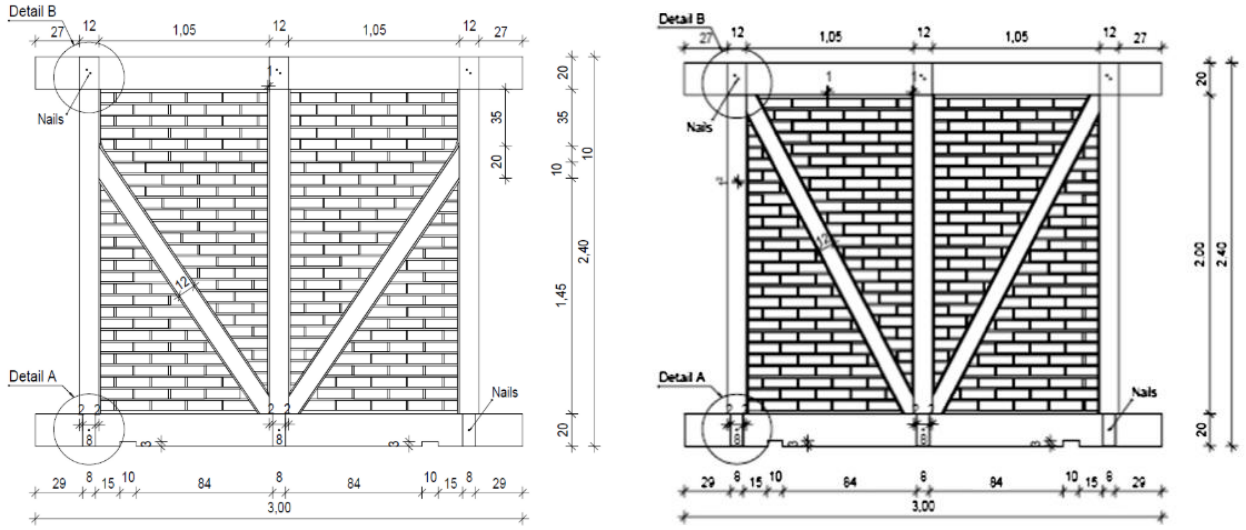

(a) **(b)**

Figure 3.1 Specimen S1 (a) and S2 (b) (Dutu et al. 2018b).

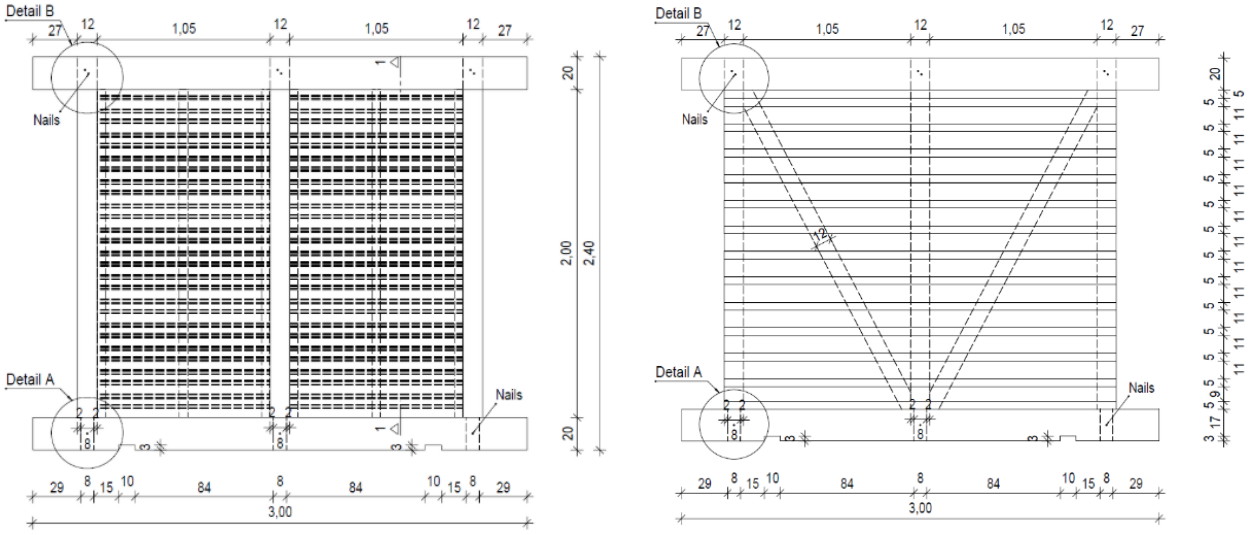

(a) **(b)**

Figure 3.2 Specimen S3 (a) and S4 (b) (Dutu et al. 2018a).

(a) **(b)**

Figure 3.3 Timber joints: mortise and tenon type (a), cross halved type (b) (Dutu et al. 2018a; b).

3.2 Material Properties

All the materials used to build the specimens should be characterized in terms of mechanical properties to calibrate a consistent numerical model that matches the experimental results and predicts the structural capacity. Several tests were conducted on masonry specimens to estimate their compressive and shear strength. Since all the panels have infill with mud mortar ranging from masonry infill to wattle and daub system, cylindrical mortar specimens were tested as well. However, few data relate to Romanian timber, *Pinaceae*, which was used to build the frame. Its mechanical properties are estimated indirectly by other experimental tests performed on the same wood species, even though these properties may be highly affected by the presence of defects and moisture content. Thus, the following experimental results related to timber properties may provide a qualitative estimation and are taken as reference values for the numerical model.

3.2.1 Compressive and Shear Tests on Masonry

Regarding masonry properties, compressive tests were performed on four masonry prisms at the laboratory of the Department of Reinforced Concrete Constructions (Technical University of Civil Engineering of Bucharest - UTCB), Figure 3.4a and b. They consist of mud bricks bonded with stabilized mud mortar. An average compressive strength of 1.86 MPa was measured and a Young's modulus of 0.6 GPa was determined as the secant stiffness crossing 1/3 of the maximum strength value, Table 3.1. The damage pattern, consisting of almost vertical cracks, can be observed in Figure 3.5a, b and c (Dutu 2017).

(a) (b)

Figure 3.4 Compression test on masonry specimen (Dutu 2017).

Table 3.1 Size and compressive strength of masonry specimens (Dutu 2017).

Specimen	Length [mm]	Width [mm]	Height [mm]	Area [mm2]	Force [kN]	Strength [MPa]
1	228	120	188	27360	48.81	1.78
2	230	114.4	191.4	26312	43.89	1.67
3	231	116.9	189.2	27003.9	57.48	2.13
4	233.2	116.5	191.2	27167.8	51.19	1.88
Average						1.86

(a) (b) (c)

Figure 3.5 Damage pattern after compressive tests for specimen 1 (a), 3 (b) and 4 (c).

Moreover, three specimens were tested to estimate the shear strength of masonry under low compression (0.1 MPa) according to SR EN 1052-3 (2003), Figure 3.6. The mortar was left to set under normal environmental conditions (temperature and humidity). Table 3.2Table 2.1 shows the dimensions of the specimens and the measured maximum forces. The average shear strength was 0.069 MPa, around 1/30 of the mean compressive strength, 1.86 MPa (Dutu 2017).

Figure 3.6 Shear test on masonry specimen (Dutu 2017).

Table 3.2 Size and shear strength of masonry specimens (Dutu 2017).

Specimen	Length [mm]	Width [mm]	Force [kN]	Strength [MPa]
1	150	111	1.08	0.065
2	143	111	1.00	0.063
3	163	113	1.48	0.080
Average				0.069

3.2.2 Compressive Tests on Mud Mortar

The mechanical properties of mud mortar were determined by compressive tests as well, Figure 3.7 (UTCB). The average compressive strength of cylindrical specimens was 2.62 MPa for mud mortar without straw representative of specimens S1 and S2, while 0.56 MPa for mud mortar with straw applied in S3 and S4, Table 3.3 and Table 3.4.

Figure 3.7 Compression test on mud cylinders (Dutu 2017).

Table 3.3 Size and compressive strength of mud mortar specimens without straw (Dutu 2017).

Specimen	Wall	W/wo straws	Obs.	Length [mm]	Diameter [mm]	Force [kN]	Strength [MPa]
1	S1 + S2	Without straw	Explosive failure	178	90	17.4	2.74
2				175	91	19.8	3.05
3				178	92.5	14	2.08
Average							2.62

Table 3.4 Size and resistance of mud mortar specimens with straw (Dutu 2017).

Specimen	Wall	W/wo straws	Obs.	Length [mm]	Diameter [mm]	Force [kN]	Strength [MPa]
1	S3 + S4	With straw	Not explosive failure	-	92	3.85	0.58
2				195	92.83	3.4	0.50
3				195	97	4.4	0.60
Average							0.56

3.2.3 Compressive Tests on Timber Elements

Regarding the buildings' wooden skeleton, two timber species were found during the field investigation: softwood (fir) for the superstructure and hardwood (oak, chestnut, etc.) for foundation piles but also for inferior stringers called "soles", Section 0. Experimental campaigns were aimed at estimating the mechanical properties of softwood species. The Romanian fir (*Pinaceae*) applied in the wall specimens has an average density of 385 kg/m^3 and an average moisture content of 15% (Dutu et al. 2018b). Timber quality was classified as Class B/CEE that corresponds to standard quality timber, including wooden elements with a starting drying state and with negligible defects such as curvature, twisted yarn, conicity, knots, eccentricity, contour irregularities or other isolated defects (Dutu 2017).

Experimental tests on timber specimens were carried out in INCERC laboratory, Bucharest. They comply with the standards SR EN 14801: 1, SR EN ISO 408, A1: 2016 (Dutu 2017). The equipment was calibrated and checked before each testing procedure, following PTE BSGF-39. Prismatic elements were tested and the resulting compressive strengths parallel and perpendicular to the grain are presented in Table 3.5 and Table 3.6. The average compressive strength parallel to the grain was 34.30 MPa, while 5.06 MPa if the load is applied perpendicular to grain direction. Figure 3.8 shows the damaged specimens tested parallel to grain direction with detached and broken fibers. It is worth to point out that the detachment at failure is even more severe in compressive tests perpendicular to the grain due to the low tensile strength perpendicular to rings, Figure 3.9.

Table 3.5 Size and compressive strength parallel to grain direction of tested specimens in INCERC, Bucharest (Dutu 2017).

Specimen	Length [mm]	Width [mm]	Force [kN]	Strength [MPa]
1	112	111	362.6	29.17
2	111	111	447	36.28
3	112	111	422.6	33.99
4	113	112	493.6	39.00
5	114	115	433.7	33.08
Average				34.30

Figure 3.8 Damages on timber specimens after compression test parallel to fiber direction (Dutu 2017).

Table 3.6 Size and compressive strength perpendicular to grain direction of tested specimens in INCERC, Bucharest (Dutu 2017).

Specimen	Length [mm]	Width [mm]	Force [kN]	Strength [MPa]
1	112	107	59.9	4.99
2	111	105	63.6	5.45
3	108	104	63.9	5.68
4	108	111	56.8	4.73
5	111	107	52.6	4.42
Average			59.36	5.06

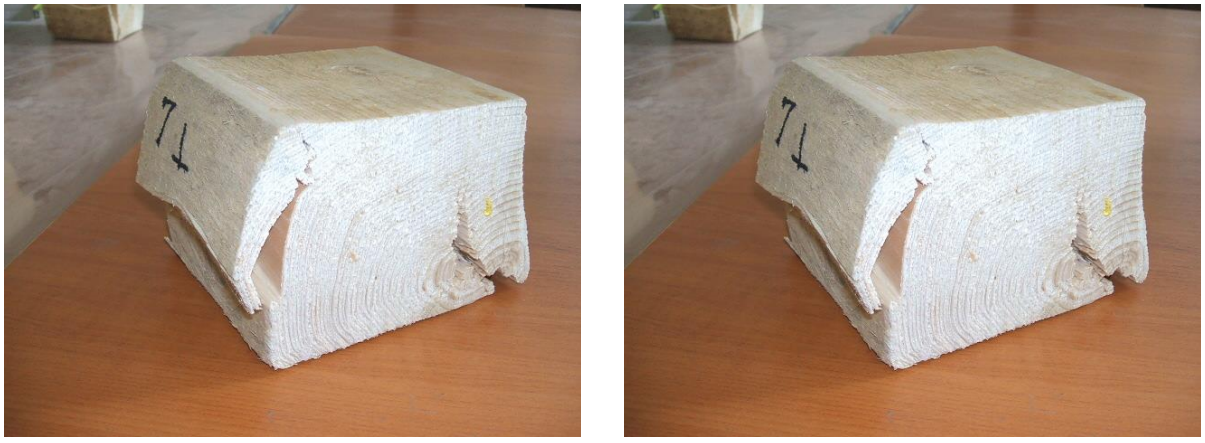

Figure 3.9 Damages on timber specimens after compression test perpendicular to grain direction (Dutu 2017).

The previous outputs are compared with those resulting from tests performed on the same timber species (Romanian fir) in Japan (Dutu 2017). They are presented to better characterize timber mechanical properties such as compression perpendicular to the grain. In this case, both cubic and rectangular specimens were tested in BL-Institute, Figure 3.10. The average ultimate strength of cubic specimens was 4.38 MPa, Table 3.7 and a similar value (5.02 MPa) was obtained for rectangular ones, Table 3.8. Both values are comparable with the compressive strength perpendicular to the grain measured in the previous experimental tests (5.06 MPa). In addition, the mean yielding strain of cubic specimens (2.8%) is almost half of the one for rectangular specimens (5%), Table 3.7 and Table 3.8. In terms of average initial stiffness, cubic specimen showed more stiffness, 175.24 MPa, than the rectangular ones, 102.67 MPa.

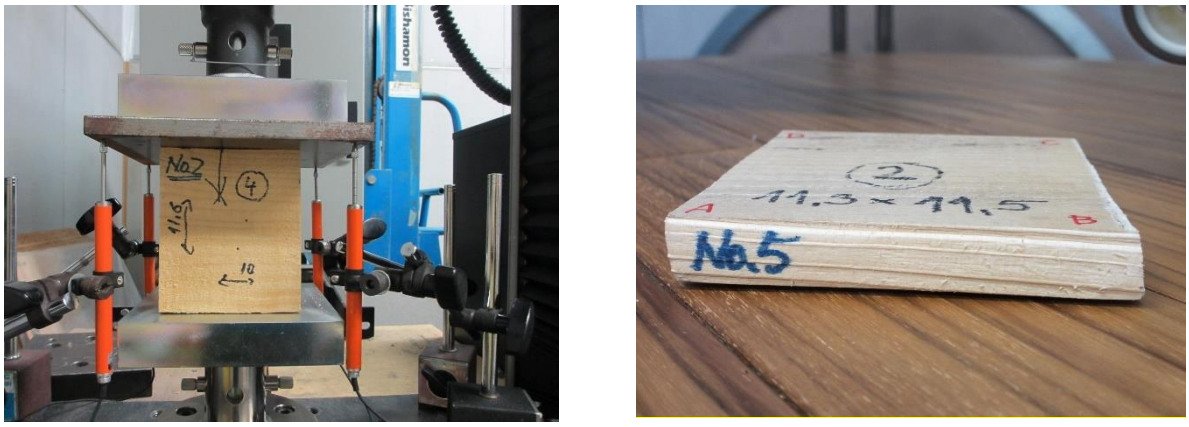

(a) **(b)**

Figure 3.10 Compressive tests on timber specimens: cubic (a) and rectangular (b) (Dutu 2017).

Table 3.7 Test results on cubic specimens (BL-Institute) (Dutu 2017).

Specimen	Max Strength [MPa]	σy [MPa]	εy	E1 [MPa]	E2 [MPa]	Maximum Force [kN]
1	3.80	3.62	0.035	113	2.28	37.39
2	4.27	4	0.026	207	3.27	41.07
3	5.06	3.63	0.023	206	14.08	49.88
Average	4.38	3.75	0.028	175.24	6.54	42.78

Table 3.8 Test results on rectangular specimens (BL-Institute) (Dutu 2017).

Specimen	Max Strength [MPa]	σy [MPa]	εy	E1 [MPa]	E2 [MPa]	Maximum Force [kN]
1	5.20	4.92	0.044	105	14.74	69.03
2	4.84	2.98	0.053	101	11.31	64.47
Average	5.02	2.95	0.05	102.67	13.03	66.75

3.2.4 Bending Tests on Timber Beams

Three-point bending tests were also carried out to obtain an estimation of the average bending strength in INCERC, Bucharest, Figure 3.11. Timber specimens were built according to the product standards and their dimensions were 95 x 120 x 2400 mm, (Dutu 2017). The resulting bending strength, f_m, was determined by the following formula (1).

$$f_m = \frac{3 \cdot F_{max} \cdot l}{2 \cdot b \cdot h^2} \tag{1}$$

where F_{max} is the maximum force, l the distance between the supports (2000 mm), b and h the dimensions of the cross-section. Table 3.9 shows the average bending strength per specimen and the mean value of 3.59 MPa, while the types of failure mechanisms are shown in Figure 3.12.

(a) **(b)**

Figure 3.11 Bending tests on timber specimens: first (a) and ultimate (b) step (Dutu 2017).

Table 3.9 Size and bending strength of tested specimens in INCERC, Bucharest (Dutu 2017).

Specimen	Base [mm]	Height [mm]	Force [kN]	Bending Strength [MPa]
1	97	118	1.81	4.02
2	98	120	1.88	4.00
3	94	117	1.18	2.75
Average				3.59

Figure 3.12 Types of failure mechanisms of 3-point bending test (Dutu 2017).

Additional data resulting from another experimental campaign performed at Technical University of Bucharest are presented in this section to assess the modulus of elasticity parallel to the grain of timber specimens, Figure 3.13. This parameter was taken as a reference value to define the material properties in the numerical model. Table 3.10 and Table 3.11 shows the average modulus of elasticity determined by four-point bending tests on two sets of timber specimens (bought from 2 different batches), 11.2 and 8.9 GPa respectively. In the present experimental tests on TFM walls, the timber frame consists of elements made of timber with similar properties as those tested in bending. The lower value was considered, to take into account the frequent possibility of low-quality timber use in existing buildings.

Figure 3.13 Four-point bending test on timber specimen.

Table 3.10 Modulus of elasticity parallel from bending test on set 1.

Specimen	Force [kN]	Em [GPa]
1	9.4	10.2
2	15.7	14.4
3	11.5	9.1
Average	12.2	11.2

Table 3.11 Modulus of elasticity parallel from bending test on set 2.

Specimen	Force [kN]	Em [GPa]
1	8.1	7.9
2	8.1	7.2
3	12.1	11.5
Average	9.4	8.9

3.2.5 Timber characterization

All experimental mean values were converted into characteristic ones according to the procedure provided by Annex D 7.2 of Eurocode 0 (EN 1990-2002), Table 3.12. Once characteristic properties are obtained, equivalent softwood strength classes can be estimated according Table 1 of EN 338 (2009). Even though they range widely, possibly depending on different test setups, quality of timber and shape effects, a correlation may be found among all the experimental results. Thus, Romanian timber may be classified between C18 and C20 according to its compressive strength perpendicular to the grain, mean modulus of elasticity and density. However, it is worth to point out that the characteristic bending strength is very low compared with those of C18 / C20 as well as the characteristic modulus of elasticity. Both values are even lower than the minimum value related to C14. The underestimation of modulus of elasticity ($E_{0,0.05}$) may be due to the large standard deviation related to the measurements for the specimens subjected to four-point bending test (7.82 and 5.32, respectively). Regarding the outputs from Romanian compressive tests, both characteristic compressive strengths parallel and perpendicular to the grain are higher than those related to C18 / C20.

Table 3.12 Mechanical properties of Romanian fir (*Pinaceae*).

Strength properties				
Bending	$f_{m,k}$	[MPa]	1.14	$f_{m,k}$ < C14
Compression parallel	$f_{c,0,k}$	[MPa]	25.75	C35 < $f_{c,0,k}$ < C40
Compression perpendicular	$f_{c,90,k}$	[MPa]	3.86 (Romania)	$f_{c,90,k}$ > C50
			2.23 (Japan)	C18 < $f_{c,90,k}$ < C20
Stiffness properties				
Mean modulus of elasticity parallel	$E_{0,mean}$	[GPa]	11.23	C24 < $E_{0,mean}$ < C27
			8.87	C16 < $E_{0,mean}$ < C18
5% modulus of elasticity parallel	$E_{0,0.05}$	[GPa]	1.81	$E_{0,0.05}$ < C14
			1.09	$E_{0,0.05}$ < C14
Density				
Mean density	ρ_{mean}	[kg/m^3]	385	C18 < ρ_{mean} < C20

3.3 Experimental Setup and Testing Program

In-plane tests were performed in a quasi-static cyclic regime and their setup is shown in Figure 3.14a, where the external vertical load of 26 kN is transmitted by a vertical hydraulic jack and the horizontal displacements by two hydraulic jacks. Both vertical and horizontal jacks imposed their pressure on a steel loading beam that can be considered rigid and only allows horizontal displacements due to the pantograph system between the reaction frame and the steel beam itself. It is worth to point out that the loading beam is connected to the timber one by steel bolts to have the same horizontal displacements and it transmits the vertical load by three steel plates placed above the columns. Moreover, the panel was fixed at the bottom platform by steel bolts and their relative displacements were measured by inductive transducers as well as those between the upper timber beam and the steel loading one. Both vertical loads and horizontal displacements were controlled manually; nevertheless, accurate results were obtained despite the low strength of the wall specimens compared to the reaction frame and a ±20% variation of the vertical load (Dutu et al. 2018a). Displacements were recorded by transducers located in four points: horizontal displacements were measured at the top and middle of the wall, vertical uplifts at the bottom of external columns. Moreover, rotations of the bottom connections were obtained by dividing the vertical uplifts with the distance between transducers. Figure 3.14b shows the loading protocol (CUREE Caltech) that was selected to compare the results with previous experimental tests (Dutu et al. 2018b). The shear angle, δ, was considered to correct the rocking by subtracting from the drift the wall deformation due to the uplift in the bottom connections.

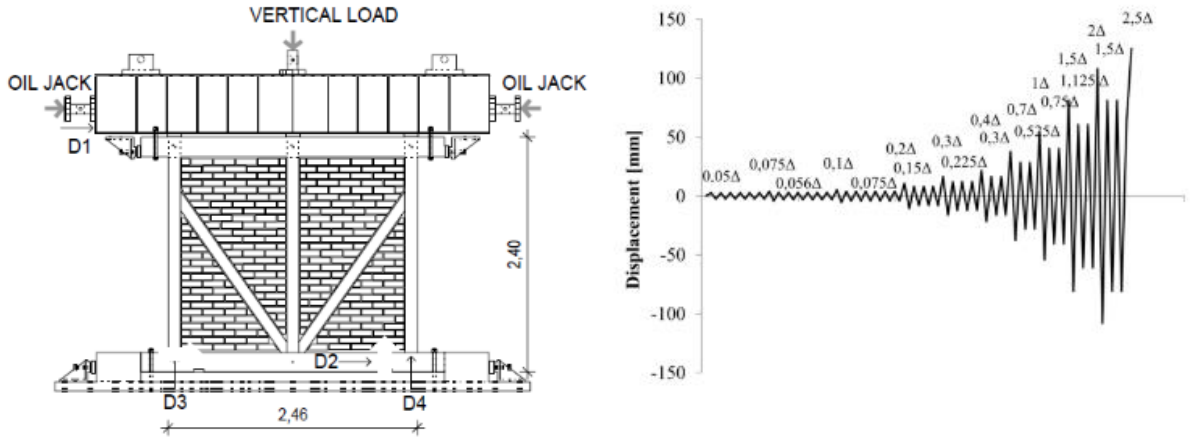

Figure 3.14 Experimental setup (a) and loading protocol (b) (Dutu et al. 2018a).

3.4 Experimental Results

The four specimens are compared in terms of initial stiffness, ultimate capacity, ductility ratio and damage pattern to better understand the influence of the bracings, type of infill and progression of damages.

Figure 3.15a and b show the two hysteretic curves related to S1 and S2. The two specimens reach the same ultimate strength but, as expected, S2 has a higher stiffness than S1 since the bracings are arranged along the actual diagonal of the frame (S2), thus they contribute to the in-plane stiffness from the very beginning of the test (Dutu et al. 2018b). However, it is worth to point out that the force related to the 7th cycle of the hysteretic curve of S1 (82 mm) does not reach the envelope curve. This may be due to the proximity between two consecutive target peak displacements (73.4 and 82 mm), resulting in lower base force because of the pinching effect. In addition, S1 test was carried out in two different phases with top displacements cycles from 0 to 82 mm and then from 55.6 to 119.6 mm meaning that some cycles were repeated twice. Thus, the accuracy of the last cycle may be lower compared to the previous ones due to stiffness degradation and increasing of damage at the connections. In terms of energy dissipation, S1 has a higher value than S2, 3.22 and 2.68 kNm, respectively. The damping ratio for S1 is higher than that for S2 too.

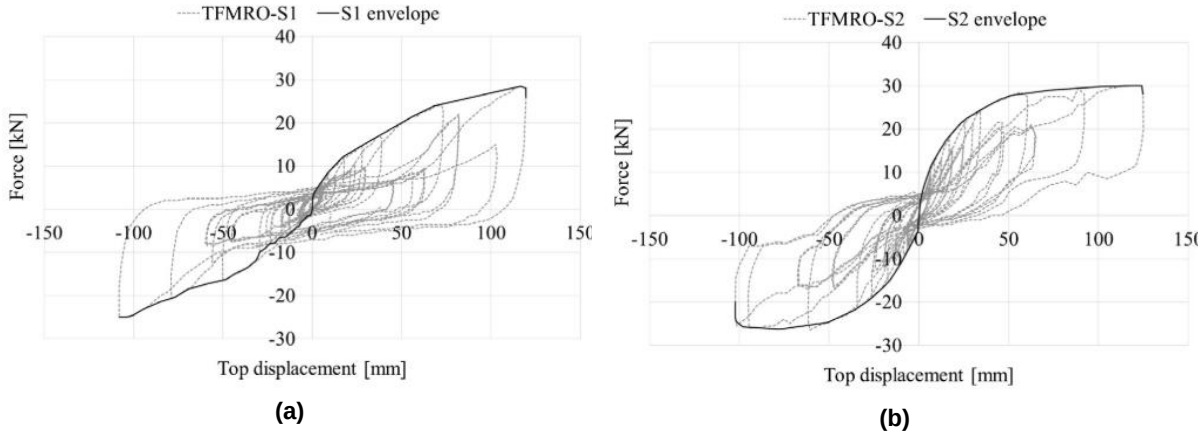

(a) **(b)**

Figure 3.15 Hysteresis loop and envelope of the first cycle for S1 (a) and S2 (b) (Dutu et al. 2018b).

Although S2 is more damaged than S1, both specimens show a similar pattern at their last step such as local compression perpendicular to the grain in the upper cross-halved joint and pull-out of the diagonal bracing subjected to tension which goes back to the initial position during the reverse cycle, Figure 3.16a and b. Specimen S1 does not show significant uplifts in the timber joints (around 1 mm in the bottom connection as long as the transducers worked properly), while S2 reveals larger uplifts in the lower (up to 25 mm) and upper connections, Figure 3.17a and b. This is due to the arrangement of the bracings that push against the upper beam in S2. It is important to note that brick masonry infill is prone to out-of-plane collapse in case of earthquakes since the infill-to-frame adhesion is very low. The infill does not increase significantly the wall stiffness because it was already cracked due to shrinkage almost from the beginning and it detached from the timber frame after the first cycle. However, masonry infill can prevent buckling of the diagonals due to its confinement effect and can increase the seismic energy dissipation through shear sliding. Moreover, the crack pattern and resulting amount of dissipated energy depends also on the strength of the mortar: if a weak one is applied, the dissipation will occur along the joints through cracking and sliding, while with a strong mortar and weak units the cracks will develop at the interface between mortar and units and through the elements.

(a) (b)

Figure 3.16 Specimen S1 (a) and S2 (b) in the last cycle (Dutu et al. 2018b).

(a) (b)

Figure 3.17 S1 damages: compression parallel to the grain (a) and diagonal detachment (b) (Dutu et al. 2018b).

(a) (b)

Figure 3.18 S2 damages: uplift of upper beam (a) and central post (b) (Dutu et al. 2018b).

(a) **(b)**

Figure 3.19 Out-of-plane of masonry infill S1 (a), S2 (b) (Dutu et al. 2018b).

Specimen S3 shows a lower ultimate strength (15 kN) but higher initial stiffness (1866 kN/rad) compared to S1 (1375 kN/rad), Table 3.13. This may be due to the lack of bracing. The ultimate drift is 6.13%, slightly higher than S1 and S2 (5.3% and 4.8% respectively). In terms of damages, they were similar to the previous specimens such as local compression perpendicular to the grain in the upper beam, Figure 3.22a. However, connection uplift was not observed (2 mm in the bottom connections, Figure 3.22b and infill did not experience any out-of-plane mechanisms, Figure 3.23a. As already mentioned for S1 and S2, the infill does not increase significantly the capacity of the wall since it experiences detachment from the timber frame, Figure 3.23b.

The last wall S4 has almost equal ultimate strength (30 kN) compared to S1 (29 kN) but higher stiffness (1911 kN/rad), Table 3.13. The ductility factor is the lowest 4.4 as well as the ultimate drift (4.5%), meaning that this system shows less seismic capacity compared to the other three specimens. Moreover, it showed uplift in the connections (18 mm of the bottom ones, Figure 3.24b) and infill cracked along the timber braces and between the bottom and upper beams (Dutu et al. 2018a). Figure 3.25a and b show detachment of the bracings subjected to tension as well as detachment of the upper beam due to their presence, respectively. Table 2.1 summarizes the global parameter related to the four specimens such as shear angle, maximum shear capacity, initial stiffness and ductility factor.

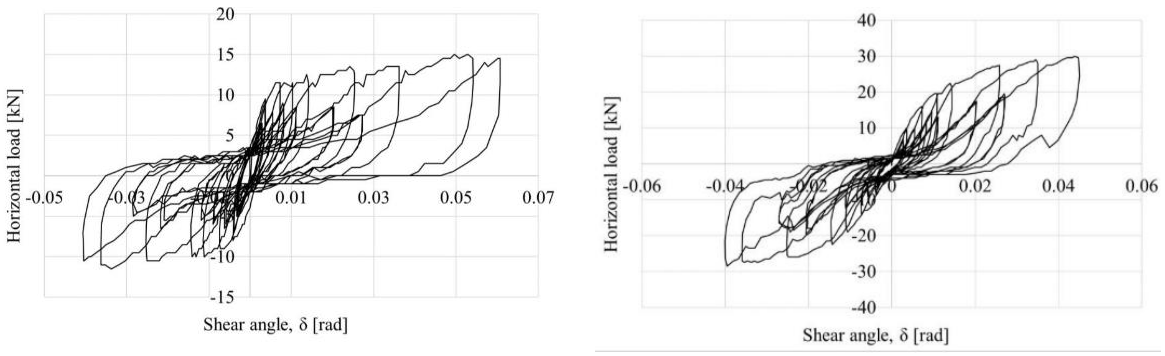

(a) **(b)**

Figure 3.20 Hysteresis curves for S3 (a) and S4 (b) (Dutu et al. 2018a).

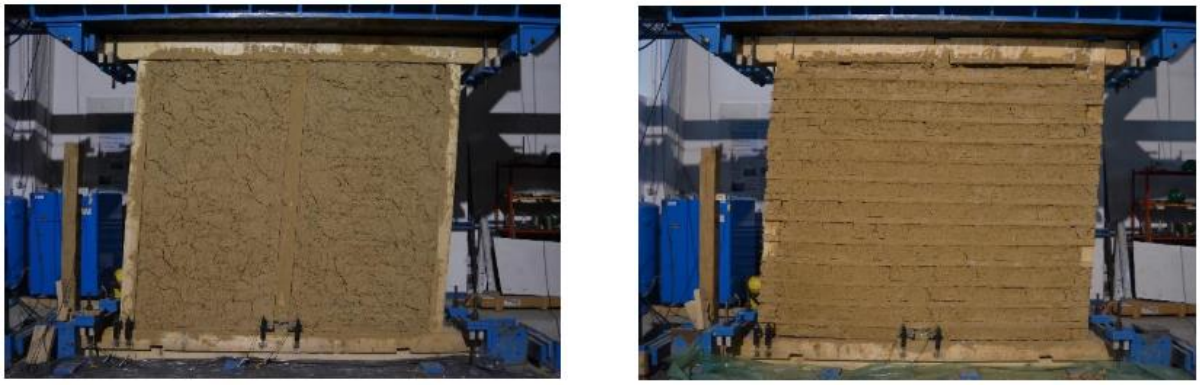

(a) **(b)**

Figure 3.21 S3 (a) and S4 (b) in the last cycle (Dutu et al. 2018a).

(a) **(b)**

Figure 3.22 S3 damages: compression perpendicular to grain (a), small uplift external connection (b) (Dutu et al. 2018a).

(a) **(b)**

Figure 3.23 S3 damages: no out-of-plane mechanism (a), detachment of infill (b) (Dutu et al. 2018a).

(a) **(b)**

Figure 3.24 S4 damages: compression perpendicular to grain (a), uplift of external connection (b) (Dutu et al. 2018a).

(a) **(b)**

Figure 3.25 S4 damages: central connection with detachment of bracings (a), detachment upper beam (b) (Dutu et al. 2018a).

Table 3.13 Summary of global parameter for each specimen.

Specimen	Shear Angle [%]	Max Shear Capacity [kN]	Initial Stiffness [kN/rad]	Ductility Factor
S1	5.3	29	1375	6.5
S2	4.8	30	2150	4.8
S3	6.13	15	1866	9.7
S4	4.5	30	1911	4.4

The experimental campaign on Romanian TFM walls showed that these structures have a good deformation capacity when subjected to in-plane quasi-static loading. The more resistant the wall, the less ductile it is in terms of shear angle and ductility factor. Indeed, S3 wall has the highest ductility factor and the lowest shear capacity. The type of infill does not change significantly the global response but can play a role for the energy dissipation. It is worth to point out that the stiffness of each wall is mainly controlled by the presence and the arrangements of diagonal elements that play a role even for the energy dissipation and damage mechanisms. Indeed, most of the damages are due to the action of bracings such as uplift of the external posts or the upper beam, especially in S2 and S4 where the diagonal members are joint at the frame corner. Moreover, the deformed shape is highly influenced by the arrangement of these elements, for example between S1 and S2 walls. Regarding the observed damage, the main mechanisms can be summarized as follows: (1) axial detachment and vertical sliding of bracings, when connected just to the posts (S1), in the lower and upper joints respectively; (2) vertical uplifts of external posts and upper beam for bracings aligned along the actual diagonal of the timber frame (S2 and S4); (3) detachment of masonry infill and activation of out-of-plane mechanisms (S1 and S2). Neither timber elements nor their connections showed severe damages except minor cracks or increase in the initial gaps due to local compression perpendicular to the grain direction.

S1 specimen was considered representative for the Romanian TFM walls since many buildings showed diagonal elements connected along the posts during the field investigation. Thus, the following analysis are aimed at studying its global behaviour under in-plane cyclic quasi-static loading.

4 CALIBRATION OF CONNECTIONS

The seismic behavior of TFM structures, such as the tested walls, is strongly affected by the performance of timber connections. Therefore, the latter were investigated and calibrated through experimental tests. The aim is to characterize their hysteretic behavior under in-plane monotonic or cyclic loads, which can be represented by non-linear springs for each degree of freedom such as horizontal, vertical and rotational. Since the actual connections were not tested before building the wall specimens, three experimental campaigns performed in Technical University of Bucharest, Japan and Malaysia were studied to calibrate the non-linear springs as comparable as possible to those of the Romanian walls.

The bottom connections of S1-S4 walls are mortise and tenon type (MT) while the upper ones are cross-halved type (CH) with plain nails as fasteners and some gaps due to the construction process, as already described in Section 3. Regarding the MT joints, they are commonly simplified as pinned connections but, in the present study, they are modelled as non-linear translational and rotational springs with a certain hysteretic behavior for each degree of freedom based on two selected experimental campaigns: the Japanese one by Sakata *et al*. (2012), considered as the most representative to calibrate the moment resisting behavior and tensile capacity, and the Malaysian one by Hassan *et al*. (2010) for shear capacity. MT joint strength is highly influenced by the width of the tenon, the dimensions of timber elements, their wood species and the presence of defects or gaps due to the construction process as well as the presence of fasteners such as dowels. Although there are some discrepancies related to geometrical characteristics, types of fasteners and timber species, both experimental tests can provide a good estimation on the performance of MT connection type. In the Japanese case, the specimens were made of another softwood, cedar instead of fir (Romanian campaign), and a timber dowel made of hardwood (oak) was applied as fastener to prevent post uplifting during the in-plane cyclic test. Whereas in the other test campaign, the medium hardwood Malaysian tropical timber (*Koompassia malaccensis*, commercial name Kempas) was used for timber elements as well as wooden dowel from Kempas. It is worth to stress that the cross-sectional dimensions are comparable with those of the Romanian walls.

4.1 Mortise and tenon joints

The Japanese experimental campaign was performed on several configurations of mortise and tenon connection type varying in cross-sectional geometry of beam and post, dimensions of tenon and dowel as well as modulus of elasticity. Figure 4.1a and b show the geometry and test setup related to in-plane bending test, where the horizontal load was applied by an actuator at 700 mm from the center axis of the lower beam that is not entirely crossed by the tenon and it is fixed to the steel foundation with anchor bolts to prevent uplifts. The reference M-θ hysteretic curve used for calibration, Figure 4.2, relates to the specimen named BD-No.5 with dimensions explained in Table 4.1. This sample has both post and beam

made of cedar (CC) with a similar moisture content that those of Romanian fir, but lower modulus of elasticity parallel to grain and higher bending strength, Table 4.2.

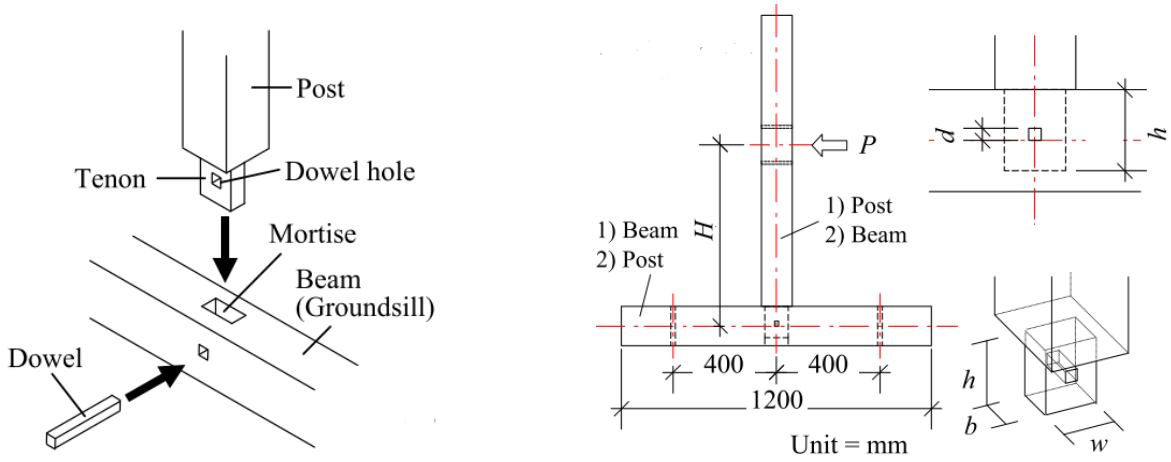

(a) **(b)**

Figure 4.1 Mortise and tenon connection with timber dowel: elements (a), geometry (b) (Sakata et al. 2012).

Table 4.1 Dimension of tested MT specimen (in-plane cyclic test) (Sakata et al. 2012).

Specimen	Post Section [mm]	Beam Section [mm]	Tenon Height h, Width w, Thickness b [mm]	Dowel Section [mm]
BD-No.5	120x120	120x150	120x90x36	18x18
Romanian MT	120x120	200x220	200x80x80	-

Table 4.2 Material properties of tested MT specimen (in-plane cyclic test) (Sakata et al. 2012).

Tree species	Specific Gravity [-]	Moisture Content [%]	Modulus of elasticity parallel [GPa]	Bending Strength [MPa]
Cedar (CC)	0.48	15.7	6.19	39.20
Romanian Fir		15	8.9	-

The M-θ curve shows a non-symmetric hysteresis that may be due to one side application of the static cyclic loading thus positive rotations and bending moments were considered representative of the MT hysteretic behavior, Figure 4.2a. Moreover, the gap between resisting moments for small (1/60 rad) and large deformations (1/15 rad) is not that significant. Figure 4.2b shows the crack pattern developed during the in-plane cyclic test with two identified failure modes: a shear failure of tenon from dowel hole to the end, a bending failure of tenon due to the high tensile stress (Sakata et al. 2012).

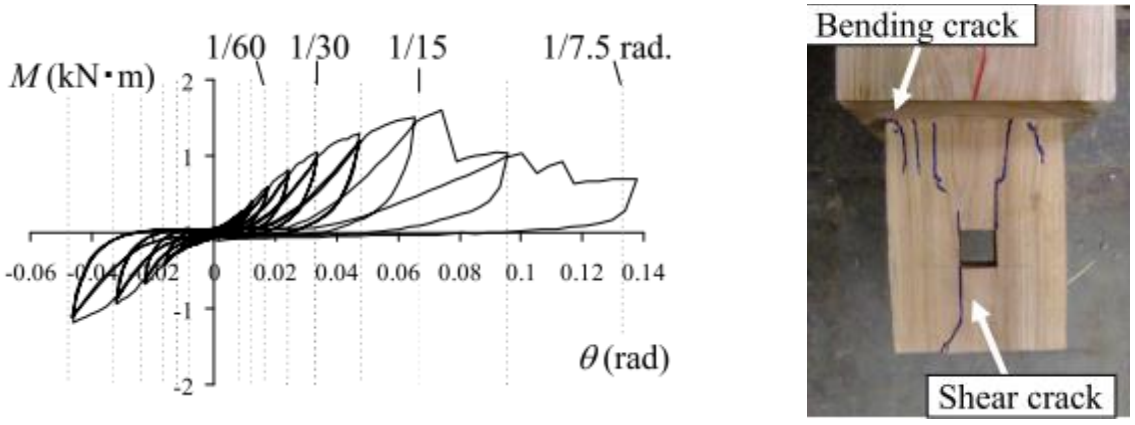

(a) **(b)**

Figure 4.2 M-θ hysteretic curve of BD-No.5 CC (a), observed failure mode (b) (Sakata et al. 2012).

The numerical model configuration is explained in Figure 4.3a consisting of a linear elastic element with all the non-linearities lumped in the rotational spring between nodes 1 and 2 that are constraint to have same vertical and horizontal displacements. Dead loads related to timber elements are neglected since they do not influence significantly the response. Once the geometrical layout and element cross-sections are defined according to the experimental setup, the moment resisting behavior of MT connection was represented by a rotational spring with a hysteretic material, SAWS, developed by Patxi Uriz, Exponent (Converted from FORTRAN code originally written by Bryan Folz). The envelope curve of SAWS uniaxial material is mainly controlled by the initial stiffness (*S0*) and its asymptotic line with slope (*R1*), defined as a ratio of (*S0*), and intercept strength (*F0*) with y axis, Figure 4.3b.

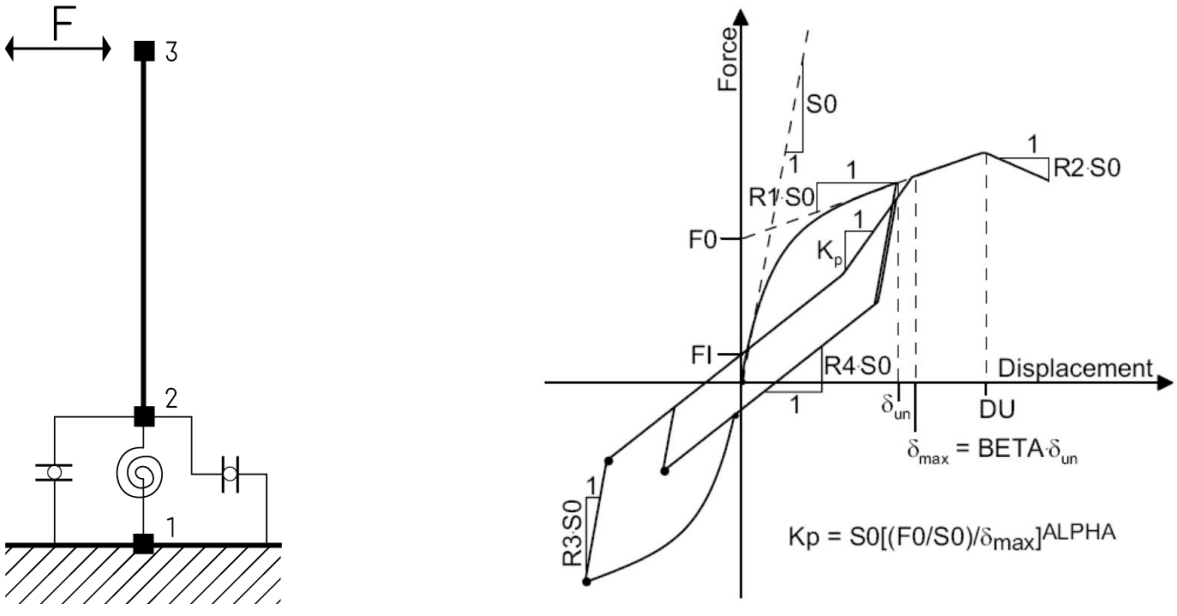

(a) **(b)**

Figure 4.3 Structural layout of in-plane cyclic test on MT joint in OpenSees (a) and SAWS material (b).

The calibration procedure is iterative and was achieved by estimating the initial stiffness (*S0*), the intercept strength of the asymptotic line of the envelope (*F0*), maximum rotation at ultimate load (*DU*) and descending branch of the experimental response (*R2*), Figure 4.3b. Once the global envelope was approached, other parameters were modified to better approach the cyclic energy dissipation, such as: unloading stiffness (*R3*) and reloading stiffness degradation (*Kp*), function of α, as well as pinching branch controlled by the slope (*R4*) and the intercept strength (*FI*), Figure 4.3b andFigure 4.4. Eventually, the cumulative dissipated energy of both experimental and numerical hysteretic curves was determined and compared to assess if their level of approximation is good enough, Figure 4.5a. Moreover, the cumulative error decreased from around -60% for negligible rotations (0.02 rad) to -26% for larger ones (0.14 rad) meaning that the experimental area is quite larger than the numerical one because the numerical last cycles do not perfectly match the experimental ones in terms of reloading stiffness degradation, Figure 4.5b.

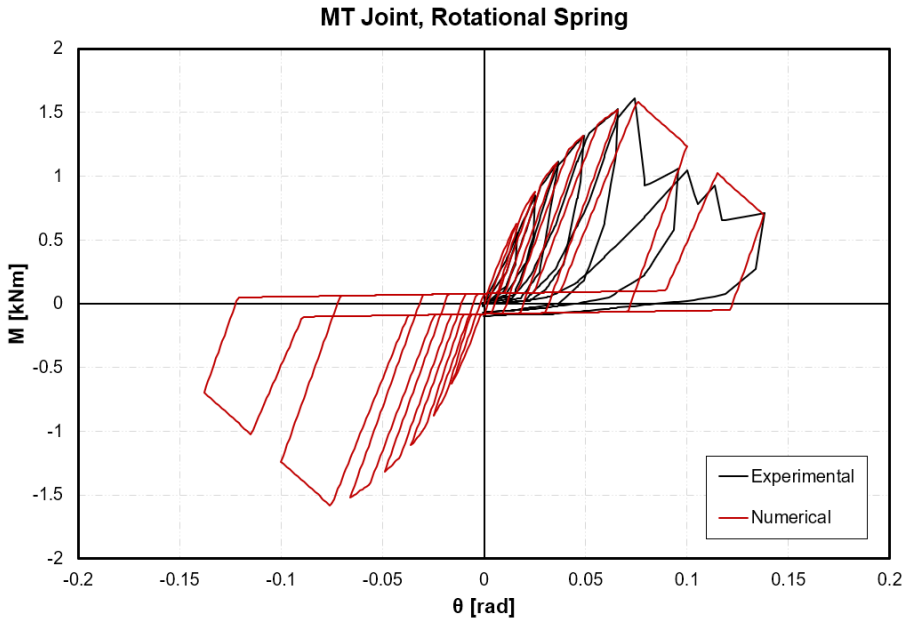

Figure 4.4 M- θ hysteretic curves for MT joint (in-plane cyclic test).

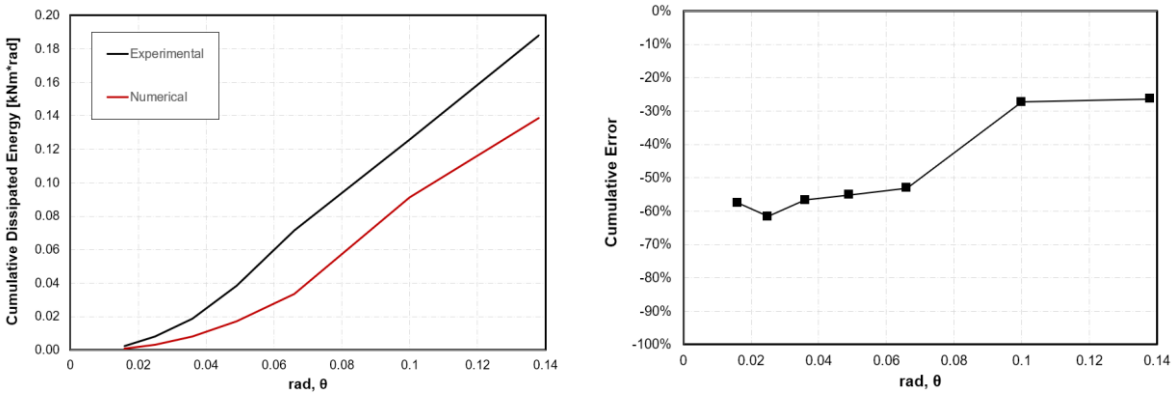

(a) (b)

Figure 4.5 Cumulative dissipated energy (a) and cumulative error (b) for MT joint (in-plane cyclic test).

The tensile capacity of MT joints was studied by pulling the post out from its initial position. In this case, the wooden dowel made of oak was substituted by a steel one to have shear failure mechanism. Table 4.3 and Table 4.4 show the geometrical characteristics and material properties of the tested specimens related to the hysteretic curve of Figure 4.7, respectively. Experimental test setup is shown in Figure 4.6 where the post, constraint by the steel dowel, was pulled by means of steel plates anchored with bolts. The global response of MT joints was quite scattered with specimens ranging from brittle to ductile failure. In the present study, ductile F-δ curve (gray curve, Figure 4.7) was taken as a reference to calibrate the vertical spring of MT connection even if it shows a lower strength compared to the brittle one.

Table 4.3 Dimension of tested MT specimen (tensile test).

Specimen	Post Section [mm]	Tenon Height h, Width w, Thickness b [mm]	Dowel Section [mm]
T-No.4	120x120	150x90x30	18x18
Romanian MT	120x120	200x80x80	-

Table 4.4 Material properties of tested MT specimen (tensile test).

Tree species	Specific Gravity [-]	Moisture Content [%]	Modulus of elasticity parallel [GPa]	Bending Strength [MPa]
Cedar (CC)	0.41	13.1	6.19	39.20
Romanian Fir		15	8.9	

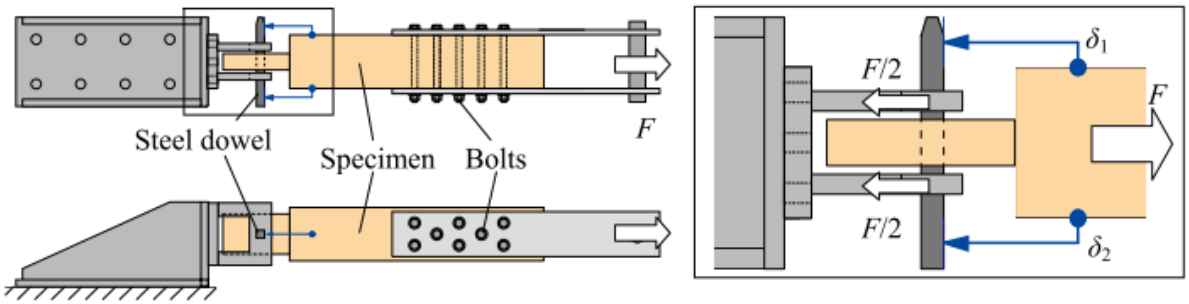

Figure 4.6 Tension test setup (Sakata et al. 2012).

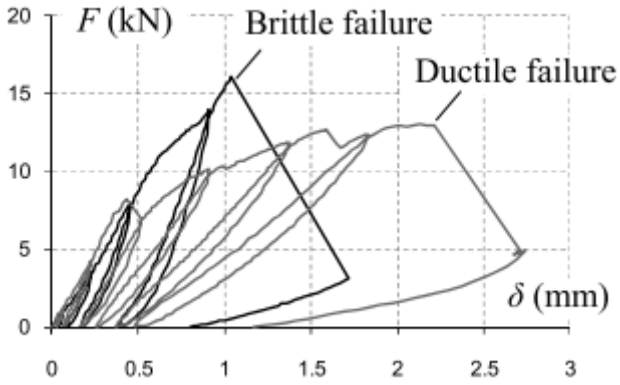

Figure 4.7 F-δ hysteretic curves of tested MT specimen (tensile test) (Sakata et al. 2012).

Figure 4.8a shows the structural configuration modelled in OpenSees; also, in this case a linear elastic element was adopted with the non-linearities lumped in the vertical spring between nodes 1 and 2 that are constraint to have the same horizontal displacements and no rotations. Dead loads are neglected as in the previous numerical model. In this case, the tensile behavior of MT connection was represented by a vertical spring with hysteretic material Pinching4, whose main parameters are shown in Figure 4.8b. The envelope curve of this uniaxial material is controlled by four points that define three branches with positive stiffness and a fourth one with a negative slope up to the last point (*ePd*$_4$, *ePf*$_4$) where the residual strength is fixed with no limit on displacements or deformations, therefore being preferable for this degree of freedom. The pinching behavior is governed by three ratios *rDisp*, *rForce* and *uForce*, that define when the reloading occurs in terms of force and displacements, and when the unloading ends, respectively.

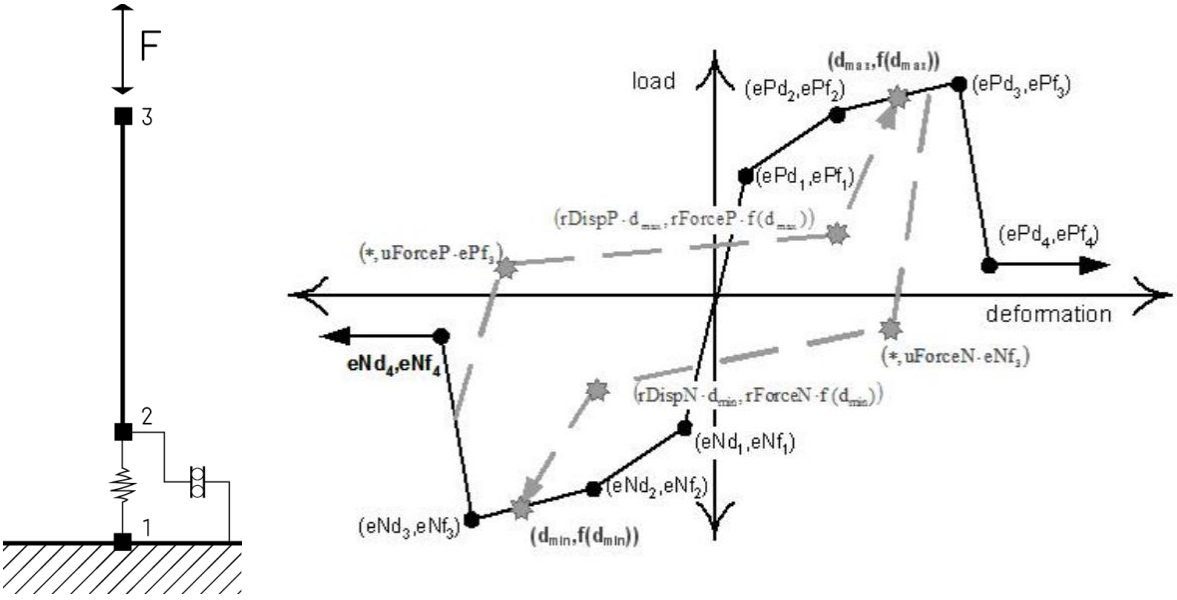

(a) **(b)**

Figure 4.8 Structural layout of tensile test on MT joint in OpenSees (a) and Pinching4 material (b).

The calibration procedure followed the same steps already explained and was achieved by estimating the initial (defined by the point *ePd₁, ePf₁*) and yielding stiffness (slope between points *ePd₁, ePf₁* and *ePd₂, ePf₂*), the maximum displacement at ultimate load (*ePd₃)* and residual force of the experimental response (*ePf₄*), Figure 4.8b. Once the global envelope was matched, secondary parameters were adjusted to better estimate the cyclic energy dissipation, such as unloading and reloading stiffness as well as pinching effect. Figure 4.9 shows the hysteretic curve with a good approximation in terms of reloading and unloading stiffness even in last cycles. The cumulative error decreased from -100% for zero deformation to -7.5% for values of ε around 0.30% meaning that the two areas are comparable and almost superimposable, Figure 4.10b.

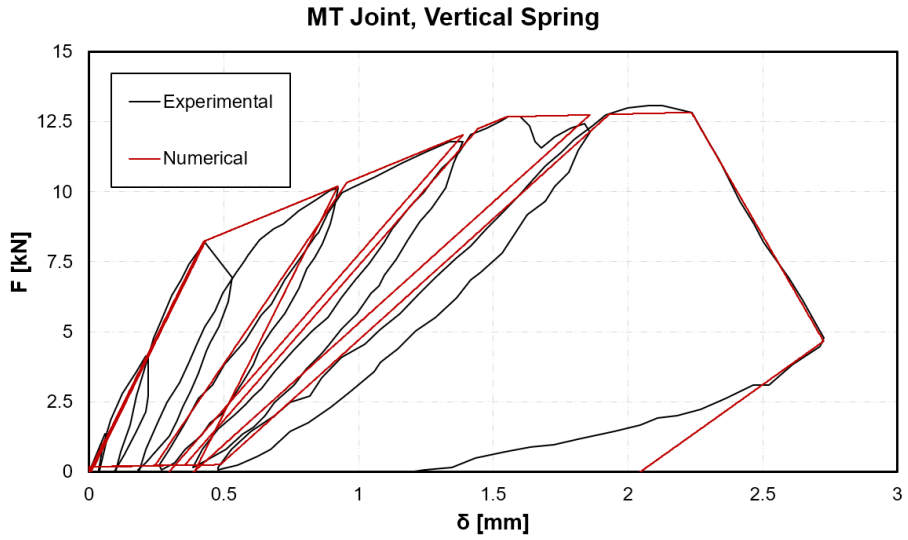

Figure 4.9 F-δ hysteretic curves for MT joint (tensile test).

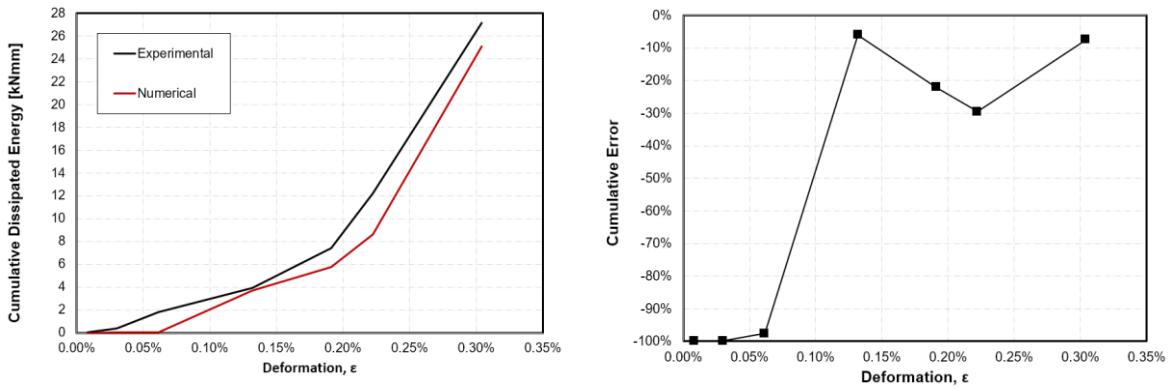

(a) (b)

Figure 4.10 Cumulative dissipated energy (a) and cumulative error (b) for MT joint (tensile test).

The second experimental campaign performed by Hassan *et al*. (2010) was aimed at studying the shear strength and capacity of mortise and tenon connections fastened with wooden dowels. In this case, timber species is a medium hardwood instead of softwood and all the elements had similar quality with almost straight fibers and no defects such as knots or splits. Timber specimens were controlled in terms of temperature (20°C) and relative humidity (60%) until they were tested (Hassan et al. 2010). Figure 4.11a and b show the shear test configuration with post and beam rotated by 90° to apply a vertical load perpendicular to the grain of the tenon member at 125 mm from the mortise one. Moreover, the horizontal element was propped with a pinned support at 900 mm from the face of vertical one that presents fixed ends.

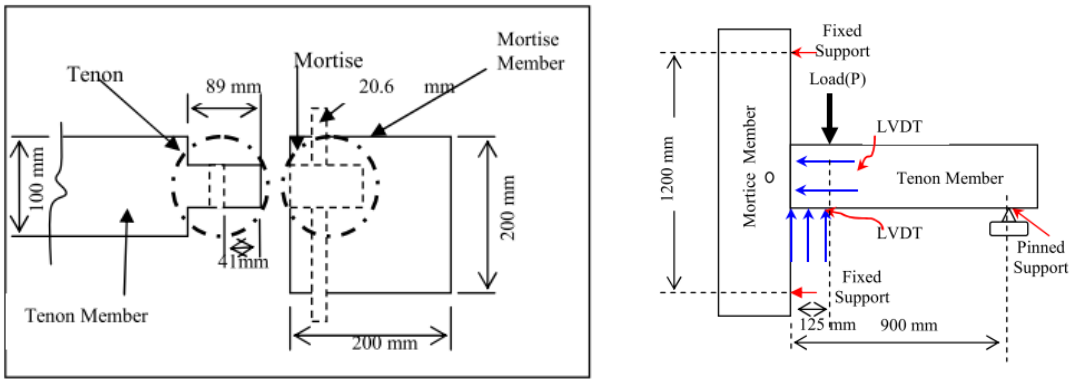

(a) (b)

Figure 4.11 Dimensions of MT connection (a) and shear test configuration (b) (Hassan et al. 2010).

Table 4.5 Dimension of tested MT specimen (shear test).

Specimen	Post Section [mm]	Beam Section [mm]	Tenon Height h, Width w, Thickness b [mm]	Dowel Diameter [mm]
MT	100x150	200x200	89x150x41	20.6
Romanian MT	120x120	200x220	200x80x80	-

Table 4.6 Material properties of tested MT specimen (shear test).

Tree species	Specific Gravity [-]	Moisture Content [%]	Modulus of elasticity parallel [GPa]
Kempas	770-1120		16-18
Fir		15	8.9

Figure 4.12a shows the F-δ monotonic curve related to MT joints with wood and steel dowel that have similar initial stiffness and displacement capacity, but, in terms of ultimate strength, the connections with a steel dowel presents higher force. The failure mechanisms of Figure 4.12b was observed at the last step of the tests where the tenon shoulder tears due to rolling shear stress.

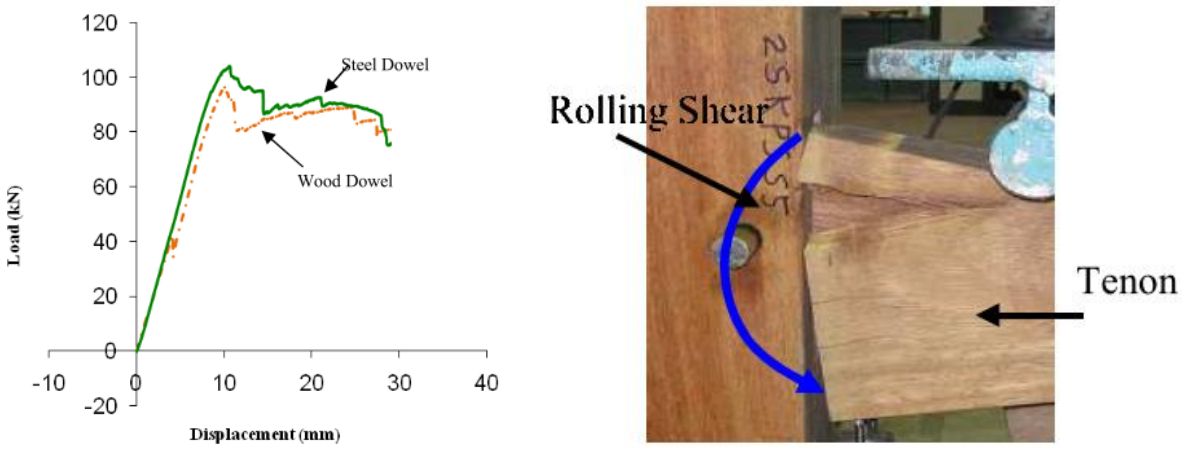

(a) **(b)**

Figure 4.12 F-δ curve of MT connection (a) and rolling shear of tenon shoulder (Hassan et al. 2010).

This setup was again modelled in OpenSees and its structural layout consists of linear elastic elements with a vertical spring between nodes 2 and 4 that are constraint to have same horizontal displacements and rotations. This spring represents the shear behavior of MT connection with Pinching4 uniaxial material, Figure 4.13b. The vertical element, which is the rotated lower beam, is fixed at both ends while the horizontal one (post) is linked with its tenon on the left and pinned at the right end.

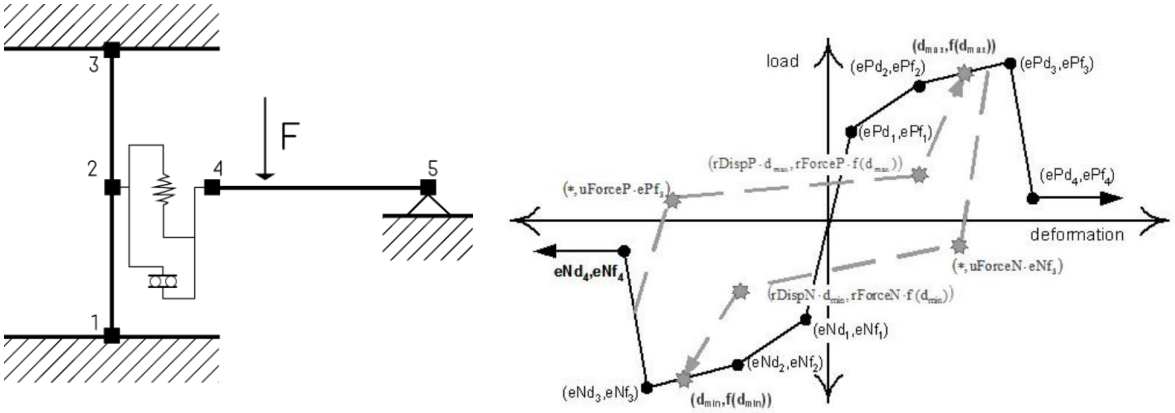

(a) **(b)**

Figure 4.13 Structural layout of tensile test on MT joint in OpenSees (a) and Pinching4 material (b).

Figure 4.14 shows the comparison between the two curves with a good approximation in terms of initial stiffness, ultimate force but also the comparable dissipated energy: 2065.43 kNmm for experimental curve and 2032.58 kNmm for numerical (error -1.59%).

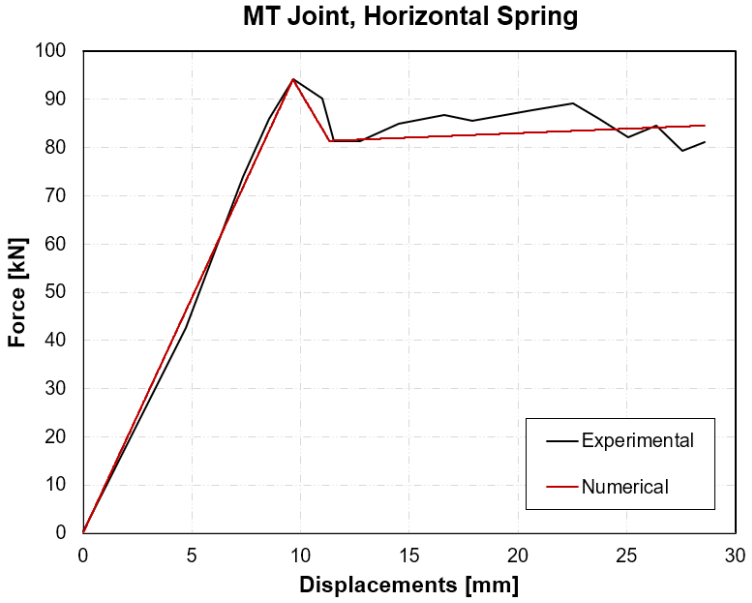

Figure 4.14F-δ curve of MT connection (shear test).

4.2 Half-lap cross-halved joints

Experimental tests on cross-halved (CH) joints were carried out at Sakata Laboratory of Tokyo Institute of Technology to characterize their moment resisting behavior (Dutu 2017). Timber elements were made of fir and cross-sectional dimensions are similar to those of Romanian CH joints, Table 4.7. The lower beam is fixed to the steel foundation by steel anchors with a diameter of 18 mm located at 100 mm from the beam ends to prevent uplift, while steel clamps at both ends avoid relative horizontal displacements, Figure 4.15. The setup consists of an actuator that applies horizontal static reverse cyclic loading at 600 mm from the beam, Figure 4.16. As already mentioned, applying the load just in one side may influence

the response of CH connections when the actuator pulls the post, resulting in non-symmetric hysteretic curve, black one in Figure 4.18. This is the reason why the calibration was performed taking as reference the curves in the 1st quadrant with positive forces and displacements.

Table 4.7 Dimension of tested CH specimen (in-plane cyclic test).

Specimen	Post Section [mm]	Beam Section [mm]	CH Thickness b [mm]
CH 1-6	120x105	160x105	52.5
Romanian CH	120x120	200x120	60

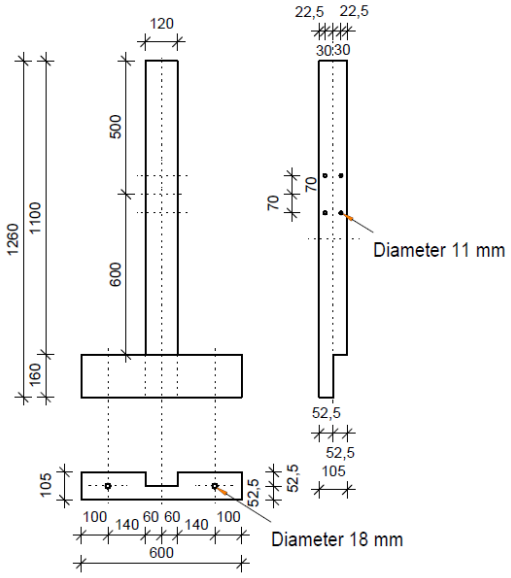

Figure 4.15 Geometry of CH connection (Dutu 2017).

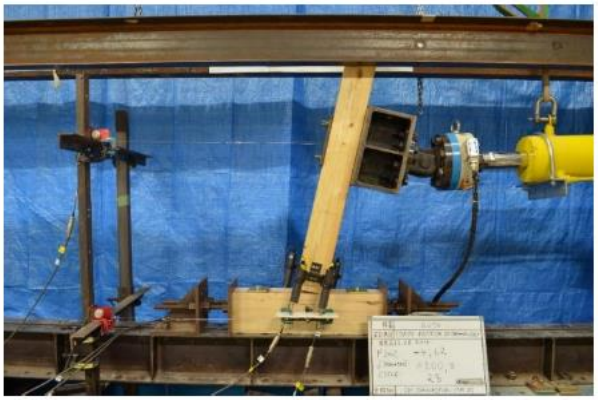

Figure 4.16 Test setup of CH connection (Dutu 2017).

Figure 4.17a shows the structural configuration modelled in OpenSees consisting of a linear elastic element with a rotational spring between nodes 1 and 2 that are constraint to have same horizontal and

vertical displacements. This spring represents the moment resisting behavior of CH connection with SAWS uniaxial material, Figure 4.17b.

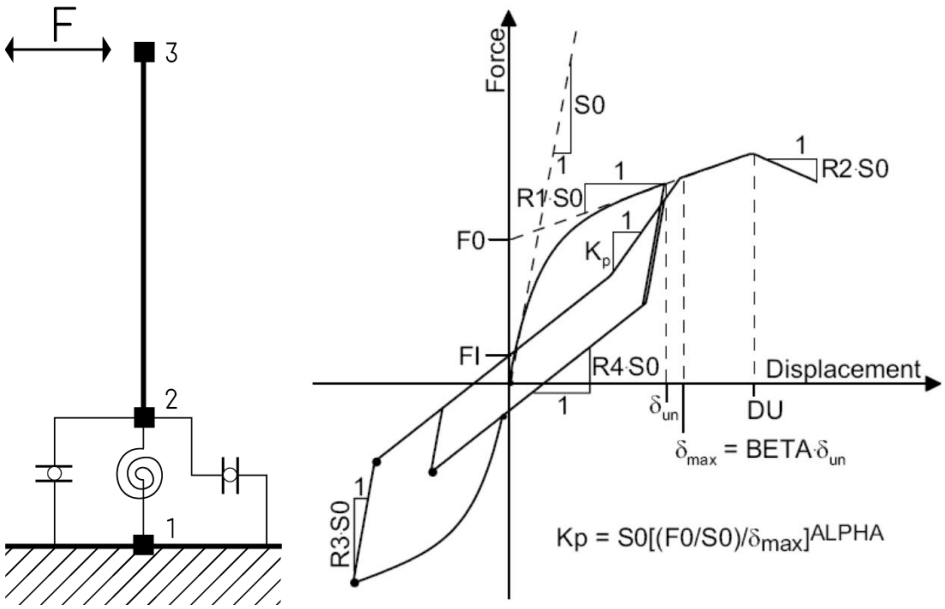

(a) **(b)**

Figure 4.17 Structural layout of in-plane cyclic test on CH joint in OpenSees (a) and SAWS material (b).

Overlapping the experimental and numerical hysteretic curves shows a good approximation in terms of reloading and unloading stiffness even in the last cycles. The cumulative error ranges from -100% for almost zero drifts (δ) to +13% for drifts around 30% with the numerical area exceeding the experimental one after around the 7% of δ due to the pinching effect, Figure 4.19b.

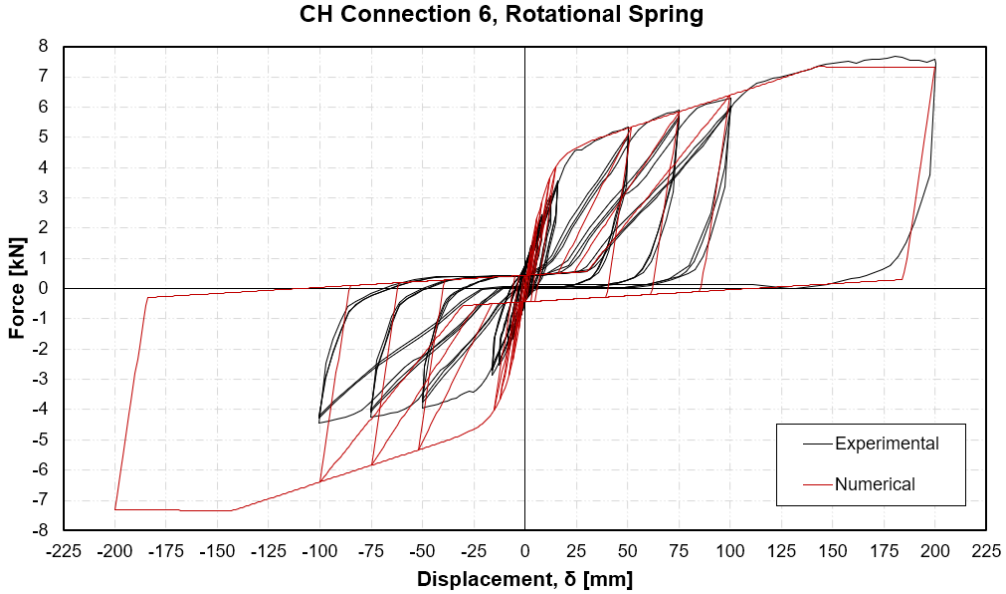

Figure 4.18 F-δ curve for CH connection 6 (in-plane cyclic test).

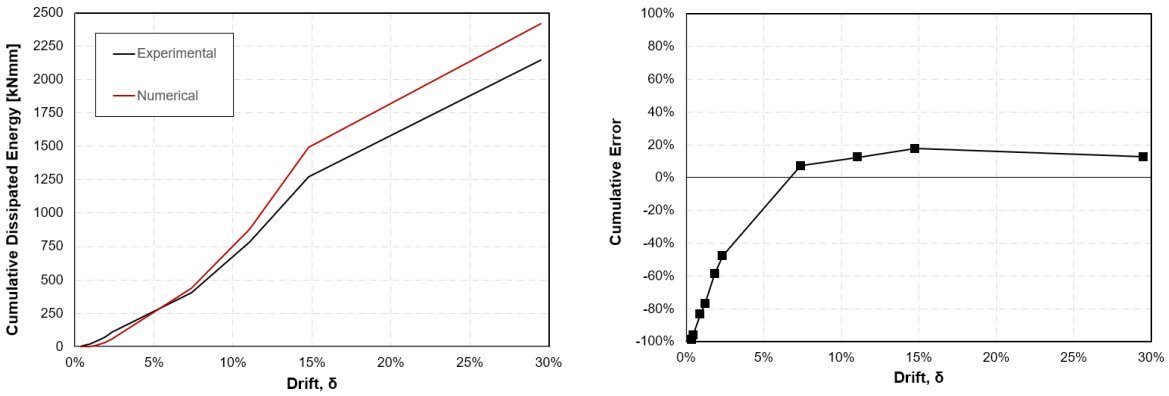

Figure 4.19 Cumulative dissipated energy (a) and cumulative error (b) for CH connection 6 (in-plane cyclic test).

Although the already explained connections are slightly different from those of the tested TFM walls in terms of geometry, element cross-sections, timber quality and level of accuracy during the construction, the resulting non-linear springs can be considered representative or at least a starting point for the following calibrations and updating since mortise and tenon and cross-halved joints are the connections in S1 wall. The two hysteretic uniaxial material *SAWS* and *Pinching4* permit to approach the measured response especially for initial stiffness, ultimate strength and deformation capacity, but, in terms of dissipated energy, good approximations can be obtained if some parameters such as reloading and unloading stiffness degradation match the experimental curves up to large deformations. However, these non-linear springs were initially applied to the joints of S1 wall and then their parameters were accurately updated to approach its global response and local measurements.

5 NUMERICAL MODEL OF ROMANIAN MASONRY WALL

The seismic behaviour of tested specimen S1 (masonry infill with lower bracings) was approached by modelling the panel in OpenSees and calibrating its response when subjected to monotonic and cyclic quasi-static in-plane horizontal loading. This response is mainly influenced by the connections between its elements which are also confined by the presence of masonry infill that limits their deformation capacity. The procedure of inverse fitting was performed to achieve a good approximation between the experimental hysteretic curve and the numerical one in terms of initial stiffness, maximum base shear and total dissipated energy. In the present section the structural scheme is described as well as the material properties applied to all the elements and especially the non-linear properties of the connections. In-plane pushover and cyclic quasi-static analysis were performed, and their results are presented and discussed to highlight pros and cons of the modelling strategy consisting of an equivalent frame with non-linearities lumped at the connections.

5.1 Geometry and Boundary Conditions

The geometry of S1 wall was simplified by modelling all the timber members with *elasticBeamColumn* elements aligned to their center axis and without representing the masonry infill that makes the panel stiffer even though it is made of mud bricks bonded with mud mortar. However, the assumption can be justified by the experimental results of Section 3 showing that the initial stiffness of the wall is mainly controlled by the presence and arrangement of timber bracings. Masonry has a role also in terms of energy dissipation since the friction between the frame elements and infill and also along masonry joints may increase it, but not significantly due to the low adherence between them with detachment from the very first cycle. Thus, its effect can be considered increasing the energy dissipated in the connections: in this case, area per cycle changes because of modification in slope of the initial and yielding stiffness and almost vertical unloading.

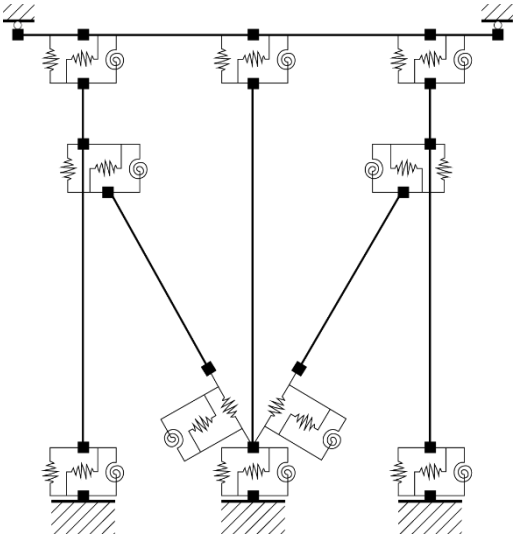

Figure 5.1 Structural scheme of S1 wall.

Figure 5.1 shows the structural scheme of S1 wall as well as its boundary conditions. The lower nodes 2, 4 and 8 are fixed since the bottom beam is constraint to the steel platform with no relative horizontal displacements between them. The pantograph system of the reaction frame was modelled by two sliding supports at the upper beam ends, nodes 22 and 24, which prevent any rotation. Moreover, the upper beams are modelled as rigid elements by applying them a large cross-sectional area (A = 10 m^2). Increasing the axial stiffness of the upper beam results in equal horizontal displacements for all the nodes 22, 24, 26, 28 and 29. The timber braces are modelled as *elasticBeamColumn* elements as well, but they can work just axially as explained in the following paragraphs, Section 5.3.3. In addition, they can slide vertically along the external posts, thus their vertical displacement is limited, but not prevented since they slid significantly (around 60 mm) along the vertical direction during the test, Figure 5.2a and b. However, there is no horizontal detachment between brace and external post, Figure 5.2a and b. Regarding braces' lower connections, they can detach if subjected to tension since the withdrawal capacity is very low and then return to their initial position in the reverse loading direction, Figure 5.3a and b.

(a) **(b)**

Figure 5.2 Vertical sliding along the post: initial (a) and final (b) position.

(a) **(b)**

Figure 5.3 Detachment along the diagonal axis: initial (a) and final (b) position.

The uplift of external vertical posts can be neglected since the transducers measured small uplifts until it worked properly, Figure 5.5. Figure 5.4a and b show the negligible vertical uplift of left post before measurement errors during the last cycles.

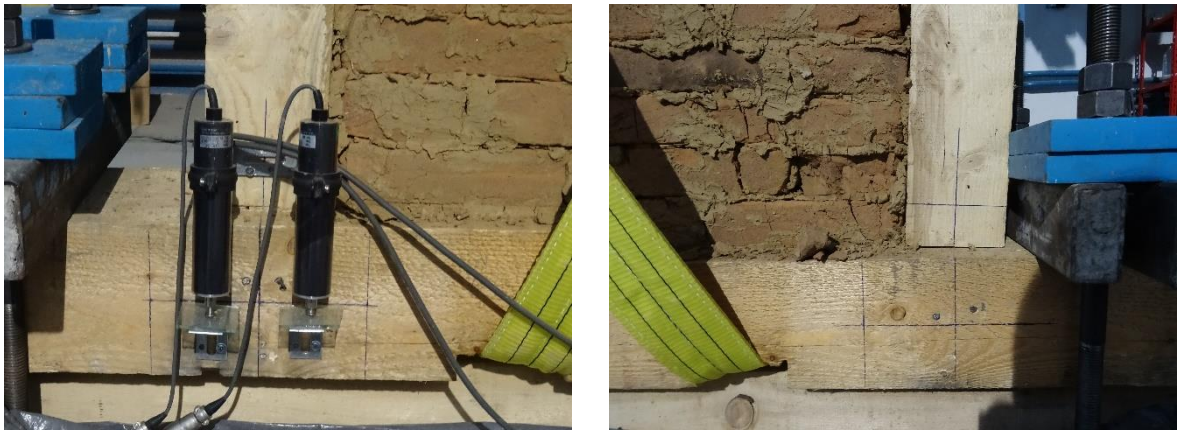

(a) **(b)**

Figure 5.4 External post uplift (a) and rotation (b).

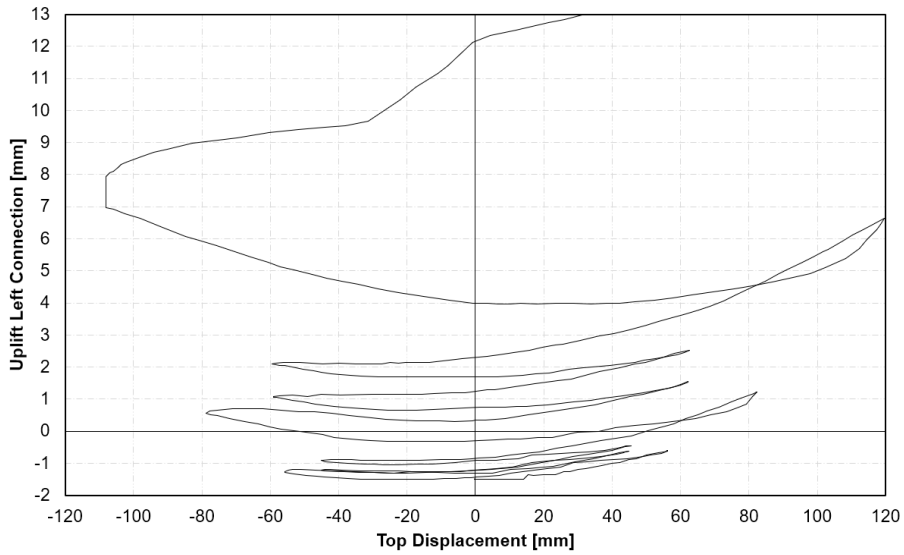

Figure 5.5 Measurement of external post uplift.

5.2 Material Properties and Loads

The weight of masonry infill was applied as point loads at the base, connection with diagonals and at the top height of the posts considering a specific weight of 19.6 kN/m^3 measured during an experimental test on comparable mortar at the Laboratory of Technical University of Civil Engineering Bucharest (UTCB) while timber elements (posts) have distributed load along their longitudinal axis with a specific weight of 385 kg/m^3. The weight of the upper beam was lumped at the nodes by determining equivalent vertical forces and concentrated moments. The total weight of S1 wall numerical model was compared with the one determined by hand calculations to check the reliability of the model. The error between them is negligible (less than 0.5%). Modulus of elasticity parallel to grain direction was set equal to 8.9 GPa in order to be conservative and consistent with the experimental test performed on similar timber batches, Section 3.1.

5.3 Connections

After defining geometry, material properties and loads, the upper and bottom connections were applied according to the previous calibration explained in Section 0 and carefully modified to consider the increase in stiffness due to masonry infill, different cross-sections of posts and beams, lack of dowel as fasteners and presence of gaps due to the construction process. In addition, they were recalibrated to approach the local measurements taken by the inductive transducers during the experimental test such as vertical displacements or rotations of the posts and, at the same time, the global response of the wall.

5.3.1 Mortise and Tenon Joints

The bottom mortise and tenon MT connections are modelled with three springs: the vertical and rotational ones are non-linear while the horizontal one is linear. The vertical springs consists of two different materials to characterize its tensile and compressive behavior. The tensile response was previously calibrated with *Pinching4* uniaxial material explained in Section 4.1, while the compressive part results from merging it in parallel with an *Elastic-No tension* uniaxial material with very high compressive stiffness (E = 10^{11} kN/m). This means that the compressive response is almost vertical with negligible displacements even for high forces to prevent the posts going through the bottom beam, Figure 5.6.

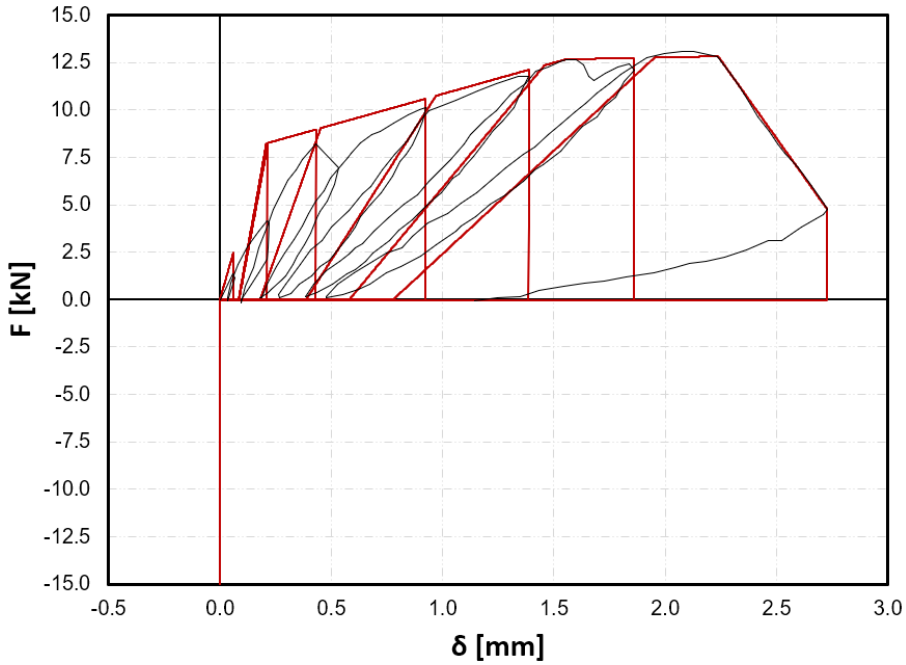

Figure 5.6 Parallel material consisting of Pinching4 in tension and elastic almost rigid in compression.

The pull-out strength was also determined as the characteristic load-carrying capacity for nailed timber-to-timber connections according to Eurocode 5 (EC5 2004).

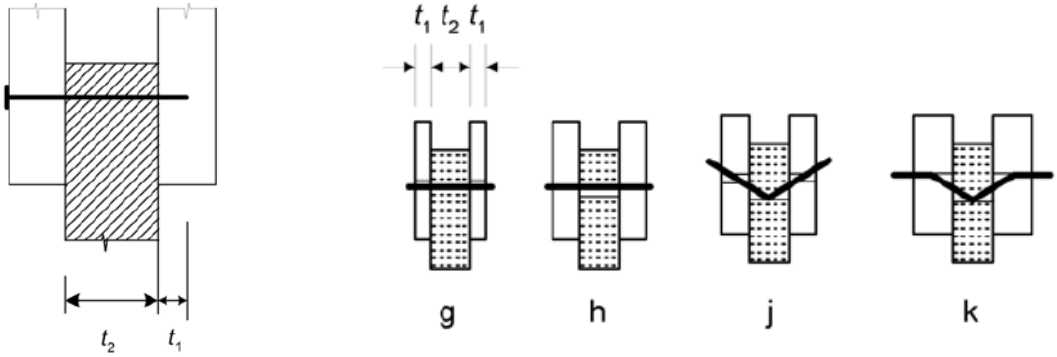

Figure 5.7 Double shear connection (a) and its failure modes (b) (EC5 2004)

The capacity per shear plane per fastener should be taken equal to the minimum of the following values of equation (3):

$$F_{v,Rk} = \begin{cases} f_{h,1,k} \cdot t_1 \cdot d & \text{(a)} \\ 0.5 \cdot f_{h,2,k} \cdot t_2 \cdot d & \\ 1.05 \cdot \frac{f_{h,1,k} \cdot t_1 \cdot d}{2+\beta} \left[\sqrt{2 \cdot \beta \cdot (1+\beta) + \frac{4 \cdot \beta \cdot (2+\beta) \cdot M_{y,Rk}}{f_{h,1,k} \cdot t_1^2 \cdot d}} - \beta \right] + \frac{F_{ax,Rk}}{4} & \text{(b)} \\ 1.15 \cdot \sqrt{\frac{2 \cdot \beta}{1+\beta}} \cdot \sqrt{2 \cdot M_{y,Rk} \cdot f_{h,1,k} \cdot d} + \frac{F_{ax,Rk}}{4} & \text{(c)} \\ & \textbf{(d)} \end{cases} \quad (2)$$

$$\beta = \frac{f_{h,2,k}}{f_{h,1,k}} \quad (3)$$

where $F_{v,Rk}$ is the is the characteristic load-carrying capacity per shear plane per fastener, t_2 is the central member thickness (tenon width is 80 mm) and t_1 the penetration depth (assumed as 40 mm); $f_{h,i,k}$ is the characteristic embedment strength in timber member i; d is the fastener diameter (6 mm); $M_{y,Rk}$ is the characteristic fastener yield moment; β is the ratio between the embedment strength of the members, equation (3), assumed equal to 1; and $F_{ax,Rk}$ is the characteristic axial withdrawal capacity of the fastener. The characteristic fastener yielding moment $M_{y,Rk}$ was determined by the equation (4) for round nails:

$$M_{y,Rk} = 0.3 \cdot f_u \cdot d^{2.6} \quad (4)$$

with f_u as the tensile strength of the wire considered as the minimum value of 600 N/mm^2. The characteristic load-carrying capacity for fasteners in double shear was around 8.94 kN considering the two plain nails for each connection. Although there are many uncertainties in the estimation of this value such as dimension of nails, its tensile strength and penetration depth, the ultimate capacity is comparable with the measured pull-out strength of 12.83 kN resulting from the experimental test by

Sakata (2012), thus the connection was not updated. Moreover, the calculated load-carrying capacity for fasteners in double shear of 8.94 kN represents the characteristic value with the fractile 5%, meaning that the experimental ones are likely to exceed this value with a probability of 95%.

The rotational spring of MT joints consists of *SAWS* uniaxial material, calibrated according to the experimental test of Section 4.1 and then modified in terms of initial and yielding stiffness as well as ultimate strength. These adjustments were required to consider the confinement effect of masonry infill and to match the envelope curve resulting from S1 test in terms of initial and yielding stiffness since the wall global response is mainly controlled by the upper and bottom rotational springs and the connections of the bracings.

Regarding the horizontal springs of MT connection, it was calibrated according to the experimental test of Section 4.1, but, since there is no relative sliding between post and lower beam, Figure 5.8, the spring was modelled as a linear elastic spring with high stiffness (E = 10^9 kN/m) to prevent any relative displacements between the fixed points and the bottom ends of the posts.

Figure 5.8 Negligible sliding between post and lower beam.

5.3.2 Cross-halved Joints

The upper cross-halved connections have three springs as well: the horizontal and vertical ones are linear, the rotational one is non-linear. The rotational spring of CH joints consists of *SAWS* uniaxial material, calibrated according to the experimental test of Section 4.2and then updated in terms of initial and yielding stiffness as well as ultimate strength. These modifications were performed for the same reason explained for the MT rotational springs such as confinement effect of masonry infill, Section 5.3.1, and to approach the envelope curve resulting from S1 test in terms of initial and yielding stiffness. The two linear springs were modelled with *Elastic* uniaxial material with high stiffness (E = 10^9 kN/m) to avoid any relative horizontal or vertical displacement between the upper beam and the posts, Figure 5.9.

Figure 5.9 Negligible sliding between post and upper beam.

5.3.3 Bracing Joints

Since the stiffness of the wall is mainly controlled by diagonal elements, their connections were calibrated accurately to match the global envelope and, at the same time, by checking two parameters: vertical sliding along the external posts and diagonal detachment from the central lower connection. Thus, the upper and lower connections differ in their alignment: the first ones are consistent with the global axis (red) while the lower ones are aligned along the center axis of the diagonals (green), Figure 5.10.

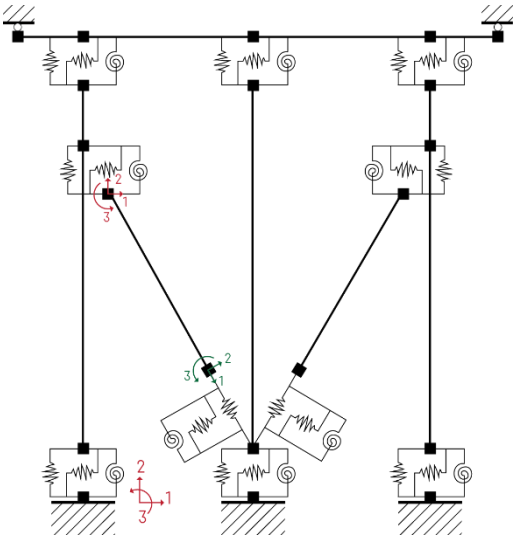

Figure 5.10 Global and local axis of diagonal elements.

The upper joint with external posts has three springs: two linear, horizontal and rotational, and one non-linear, vertical. The horizontal spring was modelled with *Elastic* uniaxial material with high stiffness (E = 10^9 kN/m) to have equal horizontal displacements between nodes 17 and 18, while the elastic stiffness of the rotational spring (*Elastic* uniaxial material) was fixed at 10^{-3} kNm/rad resulting in negligible transfer of bending moments to represent the behavior of truss elements. The calibration of the elastic stiffness related to the non-linear vertical spring was performed iteratively by comparing the experimental global

response of the wall subjected to in-plane horizontal loading with the numerical one as well as controlling the sliding along the external post. This inverse fitting ended with an elastic stiffness of 846 kN/m that was applied to the *Pinching4* uniaxial material with almost vertical unloading, Figure 5.11. The choice of this hysteretic material can be supported by the photos taken during the experimental test showing significant vertical sliding that increase the total dissipated energy through friction and yielding of the nails, Figure 5.2.

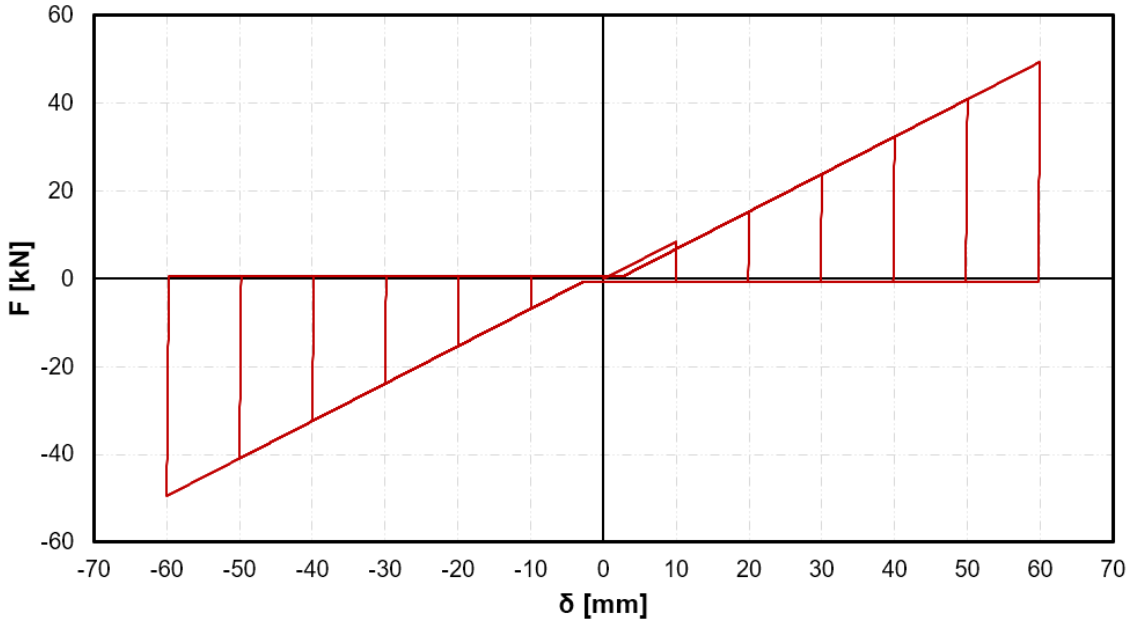

Figure 5.11 Pinching4 material applied to the verical non-linear spring of diagonal elements.

Regarding the central lower connection between diagonals and post, it was modelled with three linear springs: the one oriented with the bracing center axis has an *Elastic-No Tension* uniaxial material with high stiffness (E = 10^{11} kN/m) to prevent the diagonals going through the post, the one perpendicular to the axis has the same elastic stiffness applied to an *Elastic* uniaxial material, the rotational one has the same properties of the upper diagonal connection with low stiffness (E = 10^{-3} kNm/rad) to prevent bending moment transmission. Neglecting the tensile behavior of the lower connection was decided after determining the withdrawal capacity for slant nailing according to the EC5 (2004), Figure 5.12.

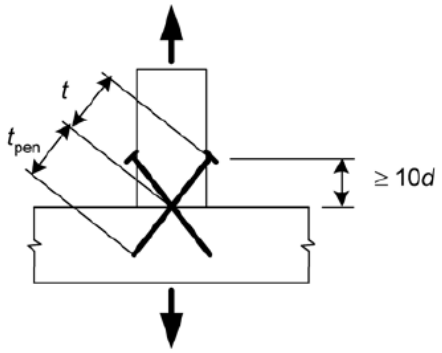

Figure 5.12 Slant nailing (EC5 2004).

This connection type can be considered comparable with the one between bracings and vertical post with smooth nails on both sides of the member. The characteristic withdrawal capacity of smooth nails $F_{ax,Rk}$ can be determined as the minimum of the following values, equation (5):

$$F_{ax,Rk} = \begin{cases} f_{ax,k} \cdot d \cdot t_{pen} \\ f_{ax,k} \cdot d \cdot t + f_{head,k} \cdot d_h^2 \end{cases} \quad (5)$$

where $f_{ax,k}$ is is the characteristic point side withdrawal strength, $f_{head,k}$ is the characteristic headside pull-through strength, d is the nail diameter, t_{pen} is is the pointside penetration length or the length of the threaded part in the pointside, t is the thickness of the head side member and d_h is the nail head diameter. Since there is no information about characteristic point side withdrawal strength and head side pull-through strength the following expressions (6) and (7) were used to determine them:

$$f_{ax,k} = 20 \cdot 10^{-6} \cdot \rho_k^2 \quad (6)$$

$$f_{head,k} = 70 \cdot 10^{-6} \cdot \rho_k^2 \quad (7)$$

where ρ_k is the timber density in kg/m^3. The two characteristic strengths were eventually multiplied by a coefficient considering that the point side penetration was smaller than $12d$. The dimensions of the nails are 6x100 mm and the point side penetration t_{pen} was assumed equal to the thickness of headside member t. The resulting characteristic withdrawal capacity was $F_{ax,Rk} = 0.0741\ kN$ that can be neglected as already mentioned.

5.4 Pushover analysis

Non-linear static analysis was performed before cyclic analysis to approach the global response in terms of initial and first yielding stiffness without considering stiffness and strength degradation related to cyclic loading.

After applying gravity loads and setting them to constant, the central control node 26 was pushed horizontally until 120 mm with displacement increments of 10^{-2} mm. Thus, the analysis was carried out

under displacement control algorithm using energy increment convergence test. This means that the inner product of the unbalanced load and displacement increments at each iteration should be lower than a certain tolerance fixed at 10^{-4}. Before running non-linear static analysis, the envelope of the experimental hysterical curve should be determined to have an upper bound comparable with the resulting numerical pushover curves. The first quadrant with positive displacements and base shear forces is taken as reference to define this envelope. Therefore, initial and first yielding stiffness were estimated considering the slope of the third cycle as the reference value for initial stiffness to neglect the behavior of the first cycles highly influenced by testing equipment's problems. Regarding the first yielding stiffness, its slope was determined by connecting the maximum base forces per main cycles except the one related to the horizontal displacement of 82 mm and the last cycle. As already mentioned, the imposed displacement of 82 mm is considered too close to the previous one (73.4 mm) according to the loading protocol and resulting in lower base force, thus it was neglected. The base force related to the last cycle was neglected as well because the damage increased significantly with stiffness and strength degradation after many repeated cycles also during the second testing phase.

An iterative inverse fitting was performed to approach the envelope by modifying the initial stiffness of the non-linear rotational springs of cross-halved and mortise and tenon connections and also the stiffness of the vertical non-linear spring in the upper connection between post and bracings until both initial and first yielding stiffness of the global response were comparable with the experimental curve. Figure 5.13 shows a good approximation between the pushover curve and the envelope of the experimental hysteretic curve except for the last main cycle. The slope of this second yielding branch can be controlled by strength and stiffness degradation of the connection during the in-plane cyclic analysis.

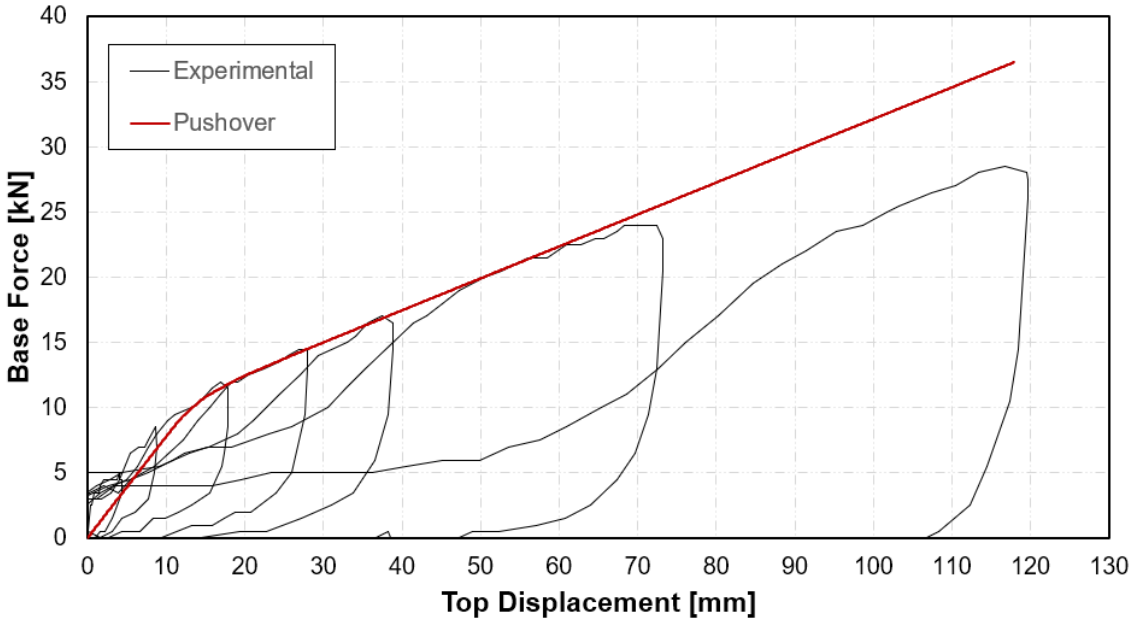

Figure 5.13 S1 pushover curve overlapped with experimental hysteretic curve.

Since the external vertical loads were not constant during the test with a maximum variation of +15% (30 kN) and -38% (16 kN) of the reference value (26 kN), three different pushover analysis were performed to understand its influence on the global response. The resulting curves are basically overlapped with no relevant influence in the global response due to the intrinsic properties of the adopted uniaxial hysteretic materials, *SAWS* and *Pinching4*.

5.5 Cyclic analysis

In-plane cyclic non-linear analysis was eventually carried out to better approximate the behavior of S1 wall when subjected to reversed cyclic quasi-static loading. In this case, strength and stiffness degradation per cycle influences significantly the global response, thus an updating on connections parameters was required.

All the settings for non-linear cyclic analysis are equal to those defined for pushover analysis. However, a vector of displacement-cycle peak was fixed according to the imposed experimental displacements neglecting the already mentioned displacement of 82 mm. This vector consists of maximum positive horizontal displacements applied by the jack. Full cycles were set even though the vector of imposed displacement-cycle peaks is not perfectly symmetric for negative and positive values in the experimental loading protocol. This means that the dissipated energy between experimental and numerical curves is not perfectly comparable. In addition, this comparison is influenced by the vertical shifting of experimental hysteretic curve which may be caused by a slightly misalignment of S1 specimen with the reaction frame during the first testing phase.

A first trial with the updated set of connections applied for pushover showed that a new set of non-linear rotational springs for cross-halved and mortise and tenon connection were required since they control the wall global response as well as bracing connections. Thus, MT and CH connections were updated due to the stiffness and strength degradation per cycle of *SAWS* uniaxial material. The experimental hysteretic curve was approached by modifying the rotational non-linear springs of these connections in terms of yielding stiffness and intercept strength of the asymptotic line to the envelope curve. Figure 5.14 shows the final numerical curve compared with the experimental one with a good approximation in terms of maximum base shear per displacement-cycle peak and reloading stiffness. The main differences are related to the pinching effect and unloading stiffness which is comparable and almost vertical up to a point where changes its slope becoming less inclined.

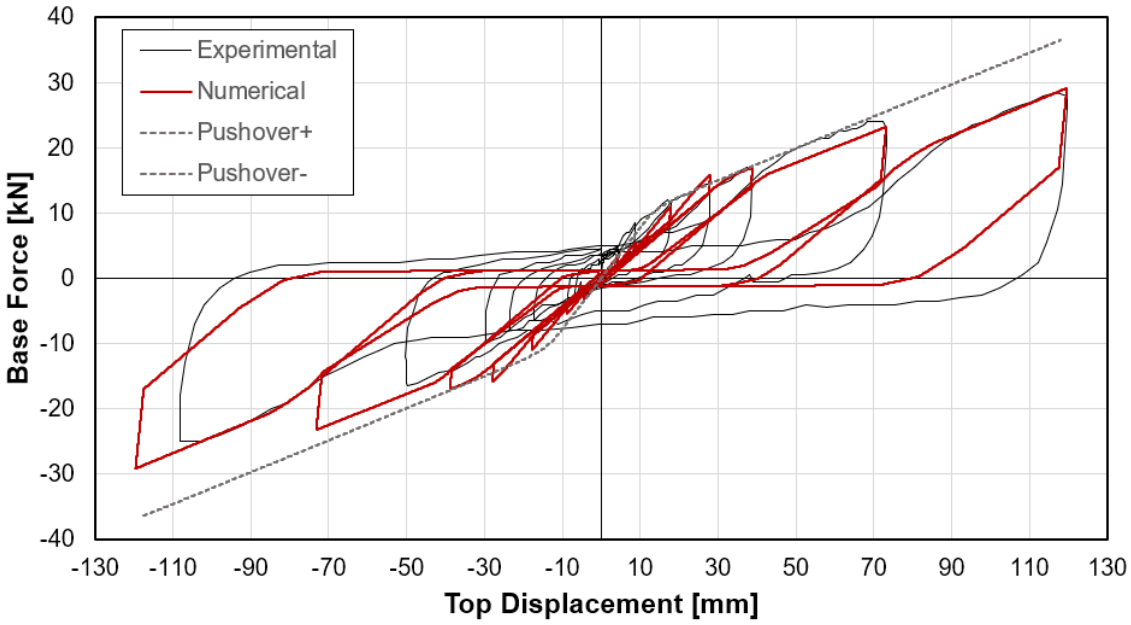

Figure 5.14 S1 cyclic analysis overlapped with experimental hysteretic curve.

Figure 5.15a shows the cumulative dissipated energy and error between the two curves. The cumulative error ranges from -89% for negligible drifts to -36% for the maximum one (5.43%) with the numerical area always smaller than the experimental one due to the pinching effect and the vertical unloading of the experimental cycles. This depends on the physical behavior of the wall that returns instantly to its original position with no pressure by the horizontal jacks while the numerical model needs to be pushed to reach its starting condition.

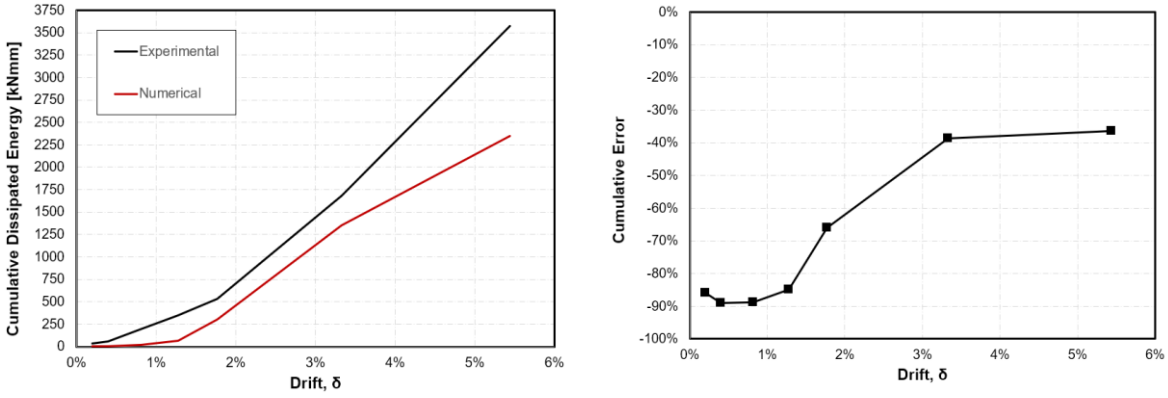

(a) **(b)**

Figure 5.15 Cumulative dissipated energy (a) and cumulative error (b) for S1 wall cyclic test.

The equivalent frame model before and after the application of vertical loads is shown in Figure 5.16a and b. Figure 5.17 shows the deformed shape of S1 wall with the expected behavior of diagonal bracings. The vertical sliding along the post is 63 mm, which is compatible with the experiment's photos, Figure 5.18, while the observed diagonal detachment is lower than the numerical one (88-107 mm), Figure 5.19. This is due to the *Elastic-No Tension* material applied to the central lower connection and also on the stiffness of the upper vertical spring related to bracing-to-post connection, which was

calibrated by assuming a vertical sliding around 65 mm according to the photos, but there are no actual measurements.

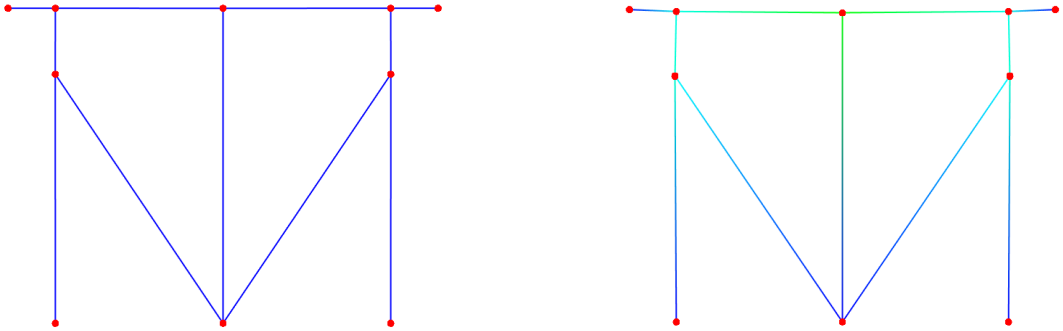

(a) **(b)**

Figure 5.16 Undeformed (a) and deformed (b) shape just under vertical loads.

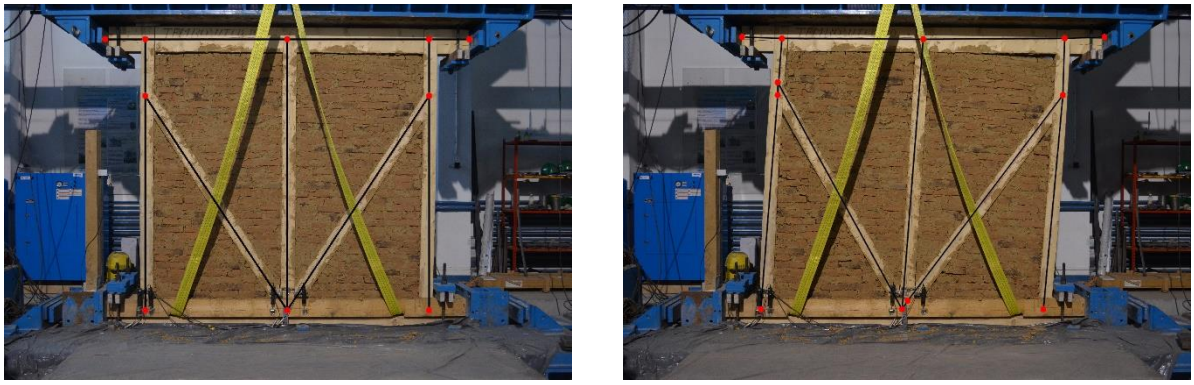

(a) **(a)**

Figure 5.17 Initial step (a) and final one (b) during in-plane cyclic test.

Figure 5.18 Vertical sliding along the post: initial and final position.

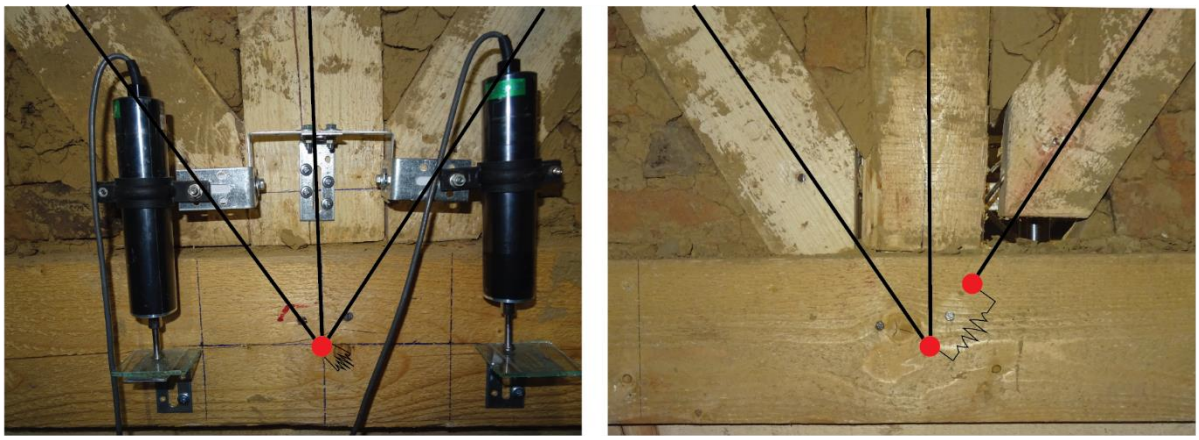

Figure 5.19 Detachment along the diagonal axis: initial and final position.

5.6 Final Remarks

The calibration of the global and local response of S1 wall was performed by following an iterative procedure of inverse fitting, starting from a preliminary calibration of the joints of the walls based on existing experimental results on carpentry joints similar to those adopted in the wall specimen. This method has some pros and cons such as it is time-consuming since it is not automatic, but allows to understand which are the main connections and non-linear springs parameter that control both global and local behaviour. It is worth to point out that both pushover and cyclic analysis are connection-dependant since *Pinching4* and *SAWS* non-linear hysteretic uniaxial material have parameters that govern reloading stiffness and strength degradation per cycle. *SAWS* material in particular has stiffness degradation intrinsic to its definition since this slope *Kp* is not a separate parameter, but depends on initial stiffness S0 and intercept strength for the asymptotic line to the envelope curve F0 and the stiffness degradation parameter alpha. The differences between the two curves are due to some limitations of the numerical model such as vertical unloading stiffness and pinching effect and also some issues during the testing phases such as the initial misalignment of the wall, the non-symmetric displacement-cycle peaks and cyclic stiffness and strength degradation caused by the repeated cycles of the second testing phase. Additional local measurements were required to better characterize the behaviour of the diagonal elements in terms of vertical sliding along the external posts and axial detachment. Thus, the results are not completely accurate, but still comparable, especially regarding the global envelope and most of the local measurements or photos taken during the test.

Nevertheless, the calibration of the wall is considered to be a good fit to the experimental results, and it may and will be used for the analysis of a whole TFM building with the same wall configuration.

6 DESCRIPTION OF A REPRESENTATIVE ROMANIAN TFM BUILDING

In the present section, a Romanian TFM building was studied and characterized in terms of geometry, structural elements, construction details as well as state of conservation to make a consistent numerical model capable of simulating its seismic behavior. The case study can be considered representative of the Romanian TFM structural typology in the Sarbova area, Timis county, to an extent that it was dismantled and rebuilt in the National Village Museum, Bucharest. Moreover, it was the first Romanian TFM building to be subjected to ambient vibration testing and analyzed in its dynamic properties (Pn-iii-p- et al. 2017).

The studied TFM building was a residential house built around 1900-1930 with just one floor and an attic under the roofing system. Although many structural features are similar to the Romanian TFM typology, *paianta,* there are some discrepancies due to the expertise of local builders such as foundation type, arrangement of diagonal elements and roofing system.

6.1 Geometrical Survey

The field investigation was performed and the geometrical dimensions are presented in the following drawings re-elaborated from those by Technical University of Civil Engineering Bucharest as well as their description. Figure 6.1a and b show the building with a rectangular shape of around 11.50x6.00 m but not completely symmetric in plan with respect to the longitudinal and transversal axis since the central space is slightly shifted to the right, Figure 6.2. Moreover, timber posts are not always aligned between parallel walls, possibly due to architectural reason and the presence of openings, Figure 6.2. An average usable height of 2.3 m was measured while the attic one ranges from 0 to 3 m of roof ridge.

(a) **(b)**

Figure 6.1 Romanian TFM building: front (a) and back (b) side view.

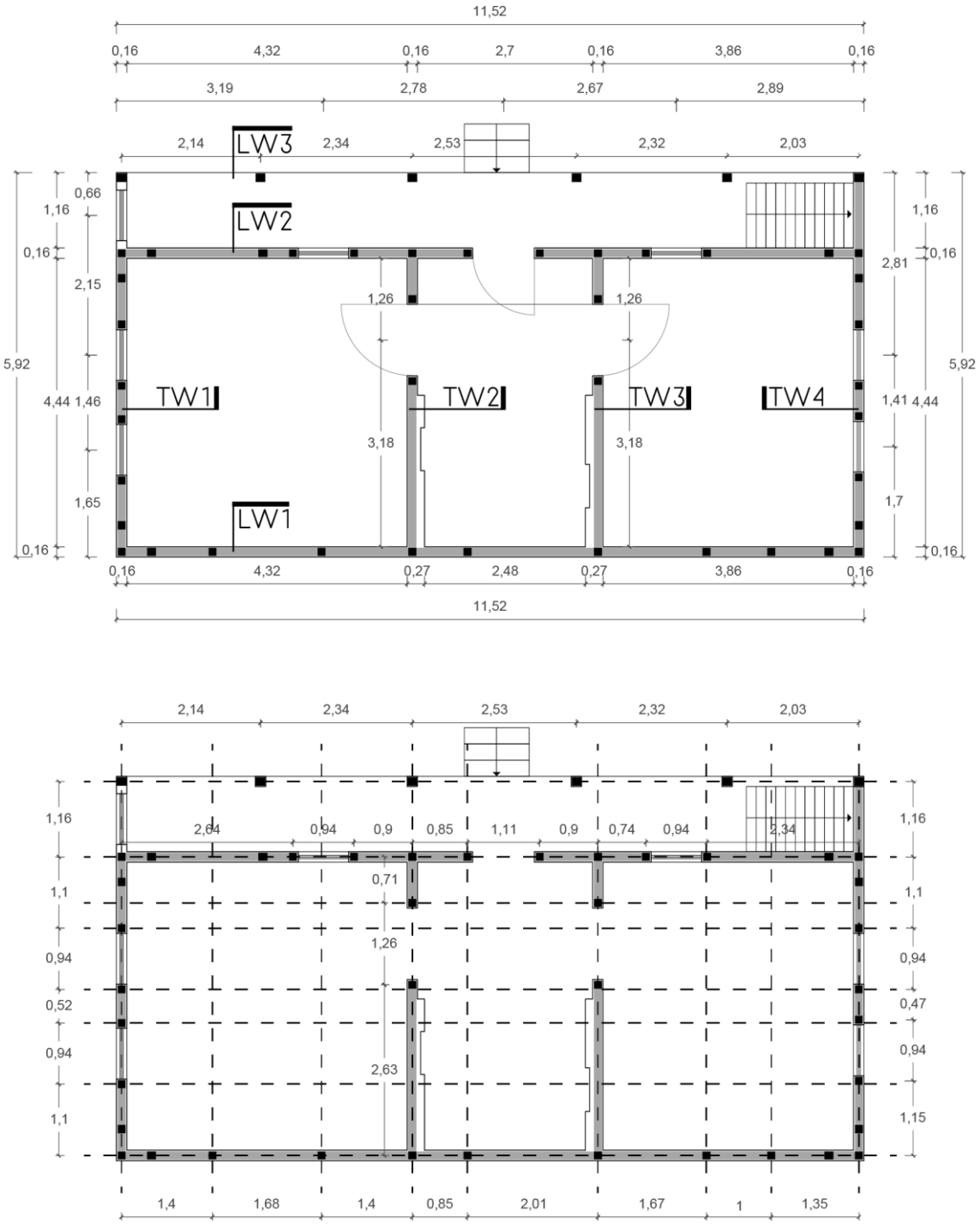

Figure 6.2 Plan configuration and structural layout.

The house is raised from the ground to avoid moisture related issues; thus, the portico is accessible by a stair with few steps made of brick masonry, Figure 6.3a. The central space may be used as living room or kitchen since there was a fireplace located close to the longitudinal wall LW1 which was not rebuilt in its position after the dismantling, Figure 6.3b and c (Pn-iii-p- et al. 2017).

(a) **(b)** **(c)**

Figure 6.3 Masonry stairs (a), central room (b) with the original chimney (c).

The left and right spaces have similar dimensions in plan and may be both bedrooms. Regarding the openings, the external transversal wall TW1 and TW4 present a non-symmetric layout, while the internal ones TW2 and TW3 have the same configuration, Figure 6.4a, c and b respectively. Longitudinal walls are not symmetric as well: LW1 has no openings may be due to its original orientation, LW2 shows three openings not perfectly centered, Figure 6.5a and b respectively.

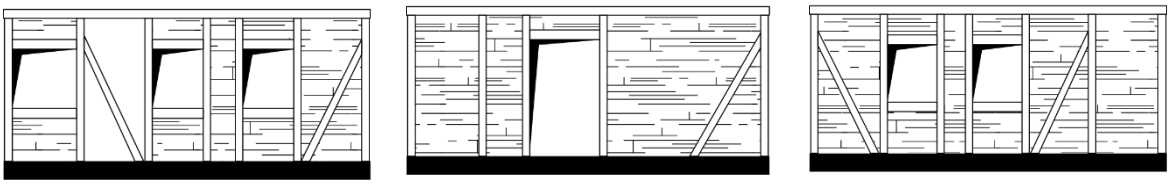

(a) **(b)** **(c)**

Figure 6.4 Elevation of TW1 (a), TW2 and TW3 (b), TW4 (c) wall.

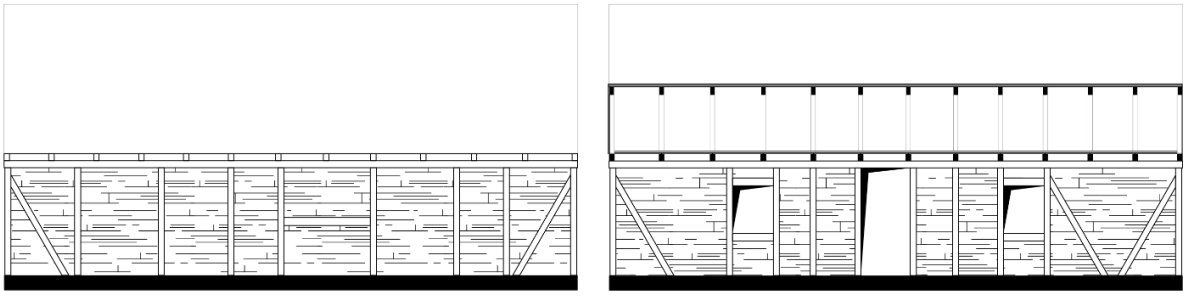

(a) **(b)**

Figure 6.5 Elevation of LW1 (a) and LW2 (b) wall.

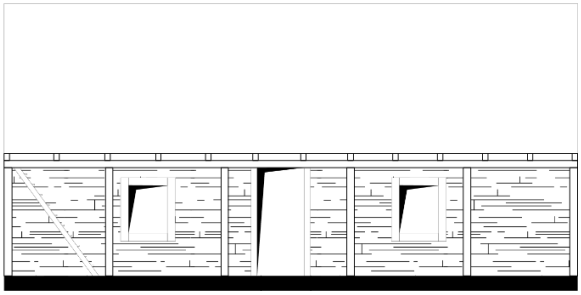

Figure 6.6 Elevation of LW3 wall or portico.

A non-habitable attic, located under a gable roof with a steep slope to avoid snow accumulation, is accessible by an external stair in the portico, Figure 6.7a. The chimney made of clay brick masonry can be observed in this space and its non-symmetric location and heavy mass may influence the global response of the building, Figure 6.7b.

(a) **(b)**

Figure 6.7 External stair (a) and chimney in the attic (b).

6.2 Structural Elements

The structural members are characterized to better understand their role, construction details as well as their connections to make a consistent numerical model based on educated assumptions.

6.2.1 Foundations

Foundations are shallow type with a continuous wall-footing made of brick masonry supporting the TFM upper structure, but its dimensions were not measured thus a thickness of around 50 cm was assumed (Pn-iii-p- et al. 2017). TFM walls rest on a beam made of hardwood (oak or acacia) with a width of about 240 mm just above the brick masonry foundations, Figure 6.8a. This beam has the role to distribute more uniformly the vertical loads and was made up of hardwood to increase its service life preventing premature rotting. Figure 6.8b shows the foundation layout that is non-symmetric with respect to both longitudinal and transversal axis.

(a)

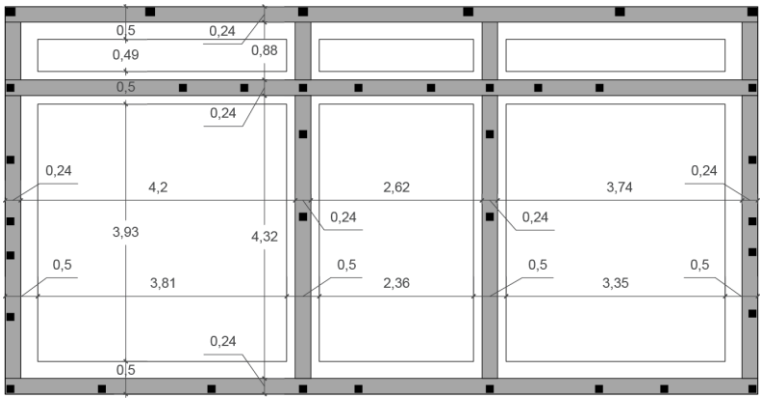

(b)

Figure 6.8 Lower beam (a) and foundation plan configuration (b).

6.2.2 Wall

TFM walls show the typical features of Romanian traditional typology but there are some differences such as the arrangement of bracings. Timber frame consists of vertical posts made of softwood (Romanian fir) located along the walls with no fixed spacing between them. Moreover, they can be found at the corner between orthogonal walls and on both sides of the openings framed with timber lintels. It is worth to point out that diagonal elements are not always constrained by two consecutive vertical posts thus they may slide horizontally at the base if the connections do not work properly, Figure 6.5. A unique horizontal beam can be observed at mid-height of the central posts of LW1, but the resulting frames are both completely infilled, Figure 6.9. The average thickness is around 16 cm; thus, a layer of plaster is applied on both sides to cover the timber skeleton (Pn-iii-p- et al. 2017).

(a)

(b)

Figure 6.9 Timber frame skeleton (a) and diagonal element (b).

6.2.3 Floor

The horizontal diaphragm consists of timber beams made of hardwood (oak) and a layer of processed planks and mud plus straw with thickness of 25 and 30 mm, respectively (Pn-iii-p- et al. 2017). Primary beams are aligned along the transversal direction and transmit loads to the secondary beams on top of each longitudinal wall LW1, LW2 and LW3, Figure 6.10. Their cross-sectional area is about 110x140 mm. Since the presence of the chimney made of clay brick masonry increases greatly the loads, an additional longitudinal beam was applied in the central part between transversal wall TW2 an TW3, Figure 6.11a and b.

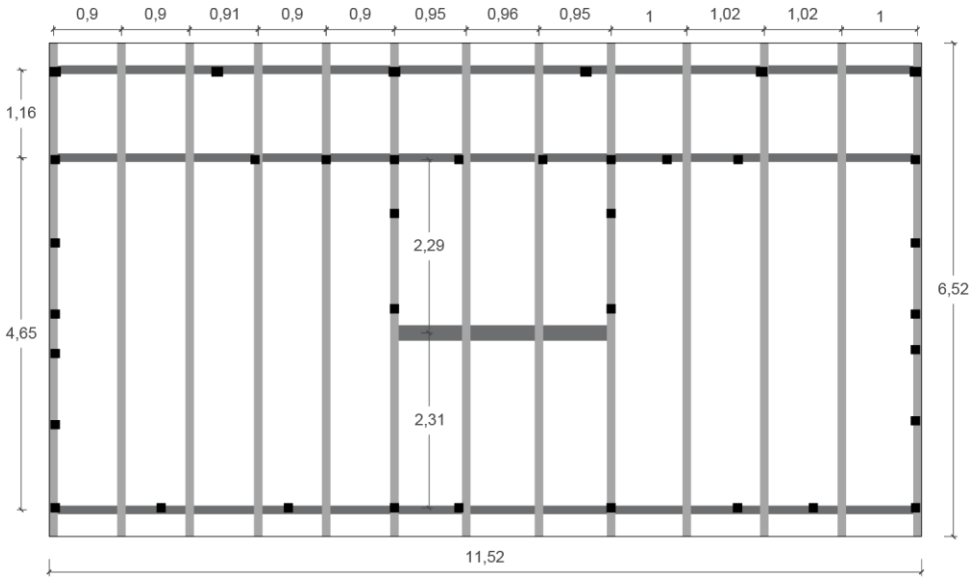

Figure 6.10 Structural layout of the floor.

(a) **(b)**

Figure 6.11 Primary beams with timber planks (a) central transversal beam (b).

6.2.4 Roofing system

The roof structure is made up of timber as well. Its frame can be considered a porch type with loads transmitted to the longitudinal wall LW1 and LW3. The roofing system consists of rafters with a cross-section of around 90x120 mm and a spacing ranging from 90 to 102 cm which support longitudinal timber strips (45x30 mm) nailed to them and applied to fix the upper ceramic tiles, Figure 6.13a. Diagonal bracings can be also observed in the fields of the roof to increase their in-plane stiffness, Figure 6.13b.

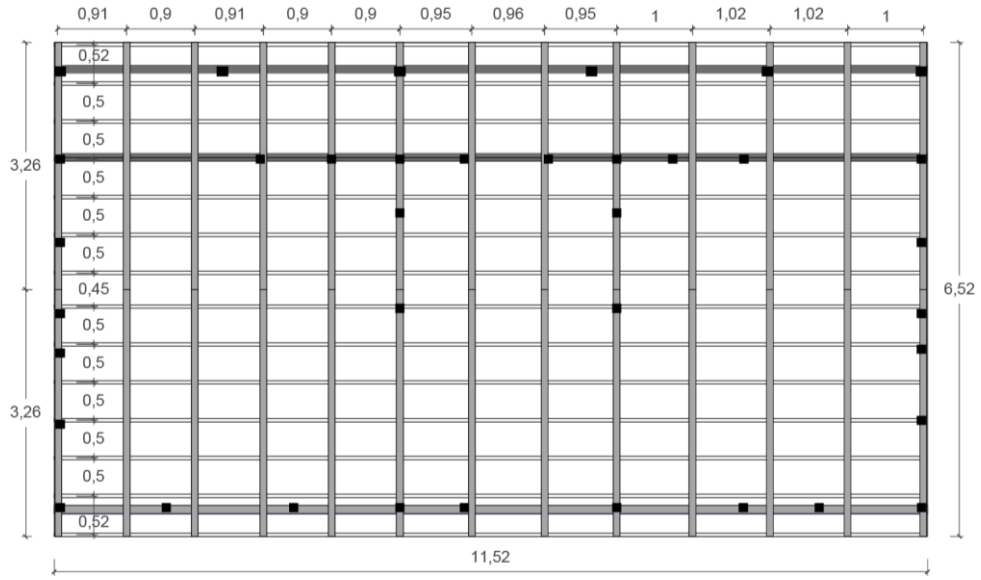

Figure 6.12 Roof plan configuration.

(a) **(b)**

Figure 6.13 Roof detail (a) and diagonal element (b).

6.2.5 Connections between Structural Elements

The connections between timber elements are similar to those observed during the field investigation explained in Section 0. Vertical posts are driven into the lower beams with mortise and tenon joints, while the latter are half-lap splice type, Figure 6.14a and b respectively. The connections between lower beams and foundations are not visible but it appears that timber elements are laid inside grooves in the continuous wall-footing to prevent any sliding, Figure 6.14c.

(a) **(b)** **(c)**

Figure 6.14 Mortise and tenon (a), half-lap splice (b) and connection with masonry foundations.

Diagonals are likely to be simply connected with nails to vertical posts as well as lintels, Figure 6.15. Sometimes bracings were used as a propping system during the construction process resulting in fast and unprocessed connections (Dutu et al. 2018b).

(a) **(b)** **(c)**

Figure 6.15 Connections between posts and diagonal elements (a) or lintels (b).

Cross-halved joints can be observed between primary and secondary beams of the horizontal diaphragm but also between rafters and diagonals on the roof fields, Figure 6.16a and b respectively. Timber rafters seems to be connected by bridle joints, Figure 6.16c.

(a) **(b)** **(c)**

Figure 6.16 Cross-halved connection between floor (a) and roof (b) members, bridle joint between rafters (c).

6.3 State of Conservation

The building is poorly maintained and showed biological colonization, coloration, minor cracks due to stress concentrations and moisture related problems leading to irreversible decay of timber elements, Figure 6.17a, b, c; Figure 6.18a and b. Moreover, other cracks can be found may be due to different construction phases between timber frame and infill or due to the excessive shrinkage of infill, Figure 6.18c.

(a) **(b)** **(c)**

Figure 6.17 Biological colonization (a), coloration (b) and moisture related problems (c).

(a) **(b)** **(c)**

Figure 6.18 Minor cracks (a), detachment of plaster (b) and crack of masonry infill (c).

Detachment of masonry infill with minor cracks can be observed due to the different physical and mechanical properties between the two materials, Figure 6.19c. Indeed, this mechanism is not prevented despite a reinforced plaster was applied to increase the deformation capacity of mortar reducing the crack width and propagation, Figure 6.19a and b.

(a) **(b)** **(c)**

Figure 6.19 Reinforced render along post (a) and beam (b), and its detachment (c).

Figure 6.20a and b show the arrangement of timber elements even if there is a coat of render to cover them. This phenomenon is evident especially in the back side of the house, LW1 wall, may be due to its orientation that does not let the timber dry.

(a) **(b)**

Figure 6.20 Moisture-related problems in TW4 (a) and LW1 (b) walls.

6.4 Dynamic Identification

The Romanian TFM building was subjected to dynamic identification to obtain natural frequencies on both longitudinal and transversal direction. The setup and output-only measurements are described and discussed in the following paragraphs.

6.4.1 Test method and instruments

The TFM building was tested under ambient vibration on November 24th, 2017, at an ambient temperature of 6°C without wind. This technique is based on output-only measurements to estimate the modal parameter of the structure. Figure 6.21a and b show the acquisition system and velocity sensors respectively; they were made by Buttan Service-Tokyo & Tokyo Soil Research Co., Ltd., Japan. The measurements were taken by setting six schemes of one direction velocity sensors CR4.5-1. GEODAS station was used as acquisition system, Figure 6.21a, with 3 or 12 channels, frequencies of sampling are 50, 100, 200, 500, 1000, 2000 Hz, and the following features related to digital to analogic conversion: resolution 24 bits, conversion speed 50 Hz and maximum input voltage ±2.5 V. When taking measurements, it is recommended to operate in a certain range of temperature and humidity such as 10-45°C and 20-80% respectively. Regarding the microtremor sensors, they are mobile velocity seismometer with just one vibration component in the horizontal direction with a sensitivity of 1 cm/s or 0.0338 V and a frequency domain ranging from 1 to 20 Hz (Pn-iii-p- et al. 2017).

(a) **(b)**

Figure 6.21 GEODAS acquisition system and velocity sensors CR4.5-1.

As already mentioned, six measurement schemes with 5 sensors were set to obtain reliable results. Four velocity sensors were located at the floor level and one on the ground just in front of the building. All the sensors were connected to the acquisition system by cables ensuring a simultaneous record of ambient vibrations for all the reference points. Two data samples for each scheme were recorded with a duration of 3 minutes and a sampling frequency of 100 Hz corresponding to 0.01 s (Pn-iii-p- et al. 2017).

Scheme 1

The first scheme is aimed at studying the transversal direction of the building; thus, all the sensors are oriented along this axis, Figure 6.22. The sensors are located on the attic floor except the fourth one that is in a position above it. Ch01 velocity sensor is aligned along TW4, Ch02 in front of the chimney, Ch03 aligned along TW2 just above the vertical post framing the door, Ch04 aligned along TW1 on the

window of the upper masonry wall. The fifth one is located on the ground close to the portico. Figure 6.23a and b show the Fourier amplitude spectra recorded per measurement sample by each sensor (Pn-iii-p- et al. 2017).

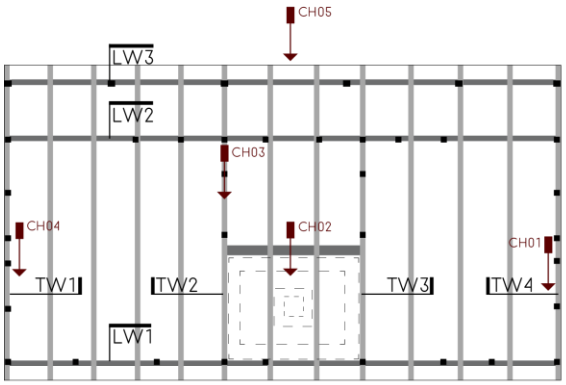

Figure 6.22 Position of velocity sensors in plan of scheme 1.

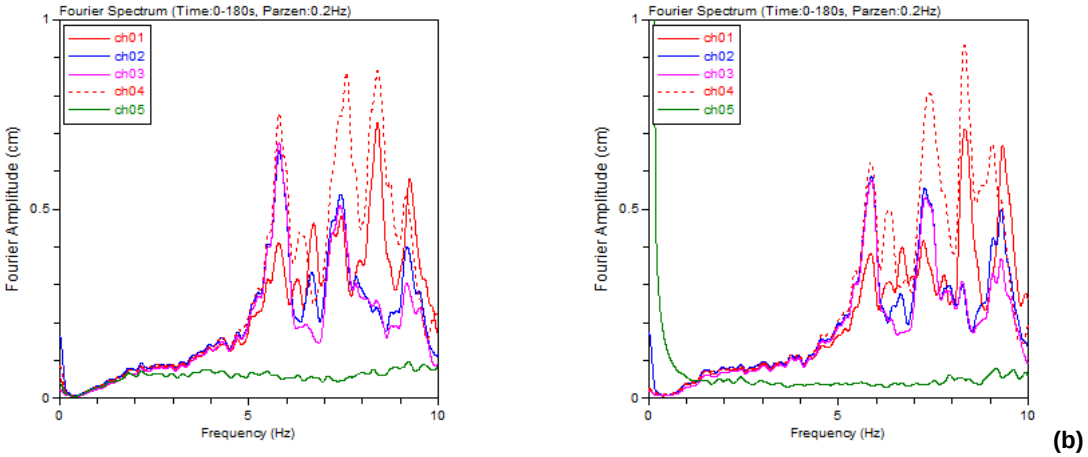

Figure 6.23 Fourier amplitude spectra sample 1 (a) and 2 (b) of scheme 1.

Scheme 2

The second scheme was set to study the longitudinal direction of the building; thus, all the sensors are oriented along this axis, Figure 6.24. The sensors are located in the same position of scheme 1 but rotated by 90°. Figure 6.25a and b show the Fourier amplitude spectra recorded per measurement sample by each sensor (Pn-iii-p- et al. 2017).

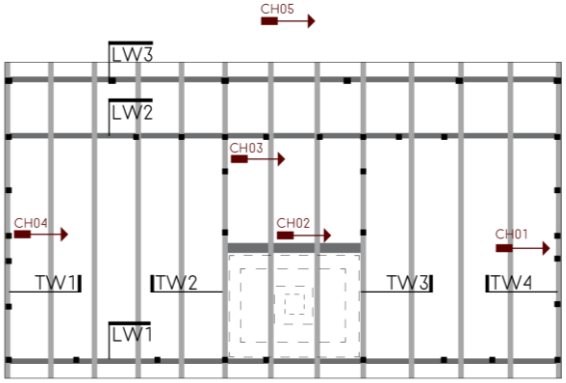

Figure 6.24 Position of velocity sensors in plan of scheme 2.

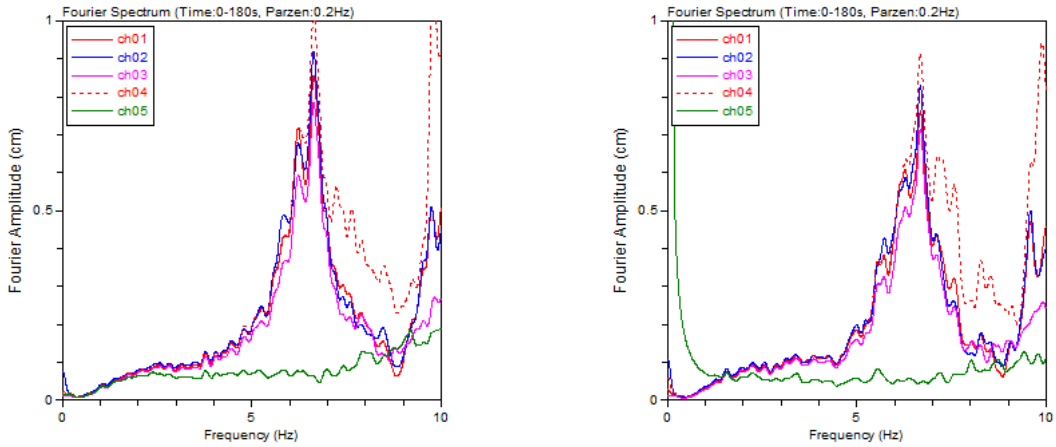

(a) **(b)**

Figure 6.25 Fourier amplitude spectra sample 1 (a) and 2 (b) of scheme 2.

Scheme 3

The third scheme was set to record both longitudinal and transversal microtremors of the building; thus, the sensors on the attic are located just in two position and oriented perpendicularly one to the other, Figure 6.26. Ch01 and Ch04 sensors are fixed in the same position of scheme 1 along TW4 wall and Ch02 and Ch03 in the one in front of the chimney. Figure 6.27a and b show the Fourier amplitude spectra recorded per measurement sample by each sensor (Pn-iii-p- et al. 2017).

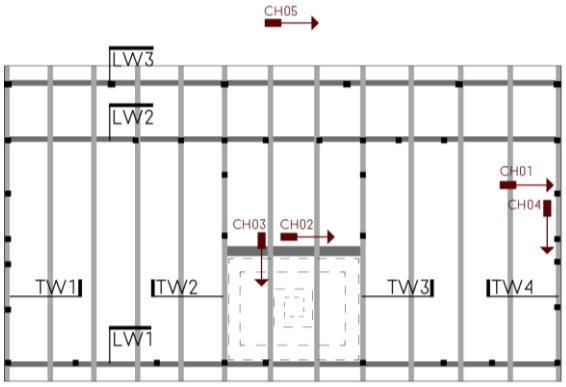

Figure 6.26 Position of velocity sensors in plan of scheme 3.

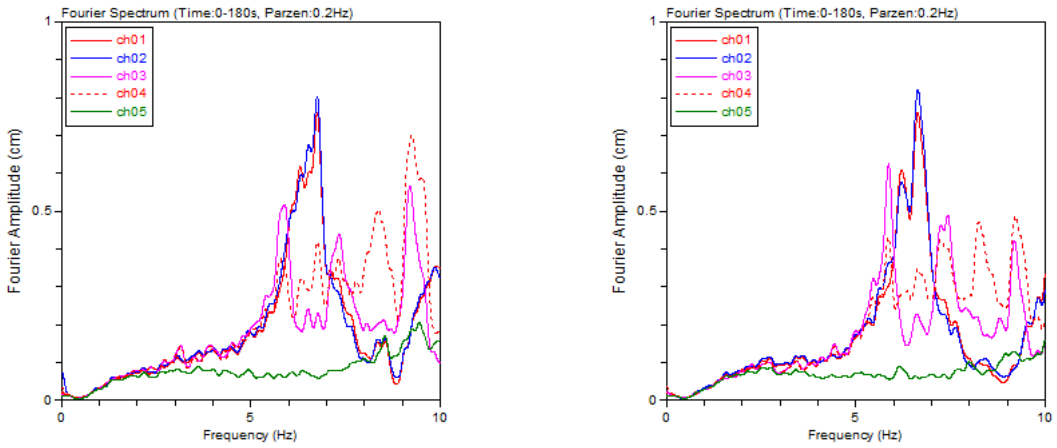

(a) **(b)**

Figure 6.27 Fourier amplitude spectra sample 1 (a) and 2 (b) of scheme 3.

Scheme 4

The fourth scheme is aimed at studying again the longitudinal direction of the building; thus, all the sensors are oriented along this axis but in different positions with respect to Scheme 1, Figure 6.28. The sensors are located on the attic floor as follows: Ch01 at the corner between LW1 and TW4, Ch02 always in front of the chimney, Ch03 and Ch04 at the corners between TW1 and LW2, TW1 and LW1 respectively. The fifth one is located on the ground close to the portico. Figure 6.29a and b show the Fourier amplitude spectra recorded per measurement sample by each sensor (Pn-iii-p- et al. 2017).

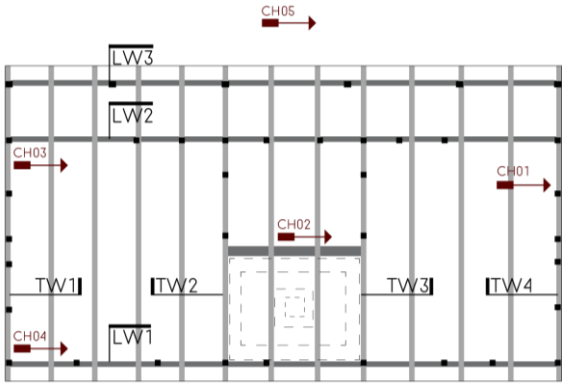

Figure 6.28 Position of velocity sensors in plan of scheme 4.

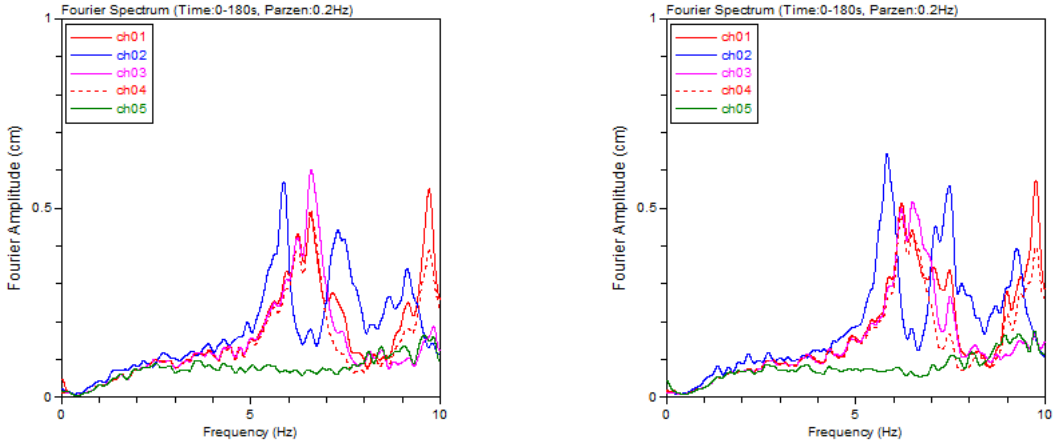

(a) **(b)**

Figure 6.29 Fourier amplitude spectra sample 1 (a) and 2 (b) of scheme 4.

Scheme 5

The fifth scheme was set to study the transversal direction of the building; thus, all the sensors are oriented along this axis but in different positions with respect to Scheme 1, Figure 6.30. Indeed, the sensors are located in the same position of scheme 4 but rotated by 90°. Figure 6.31a and b show the Fourier amplitude spectra recorded per measurement sample by each sensor (Pn-iii-p- et al. 2017).

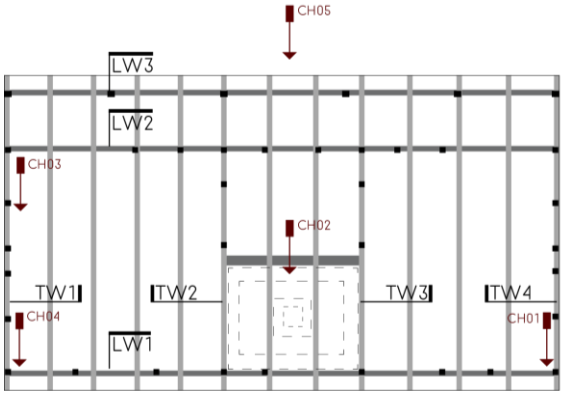

Figure 6.30 Position of velocity sensors in plan of scheme 5.

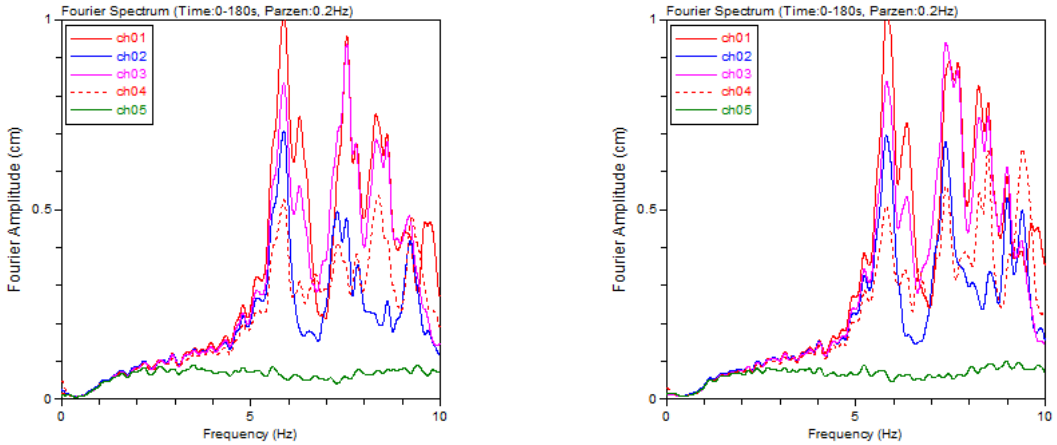

(a) **(b)**

Figure 6.31 Fourier amplitude spectra sample 1 (a) and 2 (b) of scheme 5.

Scheme 6

The sixth scheme was aimed at recording both longitudinal and transversal microtremors of the building; thus, the sensors on the attic are located just in two position and oriented perpendicularly one to the other, Figure 6.32. Ch01 and Ch04 sensors are fixed in along TW2 wall and Ch02 and Ch03 along TW3. Figure 6.33a and b show the Fourier amplitude spectra recorded per measurement sample by each sensor (Pn-iii-p- et al. 2017).

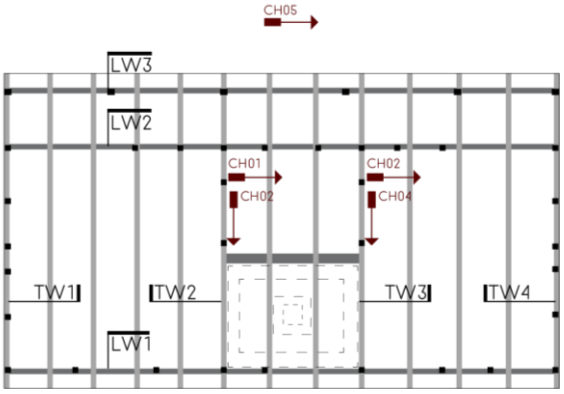

Figure 6.32 Position of velocity sensors in plan of scheme 6.

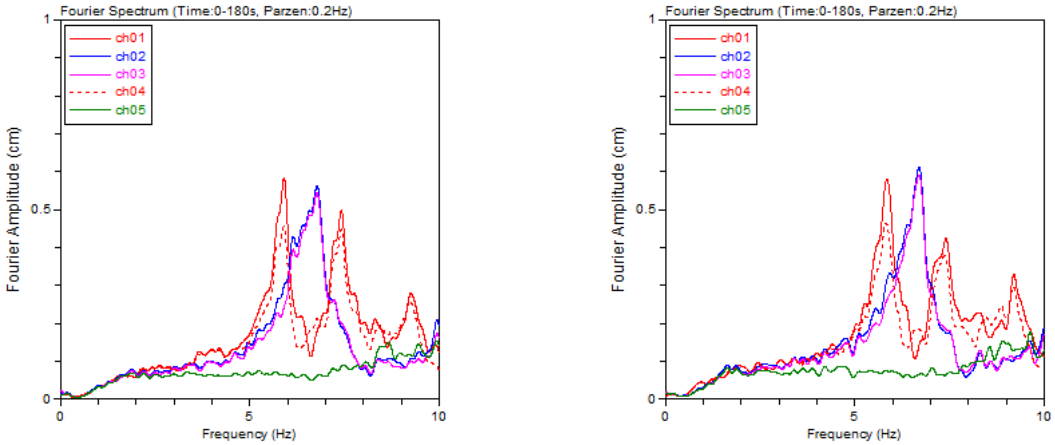

(a) **(b)**

Figure 6.33 Fourier amplitude spectra sample 1 (a) and 2 (b) of scheme 6.

6.4.2 Analysis of Results

The output related to transversal and longitudinal direction shows a different response due to geometrical layout and mass distribution. The spectra for longitudinal direction are generally straighter than those for transversal direction (Pn-iii-p- et al. 2017). Table 6.1 summarize the identified peak frequencies per scheme related to longitudinal and transversal directions by peak picking method. The first periods are very low, 0.17 s for transversal direction and 0.15 s for longitudinal one, due to the limited height of the building and the additional stiffness provided by brick masonry infill. It is worth to point out that these results can be influenced by the poor state of conservation of the building. Moreover, a simplified eigenvalue analysis should be performed on a FEM model before dynamic identification to obtain the range of frequencies and decide the best location of the sensors according to the mode shape configurations of the building. In this case, no mode shapes were obtained because there are only two sensors along the vertical direction since it is just one-storey building. Moreover, an empirical rule recommends setting the total duration of sampling around 2000 times the highest period of the structure,

in this case at least 6 minutes. Lastly, the dynamic behavior can be considered more reliable if two or more identification technique are performed.

Table 6.1 Peak frequencies corresponding to the main spectral peaks identified (Pn-iii-p- et al. 2017).

Peak frequency	f_{1TRANS} [Hz]	f_{2TRANS} [Hz]	f_{3TRANS} [Hz]	f_{1LONG} [Hz]	f_{2LONG} [Hz]
Scheme 1	5.89	7.30	9.31	-	-
Scheme 2	-	-	-	6.65	9.76
Scheme 3	5.84	7.28	9.21	6.70	9.85
Scheme 4	5.84	7.45	9.39		
Scheme 5	-	-	-	6.54	9.61
Scheme 6	5.87	7.40	9.21	6.73	9.78
Average value	5.86	7.36	9.28	6.66	9.75
Average Period [s]	0.17	0.14	0.11	0.15	0.10

7 NUMERICAL MODEL OF A REPRESENTATIVE ROMANIAN TFM BUILDING

The seismic behavior of representative Romanian TFM buildings was assessed by modelling the structure in OpenSees and calibrating its dynamic properties according to the ambient vibration tests. The global response is influenced by a set of parameters such as geometry, mass distribution, configuration of structural elements (TFM walls, floor and roofing system) as well as the connections between them and state of conservation. The procedure of inverse fitting was performed to calibrate the frequencies resulting from the numerical model with those identified by output-only measurements using peak picking technique. In the present section the structural scheme with its geometry and boundary conditions is described as well as the material properties and loads applied to all the elements, especially the linear and non-linear properties of the connections. Eigenvalue and bidirectional pushover analysis were performed, and their results are presented and eventually discussed.

7.1 Geometry and Boundary Conditions

Since the masonry panel S1 was calibrated with a modelling strategy consisting of an equivalent frame with non-linearities lumped at the connections, the same approach was applied to the building. Its geometry was simplified by modelling all the timber members with *elasticBeamColumn* elements aligned to their center axis and without representing the clay brick masonry infill that increases the in-plane stiffness more than the mud brick one of the S1 wall. In this case, it is worth to point out that the diagonal elements are not always constrained on both sides by vertical posts, thus the response may be slightly different from the tested walls and also due to their level of connection with both posts and lower beams. In addition, the in-plane response of each wall is influenced by the presence of the openings that consists of horizontal lintels pinned at their ends to the vertical posts. Moreover, neglecting the out-of-plane behavior may not be conservative since the masonry infills detach from the very beginning even during the in-plane tests, thus this mechanism is very likely to occur in case of earthquake. Table 7.1 shows the average dimensions and properties of all the timber elements of the structure according to the local reference axis.

Table 7.1 Geometrical dimension and properties of timber structural elements.

Structural Element	Width [mm]	Height [mm]	Area [mm^2]	I_y [mm^4]	I_z [mm^4]	J_t [mm^4]
Internal Columns	120	120	14400	17280000	17280000	29237760
External Columns	130	150	19500	27462500	36562500	52043550
Bracings	120	120	14400	17280000	17280000	29237760
Lintels	120	160	19200	40960000	23040000	49121280
Primary Beams	110	140	15400	25153333.33	15528333.33	
Secondary Beams	110	140	15400	25153333.33	15528333.33	
Beam supporting chymney	200	200	40000	133333333.3	133333333.3	

Rafters	90	120	10800	12960000	7290000

The structural schemes of each wall as well as its boundary conditions are presented in Figure 7.1. The lower nodes are fixed to the ground since neither differential foundation settlements nor tipping ones were observed during the field investigation due to the light weight of the structure and its continuous wall-footing. No horizontal sliding was considered as well, but this assumption may not be conservative if the lower beam is not connected to the continuous brick masonry wall footing.

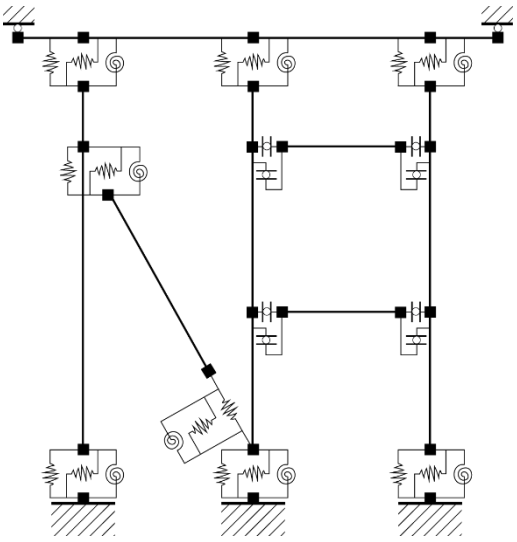

Figure 7.1 Structural scheme of walls.

Since S1 wall was calibrated considering its pure shear behavior with the application of a pantograph system that permits only horizontal displacements preventing any rotation, the horizontal diaphragm was modelled as rigid and four sliding supports were located at each corner preventing relative vertical displacements. In this case, the floor was divided in three longitudinal bands with three cells along the transversal direction to have symmetry and control relative displacements between the upper nodes of vertical posts, Figure 7.2. The rigid diaphragm was reproduced by modelling both diagonals and upper beams as rigid elements by applying them a large cross-sectional area (A = 10 m^2). Increasing the axial stiffness of these elements results in equal horizontal displacements for all the upper nodes on the floor.

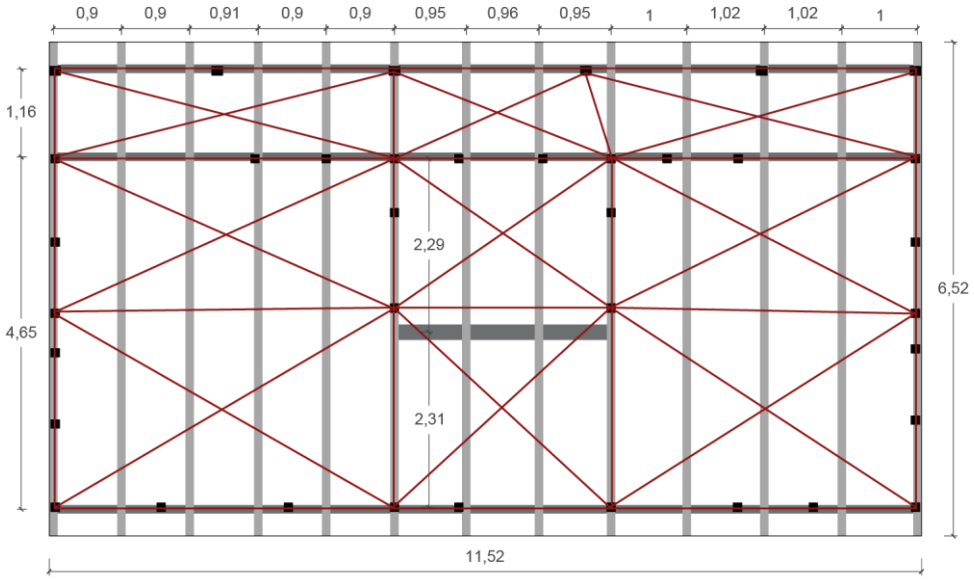

Figure 7.2 Structural scheme of floor.

7.2 Material Properties and Loads

The weight of masonry infill was converted in load per unit length considering the tributary area of each post and summed to the weight per unit length of timber. After this hand calculations, the resulting weights were applied as distributed loads along the posts considering a specific weight of 20 kN/m^3 for clay brick masonry and 385 kg/ m^3 for timber posts made of softwood (Romanian fir) to simulate the actual mass distribution of each wall. Timber beams have distributed load perpendicular to their axis with an assumed specific weight of 600 kg/m^3 since they are made of hardwood (oak or acacia). Modulus of elasticity parallel to grain direction was set equal to 8.9 GPa (softwood Romanian fir) in order to be consistent with the wall calibration, Section 5. The horizontal diaphragm and roofing system were not modelled in detail, but they were considered just as additional weight. The distributed loads per unit length per each timber beam was calculated and then lumped at fixed nodes representing the connections between the transversal primary beams and the secondary ones on top of each longitudinal wall LW1, LW2 and LW3 according to their tributary areas, Figure 7.3. The same procedure was applied to determine vertical loads from the roof trusses considering the actual tributary area of the roof field not its horizontal projection due to the steep slope, Figure 7.4.

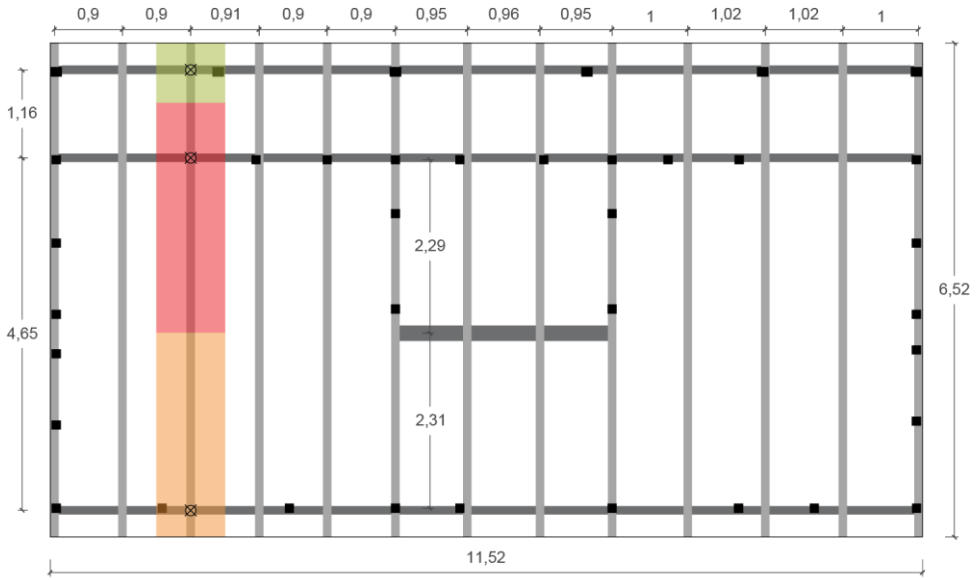

Figure 7.3 Floor tributary area of each node.

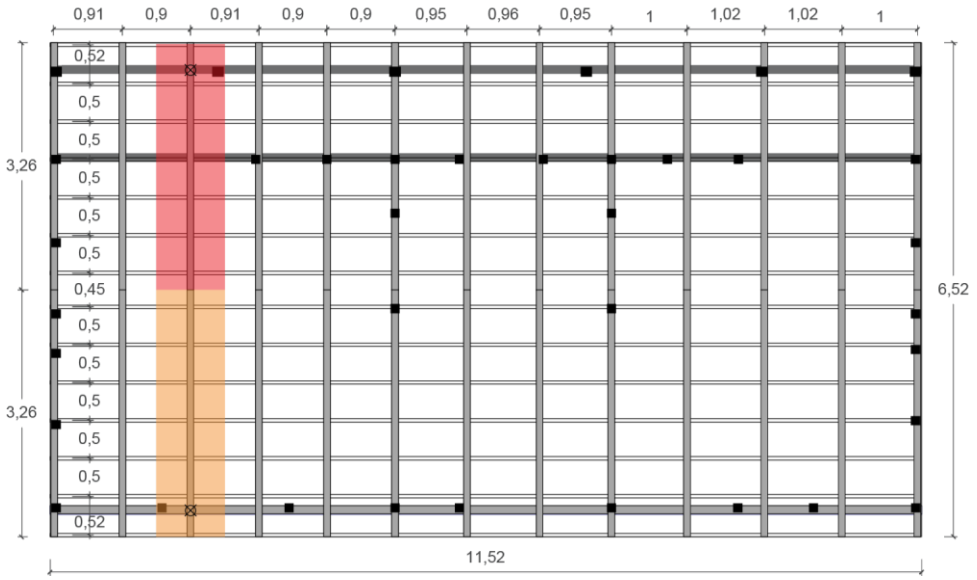

Figure 7.4 Roof tributary area of each node.

No horizontal thrust was considered since the roofing system approaches a truss structure with inclined rafters tied at the base by the transversal beams of the floor diaphragm. In this case, only dead loads were applied to be consistent with the environmental and loading conditions during the dynamic identification, Section 6.4. The presence of the brick masonry chimney was considered as lumped weight at its contour posts as well. Additional loads of brick masonry walls in the attic were lumped at the posts of TW1 and TW2, Figure 7.5.

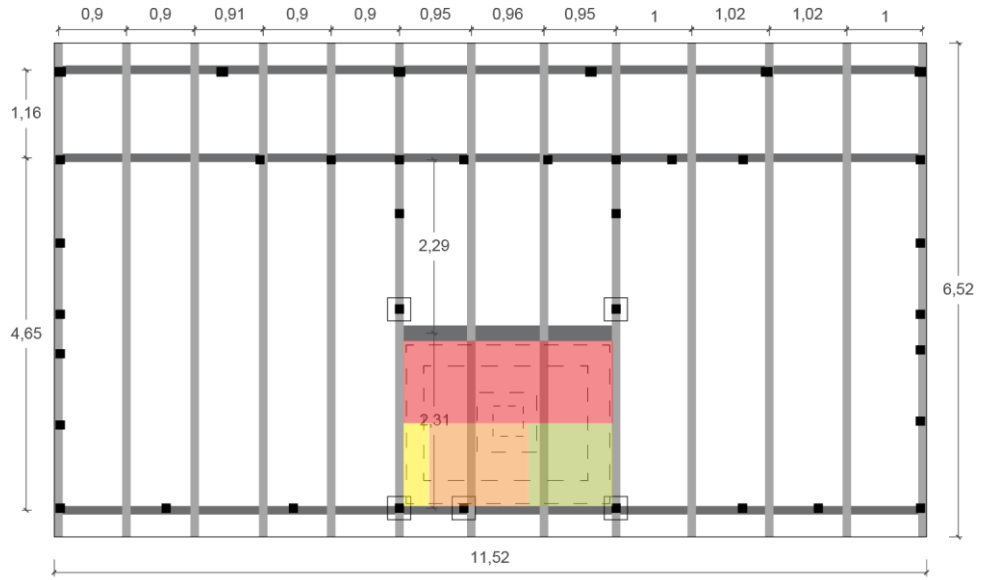

Figure 7.5 Lumped vertical loads representing the brick masonry chimney.

The total weight of numerical model was compared with the one determined by hand calculations to check the reliability of the model. The error between them is negligible (around 5%).

Table 7.2 Material properties of timber structural elements.

Timber Species	Density [kg/m^3]	Modulus of Elasticity parallel [GPa]
Softwood (Romanian fir)	385	8.9
Hardwood (oak)	600	12-

7.3 Connections

The previously calibrated set of connections for pushover analysis of S1 wall of Section 5.4 were applied to TFM walls of the building. Since in-plane stiffness is predominant, the out-of-plane stiffness was modelled as a rotational linear elastic spring (*elastic uniaxial* material) with stiffness of 3000 kN/rad, 10% of the in-plane one. The torsional inertia of each connection was modelled with a rotational linear elastic spring (*elastic uniaxial* material) with stiffness of 10^4 kN/rad.

7.4 Eigenvalue analysis

The dynamic properties of the numerical model were determined by eigenvalue analysis and then compared with the results from the dynamic identification to evaluate the reliability of the model, Section 6.4. It is worth to point out that ambient vibration tests record microtremors of structures in their elastic range. Since the initial stiffness of TFM buildings is mainly controlled by masonry infill, two models were made to compare the differences between two complementary modelling strategies: equivalent frame with non-linearities lumped at the connections (EF) and the same model with masonry infill modelled as shell elements (EFI), Figure 7.6a and b. No updating on the non-linear properties of the already

calibrated connections or on the linear material properties was performed; in particular the modulus of elasticity parallel to the grain direction was fixed at its original value of 8.9 GPa.

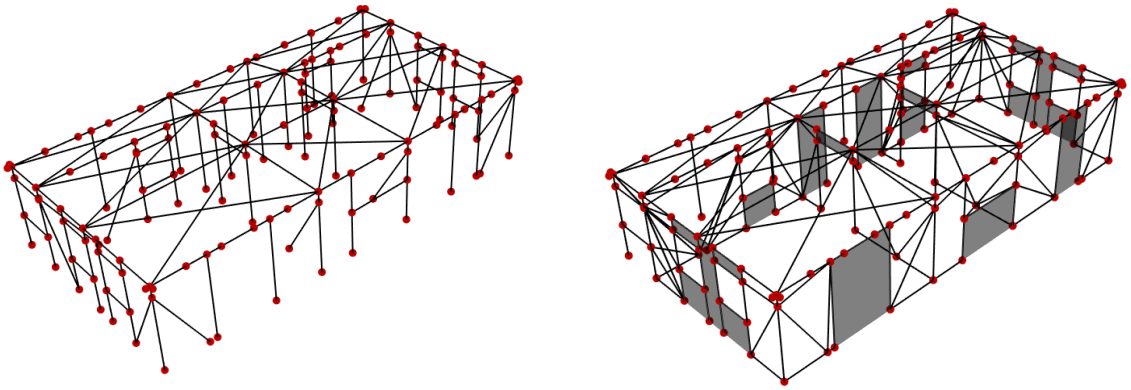

(a) **(b)**

Figure 7.6 EF (a) and EFI (b) models.

Rectangular (*ShellMITC4*) and triangular (*ShellDKGT*) shell elements were defined assigning an elastic isotropic material and updating the Young's Modulus until the measured frequencies were obtained (Poisson's ratio fixed at 0.2). The final value of *E* equal to 58.5 MPa was determined, very low compared to the one related to clay brick masonry (1.2 ÷ 1.8 GPa according to Table C8A.2.1 of Italian Circolare 2009). This value can be considered reasonable since the tested wall S1 was already calibrated with the presence of masonry infill and the increase in stiffness can be justified by the fact that mud brick masonry shows lower stiffness than clay brick masonry. Bearing in mind that the first periods are 0.17 s for the transversal direction and 0.15 s for the longitudinal one and since there are no mode shapes in the already mentioned report (Pn-iii-p- et al. 2017), the first and second periods with the corresponding mode shapes are compared between EF and EF1 models, Figure 7.7 and Figure 7.8a and b.

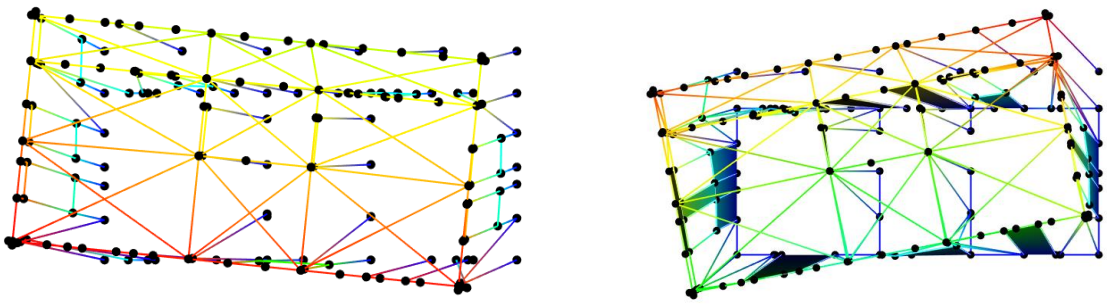

P_{1EF} = 0.374 s **P_{2EFI} = 0.154**

P_{LONG} = 0.15 s **P_{LONG} = 0.15 s**

(a) **(b)**

Figure 7.7 Mode 1 for EF (a) and EFI (b) models.

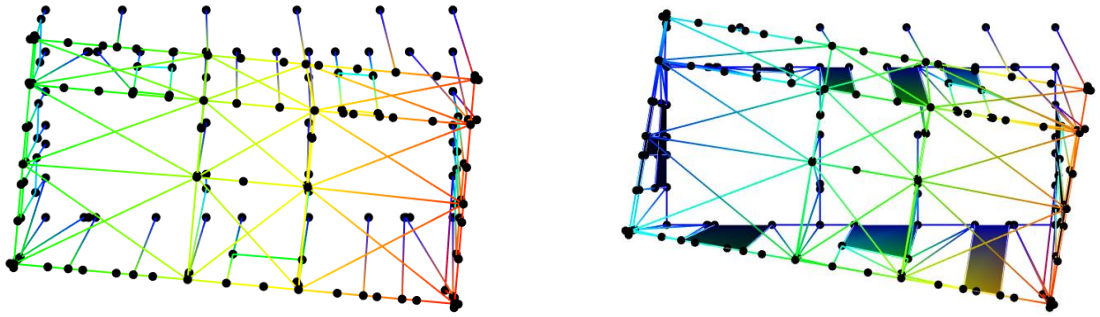

P_{2EF} = 0.333 s

P_{TRANS} = 0.17 s

(a)

P_{1EFI} = 0.17 s

P_{TRANS} = 0.17 s

(b)

Figure 7.8 Mode 2 for EF (a) and EFI (b) models.

The periods of EF model are higher than the measured ones and the corresponding mode shapes show some torsional effects due to non-symmetric layout and mass distribution. This observation was even more evident for EFI model where periods are comparable and both mode shapes experience torsional effects. Moreover, in EF model, periods and corresponding mode shapes were actually flipped; the highest period P_{1EF} was actually longitudinal not transversal and vice versa. Whereas EFI model with its masonry infill contribution shows for the highest period P_{1EFI} of 0.17 s a torsional-transversal mode, Figure 7.9a, and P_{2EFI} of 0.154 s a torsional-longitudinal one, Figure 7.9b.

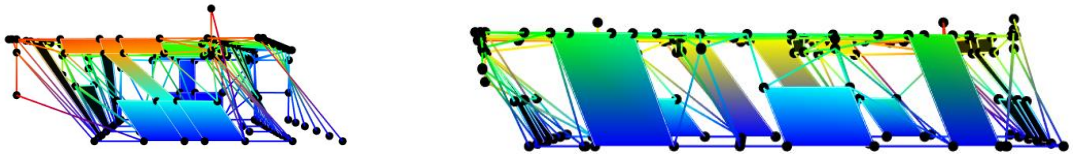

P_{1EFI} = 0.17 s

P_{TRANS} = 0.17 s

(a)

P_{2EFI} = 0.154

P_{LONG} = 0.15 s

(b)

Figure 7.9 Mode 2 for EF (a) and EFI (b) models.

The torsional effect observed in both EF and EFI models may results from the mass eccentricity due to the presence of brick masonry chimneys close to LW1 wall and also the additional weight of brick masonry along the external transversal walls, TW1 and TW2. It is undeniable that calibration of frequencies can also be performed increasing the modulus of elasticity parallel to the grain for timber elements, but this strategy was not followed because of the quality of timber in this existing TFM structure. Indeed, its state of conservation was very poor during the ambient vibration tests, thus the choice of modelling the infill was adopted.

7.5 Pushover analysis

Non-linear static analysis was performed to estimate the global response in terms of initial and first yielding stiffness without considering stiffness and strength degradation related to cyclic loading. This analysis was just performed on the EF model since EFI should have been more refined in terms of mesh size and material properties to run this type of analysis.

After applying gravity loads and setting them to constant, a central node was set as the control one and pushed up to 200 mm with displacement increments of 10^{-2} mm. Thus, the analysis was carried out under displacement control algorithm using again energy increment convergence test with the same tolerance fixed for pushover analysis of the wall (10^{-4}). Pushover analysis were performed in both directions showing different initial and yielding stiffness, Figure 7.10. Based on the observation during the experimental test of the wall S1, a maximum displacement of 63 mm was set as a reference to have failure in the TFM walls. The points corresponding to the achievement of this value are highlighted in black for y direction and red for x direction, Figure 7.10.

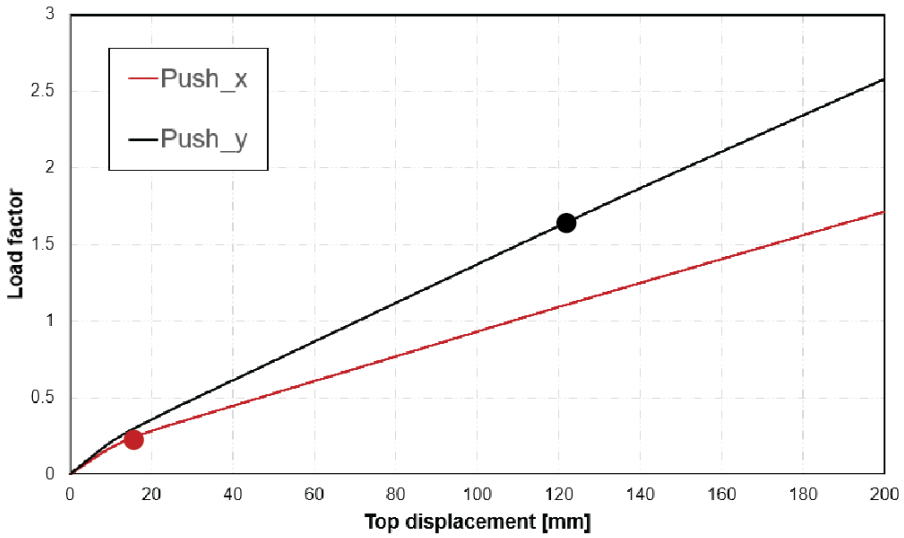

Figure 7.10 Pushover curve for x and y direction.

It is worth to stress that longitudinal direction is more vulnerable due to the fact that diagonal elements are not constrained by vertical posts but just connected to the lower beam, while in the transversal direction the final value is similar to those of the wall. Indeed the configuration is more comparable with the tested Romanian TFM wall for which the connections are calibrated.

7.6 Final Remarks

The Romanian TFM building was modelled to assess its linear and non-linear behavior by performing eigenvalue and non-linear static analysis. Two modelling strategies were adopted during the calibration of its dynamic properties since the contribution of masonry infill cannot be neglected if the building is in the elastic domain. A further calibration was required due to the different type of masonry observed in

the existing structure which is stiffer than the one of S1 infill and because the modulus of elasticity parallel to grain was not updated considering the timber quality and its state of conservation. The simplified model has other limitations such as it does not take into account the interface between the timber frame and masonry infill, but, as already mentioned in Section 5.3, its contribution in terms of dissipated energy was considered in the calibration of connections. In addition, since the masonry infill detaches from the timber frame even in the setting process, the out-of-plane mechanisms are not prevented especially in case of earthquakes, thus a further implementation of the numerical model is required. Regarding the non-linearities of the connections, they are calibrated in Section 5.3 to match the experimental curve of S1 wall subjected to a fixed vertical load and in-plane cyclic quasi-static loading. It is worth to point out that the calibrated hysteretic uniaxial materials such as *SAWS* and *Pinching4* relate to the vertical load of 26 kN representing the average load of the wall tributary area, but, due to the intrinsic properties of these materials, modifying the applied loads on the structures does not change its global response. However, the simplified EF model approaches the experimental measurements in terms of periods and provides a good estimation of the structural capacity of the building. Moreover, lumping the non-linearities at the joints allows to capture their local failures if the demand exceeds their deformation capacity. However, other measurements may be taken to better characterize the building behavior as well as some non-destructive test may be planned to estimate the mechanical properties of TFM consisting materials, infill and timber.

8 CONCLUSION

The present work was aimed at studying the non-linear hysteretic response of Romanian timber-framed structures with masonry infill when subjected to in-plane cyclic loading. These systems have proven their earthquake-resistance throughout the centuries, and they are still built nowadays even though the knowledge of local builders was almost lost. Thus, its construction details and elements should be characterized to better understand their influence on the structural behavior. Before starting with the wall calibration, a literature review on the experimental tests for the same types of connections was carried out to obtain an initial reference calibration of the hysteretic curve of the joints that can be modified during the following calibration of the wall. Although these experimental campaigns may present some differences in terms of geometry, element cross-sections, timber quality and level of accuracy during the construction, the resulting non-linear hysteretic springs can be considered representative for the mortise and tenon and cross-halved joints of the tested wall (S1). The calibration of timber connections resulted in a good approximation in terms of stiffness, ultimate strength and softening branch between the experimental and numerical results, but there are still some discrepancies in terms of reloading and unloading stiffness, especially for large deformations, that influence the comparison of dissipated energy.

During the experimental campaign on Romanian TFM walls, it was observed that the presence and arrangement of diagonal bracings controlled the initial stiffness, ultimate strength and deformation capacity of the panel with more severe damages if these elements were aligned along the actual diagonal of the frame. Thus, the choice to model the timber members as linear elastic elements is consistent with the damage observations that revealed no significant cracks along them. For this reason, the equivalent frame modelling strategy with lumped non-linearities at the joints showed its reliability in the calibration of the wall response. Performing the iterative procedure of inverse fitting can be time-consuming, but requires negligible computational effort compared to other modelling strategies and permits to understand the role of each connection and even of each parameter. The main difficulties were related to the calibration of diagonal connections that play an important role in terms of initial stiffness and influence the deformed shape of the wall. These joints along with rotational springs in the upper and lower joints between posts and beams basically control the global response of the wall.

Once all the connections were properly set, pushover analysis was performed to capture the initial and first yielding stiffness of the envelope curve obtained from the experimental test. The connections were modified until the global numerical curve matched the experimental one by the procedure of inverse fitting. It is worth to point out that when the wall was subjected to in-plane cyclic loading, a new set of connections was adopted since, in this case, the hysteretic materials are defined by parameters controlling reloading stiffness and strength degradation for each cycle. Thus, the structural response is analysis-dependent so the connections should be updated accordingly, while it is not influenced by changing the vertical loads. This limitation is intrinsic to the adopted non-linear materials *SAWS* and

Pinching4, but it is worth to point out that the connections are usually calibrated to obtain the experimental global response of the wall that is subjected to a fixed vertical load representative of the average vertical loading in a typical TFM panel. However, this is one of the reasons why the set of connections calibrated for the wall may not be representative in some posts of the building where either larger or negligible loads are applied. Regardless this limitation that can affect the building response, the wall global behavior was matched in terms of maximum base shear, initial, yielding and softening stiffness, but the approximation of the dissipated energy was not perfectly approached due to the pinching effect and almost vertical unloading in the experimental test that is difficult to obtain in a numerical model.

The loading protocol during the test was also influenced by the initial misalignment of the wall with the reaction frame, thus, in the first phase, the actuator could not exceed a maximum horizontal displacement of around 80 mm, resulting in two close cycles with a decrease of the resulting base shear related to the larger displacement. Moreover, during the second phase some cycles were repeated increasing the damages and the stiffness degradation. The positive and negative peak-displacements are different, possibly due to the manual control of the actuator, thus the hysteretic curves are not symmetric, and it is even shifted vertically may be due to the initial misalignment. Regarding the test setup, additional local measurements should be recorded to better characterize the behaviour of the diagonal elements in terms of vertical sliding along the external posts and axial detachment in addition to the already measured vertical uplift of external posts and their rotations at the base. Moreover, some inductive transducers did not work properly for large shear angles, thus their records should be corrected considering their incremental trend.

The global response of the representative TFM building was studied by applying the same set of connections calibrated for the wall, but, as already mentioned, this assumption may result in local under or over estimation of connection stiffness due to the variability of vertical loading from the fixed value of 26 kN applied to the wall specimen. Thus, the resulting frequencies and mode shapes did not exactly match with those obtained by peak picking method. In this case, a second model was considered by applying shell elements simulating the increase in stiffness due to clay brick masonry instead mud brick masonry of the tested wall S1. Updating the modulus of elasticity parallel to the grain was not considered conservative since the state of conservation was very poor and it may be even lower than the one assumed for the timber elements of the wall. However, both models were compared in terms of periods and mode shapes also with the results from dynamic identification. In this case the model with infill approached the experimental periods and the resulting mode shapes can be considered reliable with the mass distribution and the non-symmetric layout in plan. A non-linear static analysis was performed on the equivalent frame model even though this structure is more flexible than the model with infill and it showed interesting results in terms of local failure of the diagonal connections. The upper limit of their vertical sliding was fixed according to the observation during the test.

It is worth to point out that although there are some limitations in the definition of hysteretic materials and in the modelling strategy, results comparable with the tested wall and experimental measurements were obtained, meaning that the approach is still valid and reliable.

8.1 Future developments

The numerical analyses carried out in this work are a good starting point for the simplified numerical analysis of timber-framed buildings. However, it is considered that further developments can improve and optimize the numerical results obtained until now. Moreover, since new experimental campaigns are being planned on this type of structures, it is important to fill in the gaps of information necessary to carry out the numerical analyses. Further developments based on the work developed in this thesis include:

- Parametric analyses of timber-framed walls, considering the different geometrical configurations of the existing experimental campaign, mainly regarding the positioning of the diagonal elements;
- Proper representation of infill, considering its real characteristics (additional experimental data needed), out-of-plane mechanisms as well as information on the interface connectivity between frame and infill;
- Dynamic analysis on buildings.

9 REFERENCES

338, E. (2009). *EN 338: Structural timber — Strength classes - British Standards Institute*.

Aktaş, Y. D., Akyüz, U., Türer, A., Erdil, B., and Güçhan, N. Ş. (2014). "Seismic Resistance Evaluation of Traditional Ottoman Timber-Frame Himiş Houses: Frame Loadings and Material Tests." *Earthquake Spectra*, 30(4), 1711–1732.

Bianco, A. (2010). *La casa baraccata: guida al progetto e al cantiere di restauro*. (G. EditoriA, ed.), Roma.

Ceccotti, A., and Sandhaas, C. (2010). "A Proposal for a Standard Procedure to Establish the Seismic Behaviour Factor q of Timber Buildings." *World Conference on Timber Engineering, WCTE*, (January 2010).

Copani, P. (2007). "Timber-Frame Buildings and in Scandinavia: High Deformation Prevent the System from Collapse." *From Material to Structure - Mechanical Behaviour and Failures of the Timber Structures, ICOMOS IWC - XVI International Symposium, Florence, Venice and Vicenza* , (November), 11–16.

Cruz, H., Machado, J. S., Campos, A., Paulo, C., Candeias, X., Ruggieri, N., and Catarino, J. M. (Eds.). (2015). "Historical Earthquake- Resistant Timber Framing in the Mediterranean Area."

Dima, D. I., and Dutu, A. (2016). "Traditional Buildings With Timber Frame and Various Infills in Romania." *Proceedings of the WCTE 2016 World Conference on Timber Engineering, Vienna / Austria, August 22-25, 2016*, 1–9.

Dolan, J. D., and Madsen, B. (1992). "Monotonic and cyclic nail connection tests." *Journal of Civil Engireering*, 1(19), 97–104.

Dutu, A. (2017). *Metodă de evaluare seismică pentru case rezidențiale tradiționale românești*.

Duțu, A., Dima, D. I., and Bulimar, E. G. (2017). "Materials and Techniques for Traditional Romanian Residential Houses." 12–15.

Dutu, A., Niste, M., and Spatarelu, I. (2018a). "in-Plane Static Cyclic Tests on Traditional Romanian Houses ' Walls." 1–12.

Dutu, A., Niste, M., Spatarelu, I., Dima, D. I., and Kishiki, S. (2018b). "Seismic evaluation of Romanian traditional buildings with timber frame and mud masonry infills by in-plane static cyclic tests." *Engineering Structures*, Elsevier, 167(November 2017), 655–670.

Dutu, A., Sakata, H., and Yamazaki, Y. (2015). "Experimental Study on Timber-Framed Masonry Structures." *Historical Earthquake-Resistant Timber Frames in the Mediterranean Area*, N. Ruggieri, G. Tampone, and R. Zinno, eds., Springer, Cham, 67–81.

EC5. (2004). "EUROPEAN STANDARD EUROPÄISCHE NORM Eurocode 5 : Design of timber structures - Part 1-1 : General - Common rules and rules for buildings." *Design*, 1–123.

Folz, B., and Filiatrault, A. (2004). "Simplified Seismic Analysis of Woodframe Structures." *13th World Conference on Earthquake Engineering*, (245), 15.

Gioncu, V., and Marius, M. (2009). "Protection of historical buildings, Proceedings of the International

Conference of Protection of Historical Buildings." *PROHITECH 09*, 1153–1158.

Gonçalves, A. M., Ferreira, J. G., Guerreiro, L., and Branco, F. (2012). "Experimental Characterization of Pombalinos 'Frontal' Walls Cyclic Behaviour." *15th International Conference on Experimental Mechanics*, (September), 1–13.

Gülkan, P., and Langenbach, R. (2004). "The Earthquake Resistance of Traditional Timber and Masonry Dwellings in Turkey." *13th World Conference on Earthquake Engineering*, (2297).

Gupta, A. K., and Kuo, P.-H. (1985). "Behavior of wood-framed shear walls." *Journal of Structural Engineering*, 8(111), 1722–1733.

Hassan, R., Ibrahim, A., and Ahmad, Z. (2010). "Performance of Mortise and Tenon Connection Fastened With Wood and Steel Dowel." *World Conference on Timber Engineering*, 2–8.

Holliday, L., Kang, T. H.-K., and Mish, K. D. (2011). "Taquezal Buildings in Nicaragua and Their Earthquake Performance."

Indicativ P 100-1/2013. (n.d.). .

Ismail-Zadeh, A., Matenco, L., Radulian, M., Cloetingh, S., and Panza, G. (2012). "Geodynamics and intermediate-depth seismicity in Vrancea (the south-eastern Carpathians): current state-of-the art, Tectonophysics."

Kouris, L. A. S., and Kappos, A. J. (2012). "Detailed and simplified non-linear models for timber-framed masonry structures." *Journal of Cultural Heritage*, Elsevier Masson SAS, 13(1), 47–58.

Langenbach, R. (2009). *Don ' t Tear it Down !*

Lukic, R. (2016). "Numerical Modelling of the Cyclic Behaviour of Timber-framed Structures." Universidade do Minho.

Mascarenhas, J. (2009). *Sistemas de Construção V – O Edifício de Rendimento da Baixa Pombalina de Lisboa.* (HORIZONTE, ed.).

Meireles, H., Bento, R., Cattari, S., and Lagomarsino, S. (2012). "A Hysteretic Model for 'Frontal' Walls in Pombalino Buildings." *Bulletin of Earthquake Engineering*, 10(5), 1481–1502.

Mosoarca, M., Petrus, C., Valeriu, S., and Anastasiadis, A. (2014). "Seismic risk of buildings with RC frames and masonry infills from Timisoara , Banat region , Romania." *9th International Masonry Conference*, (July), 1–12.

Narita, A., Mosoarca, M., Modena, C., Da Porto, F., Munari, M., Taffarel, S., Marson, C., Valotto, C., and Roverato, M. (2016). "Behavior of Historic Buildings in Zones with Moderate Seismic Activity. Case Study: Banat Region, Romania." *Procedia Engineering*, 161, 729–737.

NDMA - National Disaster Management Authority. (n.d.). *Dhajji Construction*.

Ortega, J., Vasconcelos, G., Rodrigues, H., Correia, M., and Lourenço, P. B. (2017). "Traditional earthquake resistant techniques for vernacular architecture and local seismic cultures: A literature review." *Journal of Cultural Heritage*, 27, 181–196.

Pavel, F., Vacareanu, R., Douglas, J., Radulian, M., Cioflan, C., and Barbat, A. (2016). "An Updated Probabilistic Seismic Hazard Assessment for Romania and Comparison with the Approach and Outcomes of the SHARE Project." 173, 1881–1905.

Pn-iii-p-, R. E., Căsuță, A. D., Mocănescu, D. B.-, Niste, M., Spătărelu, I., Țăpuși, D., Erbașu, R., Târșoagă, C., Nicula, V., and Aldea, A. (2017). *Configuratii noi , cu materiale locale naturale si tehnologii moderne , pentru case traditionale romanesti (TRAROM)*.

Poletti, E., and Vasconcelos, G. (2014). "Seismic behaviour of traditional timber frame walls: experimental results on unreinforced walls." *Bulletin of Earthquake Engineering*, 13(3), 885–916.

Poletti, E., and Vasconcelos, G. (2015). "Seismic Performance of Traditional Half-Timbered Walls: Experimental Results." *Historical Earthquake-Resistant Timber Frames in the Mediterranean Area.*, N. Ruggieri, G. Tampone, and R. Zinno, eds., Springer, Cham.

Qu, Z., Dutu, A., Zhong, J., and Sun, J. (2015). "Seismic Damage to Masonry-Infilled Timber Houses in the 2013 M7.0 Lushan, China, Earthquake." *Earthquake Spectra*, 31(3), 1859–1874.

Quinn, N. (2017). "A Seismic Assessment Procedure for Historic Structures." University College London.

Ruggieri, N. (2015). "Behaviour of the Borbone Constructive System Under Cyclic Loading. Preliminary Report."

Ruggieri, N. (2016). "An italian anti-seismic system of the 18th century decay, failure modes and conservation principles." *International Journal of Conservation Science*, 7(Special Issue 2), 827–838.

Sakata, H., Yamazaki, Y., and Ohashi, Y. (2012). "A Study on Moment Resisting Behavior of Mortise-Tenon Joint with Dowel or Split Wedge." *15th World Conference on Earthquake Engineering (15WCEE)*.

Sánchez, O., Kvist, L. P., and Aguirre-Mendoza, Z. (2006). "Bosques secos en Ecuador y sus plantas útiles." *Botánica Económica de los Andes Centrales*, 188–204.

Santos. (1997). "Ensaios de paredes pombalinas."

Schacher, T. (2008). "Good Engineering without Appropriate Communication doesn ' t lead to Seismic Risk Reduction : some thoughts about appropriate knowledge transfer tools." *14 WCEE*.

SR EN 1052-3:2003. (2003). *Methods of test for masonry - Part 3: Determination of initial shear strength.*

Torrealva, D., and Vicente, E. (2012). "Experimental Evaluation of Seismic Behavior of Quincha Walls from the Historical Centre of Lima–Peru." *Proceedings of the 15th World Conference in Earthquake Engineering*.

Vieux-Champagne, F., Sieffert, Y., Grange, S., Polastri, A., Ceccotti, A., and Daudeville, L. (2014). "Experimental analysis of seismic resistance of timber-framed structures with stones and earth infill." *Engineering Structures*, Elsevier Ltd, 69, 102–115.

Vintzileou, E., Touliatos, P., Zeris, C., Repapis, K., Adami, C., Zagotsis, A., Leonardos, E., and Palieraki, B. (2004). *Evaluation and recommendations for the interventions in the buildings of Lefkada's historic settlement. Organization for the seismic design and protection.* Athens.

Wenzel, F., Sperner, B., Lorenz, F., and Mocanu, V. (2001). "Geodynamics, tomographic images and seismicity of the Vrancea region (SE-Carpathians, Romania)." *Stephan Mueller Special Publication Series*, 3, 95–104.